Modulation of the in vitro mechanical and chemical environment for the optimization of tissue-engineered articular cartilage

Brendan L. Roach

Submitted in partial fulfillment of the
requirements for the degree of
Doctor of Philosophy
in the Graduate School of Arts and Sciences

COLUMBIA UNIVERSITY

2017

ABSTRACT

Modulation of the in vitro mechanical and chemical environment for the optimization of tissue-engineered articular cartilage

Brendan L. Roach

Articular cartilage is the connective tissue lining the ends of long bones, providing a dynamic surface that bears load while providing a smooth surface for articulation. When damaged, however, this tissue exhibits a poor capacity for repair, lacking the lymphatics and vasculature necessary for remodeling. Osteoarthritis (OA), a growing health and economic burden, is the most common disease afflicting the knee joint. Impacting nearly thirty million Americans and responsible for approximately $90 billion in total annual costs, this disease is characterized by a progressive loss of cartilage accompanied by joint pain and dysfunction. Moreover, while generally considered to be a disease of the elderly (65 years and up), evidence suggests the disease may be traced to joint injuries in young, active individuals, of whom nearly 50% will develop signs of OA within 20 years of the injury. For these reasons, significant research efforts are directed at developing tissue-engineered cartilage as a cell-based approach to articular cartilage repair. Clinical success, however, will depend on the ability of tissue-engineered cartilage to survive and thrive in a milieu of harsh mechanical and chemical agents.

To this end, previous work in our laboratory has focused on growing tissues appropriate for repair of focal defects and entire articular surfaces, thereby investigating the role of mechanical and chemical stimuli in tissue development. While we have had success at producing replacement tissues with certain qualities appropriate for clinical function, engineered cartilage capable of withstanding the full range of insults *in vivo* has yet to be developed. For this reason, and in an effort to address this shortcoming, the work described in this dissertation aims to (1) further characterize and (2) optimize the response of tissue-engineered cartilage to physical loading and the concomitant chemical insult found in the injured or diseased diarthrodial joint, as well as (3) provide a clinically relevant strategy for joint resurfacing. Together, this holistic approach maximizes the chances for

in vivo success of tissue-engineered cartilage.

Regular joint movement and dynamic loads are important for the maintenance of healthy articular cartilage. Extensive work has been done demonstrating the impact of mechanical load on the composition of the extracellular matrix and the biosynthetic activity of resident chondrocytes in explant cultures as well as in tissue-engineered cartilage. In further characterizing the response of tissue-engineered cartilage to mechanical load, the work in this dissertation demonstrated the impact of displacement-controlled and load-controlled stimulation on the mechanical and biochemical properties of engineered cartilage. Additionally, these studies captured tension-compression nonlinearity in tissue-engineered cartilage, highlighting the role of the proteoglycan-collagen network in the ability to withstand dynamic loads *in vivo*, and optimized a commercial bioreactor for use with engineered cartilage.

The deleterious chemical environment of the diseased joint is also well investigated. It is therefore essential to consider the impact of pro-inflammatory cytokines on the mechanical and biochemical development of tissue-engineered cartilage, as chemical injury is known to promote degradation of extracellular matrix constituents and ultimately failure of the tissue. Combining expertise in interleukin-1α, dexamethasone, and drug delivery systems, a dexamethasone drug delivery system was developed and demonstrated to provide chondroprotection for tissue-engineered cartilage in the presence of supraphysiologic doses of pro-inflammatory cytokines. These results highlight the clinical relevance of this approach and indicate potential success as a therapeutic strategy.

Clinical success, however, will not only be determined by the mechanical and biochemical properties of tissue-engineered cartilage. For engineered cartilage to bear loads *in vivo*, it is necessary to match the natural topology of the articular surface, recapitulating normal contact geometries and load distribution across the joint. To ensure success, a method for fabricating a bilayered engineered construct with biofidelic cartilage and subchondral bone curvatures was developed. This approach aims to create a cell-based cartilage replacement that restores joint congruencies, normalizes load distributions across the joint, and serves as a potential platform for the repair of both focal defects and full joint surfaces.

The research described in this dissertation more fully characterizes the benefits of mechanical stimulation, prescribes a method for chondroprotection *in vivo*, and provides a strategy for creating a cartilage replacement that perfectly matches the native architecture of the knee, thus laying the

groundwork for clinical success of tissue-engineered cartilage.

Table of Contents

List of Figures

List of Tables

Acknowledgements

> "Wander a whole summer if you can... time will not be taken from the sum of life. Instead of shortening, it will definitely lengthen it and make you truly immortal."
>
> -John Muir

I'd like to acknowledge and thank the funding sources that made this dissertation possible. Funding from the T32 pre-doctoral training fellowship and the National Science Foundation Graduate Research Fellowship have enabled me to investigate my every question and allowed me to build a professional network in New York City and internationally.

I am eternally indebted to my committee members for their direction and support: Drs. Clark Hung, Gerard Ateshian, Helen Lu, Kacey Marra, and Roshan Shah. One of my first memories at Columbia University was a guest lecture from Helen. A lecture that ended with a grand challenge from her for the next generation of tissue engineers: regenerate the complexity of an entire joint. I hope she continues to challenge students to dream big. Many thanks to Roshan, who has indulged me in Friday night e-mails about anti-fibrotic delivery systems and provided a much appreciated clinical perspective. I have had the honor of working with and learning from Gerard, one of the few people I know who knows what he knows and also knows what he doesn't know. I owe much thanks to Kacey, who has provided expertise and guidance on polymer drug delivery systems, and made a substantial portion of this dissertation possible. And I thank her for helping to steer me away from a potentially costly decision to encapsulate TGF-β3. Above all, I am immensely grateful to Clark for taking a chance on me and being willing to listen to my ideas when I didn't yet know the potential of them. With his mentorship, support, and encouragement, I've grown as a researcher and, more importantly, as a person.

A very special thanks is due to my long time colleagues and friends, Terri-Ann Kelly and Andrea Tan. They taught me everything I know about cell culture and cartilage tissue engineering, and sacrificed much of their time and patience in the process. Their friendship, wisdom, guidance, and support during this journey has led me to where I am today. I'd

also like to thank the members of the lab currently furthering our work as well as those that have moved on, for spending the majority of their lives here with me. We worked together, laughed together, complained together and celebrated together. We've written protocols, manuscripts, and book chapters together. From the TA office to Hayden's lab to temp space to other temp space to our new lab, I appreciate every day I was able to work with and learn from you (even if I could be a little difficult sometimes). For this, I must thank Grace O'Connell, Mike Albro, Sevan Oungoulian, Brian Jones, Alex Cigan, Bob Nims, Krista Durney, Adam Nover, Sonal Sethi, Amy Silverstein, Eben Estell, and Rob Stefani. I have also had the privilege of working with several brilliant undergraduate researchers, graduate researchers, and orthopedic residents, each of whom has helped teach me how to be a better listener, mentor, and team member.

I'd like to thank my family and friends, who still don't really know what I've been doing these past five and a half years, but have been incredibly supportive none-the-less. Their encouragement and unjustified admiration have kept me grounded and provided perspective when I needed it most.

Lastly, I am most grateful to have had Marci Elpers by my side during this journey. She read my abstracts and manuscripts and inspired me to be a better lab mate, researcher, and friend. Although I rarely made it home on time and often worked late into the night, she was always my biggest cheerleader and a radiant reminder of why I was on this journey. For that, I owe her everything.

To my great grandfather, an illegal immigrant and brick-layer.
To Papa Roach, a delivery man and the son of a sharecropper.
To my parents,
for always pushing me higher,
but never letting my feet leave the ground.

Chapter 1 Introduction

Articular cartilage provides a dynamic surface that bears load while providing a smooth surface for joint articulation. When damaged, however, this tissue exhibits a poor capacity for repair, lacking the lymphatics, cellularity, and vasculature necessary for remodeling. With time, therefore, the progressive loss of articular cartilage leads to joint paint, dysfunction, and disruption in activities of daily living. Significant research efforts are directed at developing tissue-engineered cartilage as a cell-based approach to articular cartilage repair. Clinical success, however, will depend on the ability of tissue-engineered cartilage to survive and thrive in a milieu of harsh mechanical and chemical agents. In an effort to address this environment, the work presented in this dissertation aims to (1) further characterize and (2) optimize the response of tissue-engineered cartilage to physical loading and chemical insult, as well as (3) provide a clinically relevant strategy for joint resurfacing. Together, this holistic approach looks to maximize the chances for *in vivo* success of tissue-engineered cartilage.

Guiding this work, the following global hypothesis and specific aims are presented, accompanied by an assertion of the significance of this work. An introduction to cartilage biology and repair is followed by a brief review of the literature pertinent to the specific aims outlined.

1.1 Global hypothesis and specific aims

The research presented in this dissertation is comprised of three interdependent aims that work toward the central goal of facilitating successful replacement of damaged articular cartilage (Figure 1.1).

In developing a biofidelic tissue prepared for the mechanical and chemical environment *in vivo*, this work is guided by the following global hypothesis:

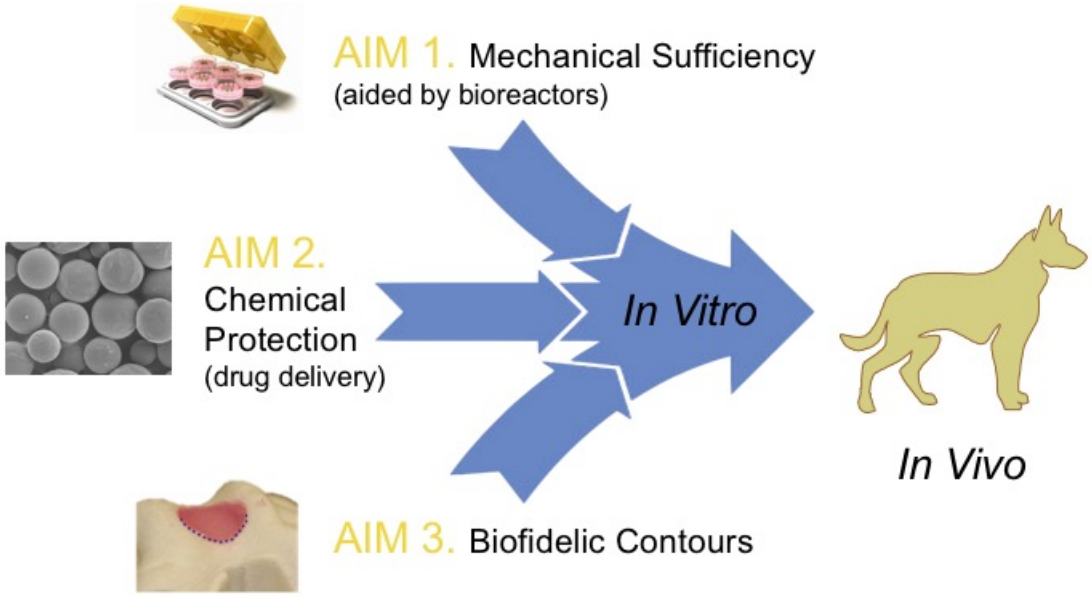

Figure 1.1: Schematic depicting the current paradigm for cartilage tissue engineering, including a canine preclinical model of OA.

Global Hypothesis: A combination of 1) optimized dynamic compressive loading and the 2) incorporation of polymer microspheres that release dexamethasone from within cell-seeded hydrogel constructs will prepare and protect constructs from the deleterious effects of mechanical and chemical exposure in the diarthrodial joint, allowing for improved cartilage repair in an unwelcoming environment.

The following specific aims outline the work necessary to investigate this global hypothesis.

Specific Aim 1A) Using a custom-designed microscope based device, assess the tensile and compressive properties of tissue engineered cartilage following culture under free-swelling and dynamic loading (displacement-controlled) conditions. Evaluate the relationships between biochemical content, culture conditions, and mechanical properties.

Tension compression nonlinearity (TCN) is a phenomenon that describes articular cartilage's complex response to tensile and compressive forces. A higher stiffness in tension versus compression allows cartilage to resist radial expansion under axial compressive loading, resulting in increased fluid pressurization and dynamic stiffness (Huang *et al.* , 2001; Soltz & Ateshian, 2000; Soulhat *et al.* , 1999). While this phenomenon has been well characterized in native cartilage explants, little is known as to the existence and characterization of TCN in engineered cartilage. These studies aim to complement native explant studies (Chahine *et al.* , 2004) and provide insight to the impact of dynamic compressive loading on TCN in engineered cartilage. Use of an osmotic swelling technique in combination with a microscope-based unconfined compression device allows for TCN characterization in a single sample (Kelly *et al.* , 2009; Chahine *et al.* , 2004; Wang *et al.* , 2001). By elucidating the impact of displacement-controlled dynamic loading on TCN in engineered cartilage, this work aims to quantify osmotic tissue swelling, with potential implications for the diagnosis of cartilage matrix damage.

Specific Aim 1B) Apply physiologic load-controlled protocols to tissue engineered cartilage using a mechanoactive tissue engineering (MATE) bioreactor. Optimize loading protocols for engineered tissues.

Displacement-controlled dynamic loading of tissue-engineered cartilage has traditionally employed systems with single actuators that allows for simultaneous and interdependent stimulation of batch tissues (Mauck *et al.* , 2003; Aufderheide & Athanasiou, 2006; Cassino *et al.* , 2007). While this allows for physiologic loading (Park *et al.* , 2004), high testing volume, and has proven to aid in the development of tissues with native mechanical properties (Lima *et al.* , 2007), this approach ignores the reality that not all tissues are of equal thickness or stage of development (Davisson *et al.* , 2002; Park *et al.* , 2004). The resulting divergences in strain across variable samples

negatively impacts tissue development (Butler *et al.* , 2009). Single station, load-controlled systems have been used in the past to investigate native explant cartilage (Park *et al.* , 2004), however, the application of independent, load-controlled deformational loading to engineered tissues is, as of yet, unexplored. By implementing the MATE bioreactor, a commercially available device, this work looks to investigate the impact of physiologic, load-controlled compressive loading on the development of tissue-engineered cartilage, and use these results to inform the optimization of future loading protocols.

Specific Aim 2A) Perform in vitro experiments to characterize DEX release profile from polymer microspheres comprised of FDA-approved poly(lactic-co-glycolic) acid (PLGA). Compare the growth of chondrocyte-seeded agarose constructs (with media supplementation of DEX) with the same tissues impregnated with DEX-loaded microspheres (without exogenous DEX). Evaluate mechanical and biochemical properties.

Specific Aim 2B) Perform parallel studies but with culture medium further supplemented with interleukin-1 (IL-1) following 4 weeks of construct development and analyze culture medium.

Inflammatory cytokines, elevated with trauma or OA (Irie *et al.* , 2003; Tsuchida *et al.* , 2014), may contribute to inferior outcomes for cartilage repair (Vanlauwe *et al.* , 2011; Filardo *et al.* , 2013; Saris *et al.* , 2003; Ozsoy *et al.* , 2009) as well as hamper cartilage regeneration (Yang *et al.* , 2006; Beekhuizen *et al.* , 2013; Rodrigo *et al.* , 1995). To this end, preliminary data suggests that early inhibition of pro-inflammatory cytokines may improve clinical outcomes (Morisset *et al.* , 2007; Elsaid *et al.* , 2015; Olson *et al.* , 2014). Dexamethasone, a critical element for cultivating engineered cartilage with native properties (Florine *et al.* , 2012), is demonstrated *in vitro* to prevent cartilage tissue degradation in the presence of pro-inflammatory cytokines (Lu *et al.* , 2011) and is used *in vivo* to suppress inflammation and provide joint pain relief. Used for joint pain relief, however, dexamethasone, and glucocorticoids more broadly, are used at high concentrations, thus hampering the immune system systemically and altering the function of disease-fighting leukoctyes. As an alternative, recent work has exploited the use poly(lactic-*co*-glycolic acid) (PLGA) systems

for the delivery of anti-inflammatory drugs, and glucocorticoids, specifically (Galeska *et al.* , 2005; Dang *et al.* , 2011; Tang *et al.* , 2010; Bae *et al.* , 2010; Hickey *et al.* , 2002b; Hickey *et al.* , 2002a; Rubin *et al.* , 2009; Kelmendi-Doko *et al.* , 2014). In fact, previous work suggests that the continuous, low dose administration of glucocorticoids provides enhanced inhibition of inflammation in OA. In an effort to exploit the anabolic and chondroprotective properties of dexamethasone, this work focuses on (A) the fabrication of a PLGA drug delivery system for dexamethasone and its application to tissue-engineered to cartilage to support growth and (B) protect the tissue from the deleterious effects of pro-inflammatory cytokines, thus preparing the engineered tissue for the harsh environment *in vivo*.

Specific Aim 3: Develop methodology to digitize the contours of the distal femur, including both the articular surface and the subchondral bone. Using digital model, reconstruct and prototype casting device that allows for the production of large cartilage surface areas while preserving joint congruities. Finally, demonstrate the ability to use chondrocyte-laden agarose to appropriately fill the topographies of the casting device.

For patients with large cartilage defects (>10 cm^2), fresh osteochondral allografts are often the only suitable treatment (Bugbee, 2002). The technical demands associated with restoring congruency of the articular surface pose a significant challenge to the success of this surgery. A seamless transition between graft and host tissue requires matching of the donor joint size to provide grafts with similar anatomical surface contours. The limited supply of suitable cartilage grafts to meet this clinical demand has prompted recent attempts at developing cell-based therapies for cartilage repair (Lima *et al.* , 2004; Vunjak-Novakovic *et al.* , 1999; Buckley *et al.* , 2012; Pazzano *et al.* , 2000). Unlike previous attempts at developing cell-based therapies of scale, it may be more clinically relevant to fabricate anatomically defined osteochondral constructs for large defects. Motivated by this clinical need, the work introduced here aims to create biofidelic engineered tissues to restore proper load distribution and allow for functional cartilage repair.

The *in vitro* studies outlined above will provide the groundwork for future *in vivo* studies in a preclinical model of OA to assess the efficacy of our functional tissue engineering strategy for

articular cartilage repair.

1.2 Significance

Articular cartilage provides a surface that bears dynamic loads and allows for smooth joint articulation. Following injury, however, cartilage's inability to assess, degrade, and rebuild the extracellular matrix poses a major challenge to cartilage health long-term. Osteoarthritis, the most common disease afflicting synovial joints, is characterized by focal and progressive loss of cartilage and is normally defined by pain, swelling, and stiffness in the joints. An estimated 27 million Americans age 25 and older suffer from OA. This number is projected to rise to more than 67 million by 2030 (Hootman & Helmick, 2006) with total costs estimated at nearly $90B a year (Leigh *et al.* , 2001). Further, 25 million of these people, or 9.3% of US adults, are projected to experience activity limitations as a result of OA (Leigh *et al.* , 2001). These trends are driven in part by an increasing number of joint injuries in young patients (e.g. tear of the ACL) (Soprano, 2005), who have a 50% chance of developing radiographic indications of OA within two decades of the injury (von Porat, 2004; Lohmander *et al.* , 2007; Englund *et al.* , 2003). In these patients, reconstruction of the knee following injury often focuses only on joint stabilization, failing to address the concomitant cartilage damage (e.g. release of type 2 collagen fragments (Lohmander *et al.* , 2003) that plays a critical role in the development of OA (von Porat, 2004; Lohmander *et al.* , 2003; Lohmander *et al.* , 2007). Patients that develop cartilage lesions larger than 2 cm^2may require therapeutic intervention, but few widely-applicable and successful approaches are available that provide the inherent benefits (mechanical function and articular contour) afforded by native tissue (Hangody & Füles, 2003; Knutsen *et al.* , 2004; Moseley *et al.* , 2010). To meet this need, extensive research has been conducted to develop a cell-based therapy for cartilage repair, often including the use of cultured cells inside a three-dimensional scaffold (Lima *et al.* , 2004; Mauck *et al.* , 2002; Mauck *et al.* , 2000a; Pazzano *et al.* , 2000; Freed *et al.* , 1993; Vunjak-Novakovic *et al.* , 1996; Obradovic *et al.* , 1999).

In an effort to prepare these scaffolds for the mechanical loads experienced in the knee, work involving mechanical stimulation has been done to generate engineered tissues with functional mechanical properties (i.e., equilibrium moduli near native values) (Mauck *et al.* , 2000a; Mauck *et al.* , 2003; Lima *et al.* , 2007; Huang *et al.* , 2009; Huang *et al.* , 2010). Unlike native explant cartilage (Wang *et al.* , 2002b; Chahine *et al.* , 2004), however, a comprehensive understanding of how these

engineered tissues respond to mechanical stimulation *in vitro*, and how that may impact function *in vivo*, has yet to be elucidated. Part I of this dissertation investigates the complex compressive and tensile forces at play within engineered cartilage and in response to mechanical stimulation (Chapter 2). Chapter 3 explores, for the first time, the application of load-controlled, independent 'batch' loading for tissue-engineered cartilage, making possible extended cultivation and physiologic stimulation of tissue-engineered cartilage meant for use in the clinic.

The studies described in Part II of this dissertation aim to develop strategies for fostering growth and providing chondroprotection for tissue-engineered cartilage. The harsh inflammatory environment of the knee presents articular cartilage, and cartilage replacements, with a milieu of pro-inflammatory cytokines and degradative enzymes. Clinical strategies, as well as those *in vitro*, have utilized glucocorticoids, and in particular dexamethasone, to quell these inflammatory agents. Long-term success of tissue-engineered cartilage in patients, however, mandates a minimalist strategy that maintains the beneficial aspects of steroid use while limiting the negative side effects. Chapter 3 details the development of a drug delivery system that aims to provide prolonged, low-dose concentrations of dexamethasone. These microparticles are then employed in Chapter 4, investigating the usefulness of this approach in cultivating mechanically and biochemically sufficient engineered tissues capable of defending themselves against physiologic levels of pro-inflammatory cytokine.

Part III of this dissertation describes efforts to ensure effective translation of tissue-engineered cartilage strategies to the clinic. While cartilage allografts, the gold standard for repair of large focal defects, are in short supply, the importance of contour matching for positive clinical outcomes of cartilage replacements remains paramount. Using a generalizable approach, and widely-applicable technologies, Chapter 5 introduces a strategy for modeling, digitizing, and recreating biofidelic tissue-engineered osteochondral constructs.

Together, these results recommend the synergistic combination of dynamic loading, dexamethasone-loaded microspheres, and biofidelic curvatures to produce clinically-sized osteochondral constructs for the successful treatment or prevention of OA.

1.3 Background

1.3.1 Articular cartilage biology, structure, and function

Articular cartilage is the dense, white connective tissue found at the ends of long bones and, in particular, in diarthrodial joints. Comprised of chondrocytes, water, and a matrix macromolecular framework, cartilage derives its form and mechanical properties from its matrix. This extracellular matrix (ECM) consists of two components: a mobile interstitial fluid phase (mostly water) and a solid matrix (consisting of primarily type II collagen fibrils and proteoglycans) (Buckwalter, 2004a). Proteoglycans, occupying 25-35% of the dry weight of cartilage, are lined with negatively-charged (SO_3^- and COO^-) glycosaminoglycan (GAG) side chains that create a high fixed-charge density in the tissue (Mow *et al.* , 1984; Mow *et al.* , 1998; Mow & Lai, 1990). This ion gradient attracts mobile cations and subsequently, interstitial water, into the tissue in an effort to maintain electroneutrality. Collagen, comprising ~60% of the dry weight of cartilage, provides a dense fibrillar network that resist expansile forces created within the tissue (Setton *et al.* , 1998). The resulting Donnan osmotic pressure from GAG concentration swells the tissue against this constraining fibrillar collagen framework, thus imparting cartilage with its dynamic mechanical properties. To maintain this complex extracellular structure, chondrocytes, which make up only 1% of the tissue volume in mature adults (Stockwell, 1967), actively synthesize and assemble appropriate types and amounts of macromolecules into this highly ordered framework.

The complexity of cartilage is further evident from the changes in tissue composition and organizational structure observable through the depth of the tissue (Guilak *et al.* , 1995). From a sagittal cross-section, articular cartilage is classified into blurred zones: the superficial (SZ), middle (MZ), and deep (DZ) zones (Sophia Fox *et al.* , 2009; Buckwalter, 2004a). The SZ is the thinnest zone of articular cartilage. Chondrocytes in this zone synthesize a matrix high in collagen and low in proteoglycans, aligning the collagen fibrils in a dense network parallel to the joint surface. The MZ contains the highest concentration of proteoglycan in the tissue (Buckwalter, 2004a) and large-diameter collagen fibrils, aligned obliquely to the joint surface (Sophia Fox *et al.* , 2009). In the deep regions of the MZ, and transitioning into the DZ, collagen fibrils begin to orient themselves perpendicularly to the joint surface and chondrocytes begin to become hypertrophic as collagen fibrils anchor into the subchondral bone and the tissue becomes calcified.

The depth-dependent composition and organization of cartilage define its unique mechanical characteristics. The interplay of collagen and GAG in the SZ and DZ gives rise to cartilage's unique non-linear transition from tension to compression (Chahine *et al.* , 2004), where the tensile modulus of the tissue (E_{+Y}=3-6 MPa, (Kempson *et al.* , 1968; Williamson *et al.* , 2003b; Williamson *et al.* , 2003a)) is over an order of magnitude higher than the compressive modulus (E_{-Y}=0.1-1 MPa, (Wang *et al.* , 2002a; Wang *et al.* , 2002b; Park *et al.* , 2004)). This relationship is critical to the proper function of articular cartilage as a dynamic load bearing tissue. A higher stiffness in tension versus compression allows cartilage to resist radial expansion under axial compressive loading, resulting in increased fluid pressurization and dynamic stiffness (Huang *et al.* , 2001; Soltz & Ateshian, 2000; Soulhat *et al.* , 1999). This plays out following instantaneous loading, when fluid cannot exude rapidly from within the dense ECM, causing initial deformation to be nearly isochoric as fluid pressures rise considerably to resist the compressive load. In order to distribute and absorb loads in a manner similar to native cartilage, engineered cartilage should exhibit similar properties of tension-compression nonlinearity.

1.3.2 Articular cartilage injury and repair

OA, the most prevalent form of joint disease, is characterized by pain and dysfunction. While the etiology of the disease is largely unknown, certain events are known to expedite its development. Traumatic injury, via ligament or meniscal tear, leads to early-onset osteoarthritis in nearly 50% of injured patients (von Porat, 2004; Lohmander *et al.* , 2007; Englund *et al.* , 2003). This is due in part to repair strategies that focus largely on joint stabilization in an attempt to restore normal joint kinematics, ignoring concomitant, and potentially more egregious, injuries to the chondral surface (e.g., release of type 2 collagen fragments (Lohmander *et al.* , 2003)). In fact, the disruption of the macromolecular framework of the matrix, manifest in the appearance of fibrillation, is often the first stage of disease (Eyre & Wu, 2005; Farquhar *et al.* , 1996; Buckwalter & Brown, 2004; Buckwalter, 2004b). This leads to a decrease in proteoglycan concentration and may allow further swelling of the tissue. Importantly, disruption of the matrix leads to an increase in permeability, and thus water content, decreasing the stiffness of the matrix and the ability of the tissue to support loading. The progressive softening of the matrix increases the vulnerability of the tissue to additional mechanical damage with time (Bank *et al.* , 2000).

Chondrocytes are quickly able to detect this macromolecular event through alterations in its extracellular environment. In an attempt to repair the injured tissue, chondrocytes begin producing a series of anabolic and catabolic factors, including matrix constituents, in an effort to replace the lost tissue (Martin & Buckwalter, 2000; Martin *et al.* , 2002; Buckwalter, 2004a; Buckwalter, 2004b). With continued mechanochemical insult, however, and with a limited capacity for repair, the balance between anabolic (TGF-β, IGF-1, TIMP-3) and catabolic factors (IL-1, TNF-α, IL-6, IL-17, ADAMTS-4,5, MMP-13 (Goldring & Goldring, 2004; Mueller & Tuan, 2011)) begins to shift in favor of degradation. For this reason, any cell-based therapy for cartilage repair must consider the impact of pro-inflammatory cytokines on the health of the tissue.

The combined effects of abnormal kinematics and a harsh chemical environment often leads to progressive loss of articular cartilage and a diminished anabolic and proliferative response in chondrocytes (Mankin & LIPPIELLO, 1970; Mankin, 1974; Mankin *et al.* , 1981). With time, focal areas of damage grow until the degradation is significant enough that the joint space has collapsed and bone-on-bone articulation causes disabling pain and discomfort. Current strategies for repair, however, are dependent on the joint involved, the size, location and severity of the defect.

For focal articular cartilage lesions ($<$2 cm^2), minimally invasive reconstructive surgical approaches including microfracture (Steadman *et al.* , 2001), autograft transfer via periosteal grafts (O'Driscoll *et al.* , 2001), osteochondral autograft transfer system or mosaicplasty (Hangody *et al.* , 1997), and autologous chondrocyte implantation (Brittberg *et al.* , 1994) are currently utilized. While addressing symptoms of pain and providing improvements in function, these strategies have not shown long-term durability, are often limited by tissue availability, and in the case of osteochondral grafts, can result in suboptimal tissue properties (Ahmad *et al.* , 2001) and significant donor site morbidity (Lee *et al.* , 2000a; Lee *et al.* , 2000b). For larger lesions, greater than 10 cm^2, when articular cartilage loss has distorted the morphology of the condyle, fresh osteochondral allografts are ideal (Bugbee, 2002). The technical demands associated with this procedure (i.e., attaining a flush fit of the graft with the surrounding host cartilage tissue), however, and the limited supply of suitable grafts, necessitate the development of alternative strategies for repair, including tissue-engineered constructs of cultured cells in three-dimensional scaffolds (Lima *et al.* , 2004; Mauck *et al.* , 2000a; Pazzano *et al.* , 2000; Vunjak-Novakovic *et al.* , 1999). For engineered constructs to functionally bear the loads experienced *in vivo*, these tissues must capture the natural topology

of the articular surface to fully recapitulate normal contact geometry and load distribution profiles across the joint (Hung *et al.* , 2003; Cooney & Chao, 1977; Ateshian *et al.* , 1992; Ateshian *et al.* , 1995; Eberhardt *et al.* , 1990; Huberti & Hayes, 1984). While progress has been made, there is currently no tissue-engineered product able to meet these design challenges, thus warranting further investigation.

1.3.3 Functional tissue-engineered articular cartilage

Functional cartilage tissue engineering as a strategy for the repair of injured cartilage tissue relies on the use of an appropriate scaffold, cell source, and exogenous factors to foster the growth, *in vitro*, of a tissue replacement capable of withstanding the mechanochemical demands of the joint environment (Butler *et al.* , 2000). In this effort, our laboratory and others have modified this paradigm, incorporating aspects of modern tissue culture techniques and research trends in order to produce engineered cartilage with functional properties. Central to this approach are three important factors: 1) scaffold type, 2) cell source, and 3) exogenous (mechanical and/or chemical) factors.

1.3.3.1 Scaffold choice While scaffolds are not required for laboratory-based cartilage formation (Huang *et al.* , 2016b; Huang *et al.* , 2016a; Elder *et al.* , 2011; Bhumiratana *et al.* , 2014), hydrogels as a scaffold for cartilage growth offer baseline properties similar to those observed in other soft hydrated tissues (i.e. high water content) (Smetana Jr & Vilím, 1991). Polymers that are capable of forming hydrogels stem from natural (e.g., hyaluronic acid (Burdick & Prestwich, 2011), alginate (Bonaventure *et al.* , 1994), chitosan, chondroitin sulfate, collagen, agarose, silk (Wang *et al.* , 2005)) or synthetic (e.g. poly(lactide-*co*-glycolide), poly(ethylene glycol) (Hwang *et al.* , 2010), poly(vinyl alcohol)) origins. Each hydrogel carries advantages and disadvantages and are appropriate for applications depending on the intended outcome.

Agarose, a hydrophilic linear polysaccharide derived from red seaweed, has been used in applications such as gel electrophoresis (Hammarlund & Rising, 1953), 3D printing (Campos *et al.* , 2012), and for the creation of complex curved shapes (Hung *et al.* , 2003). A low-melt polymer, agarose (type VII) allows for the encapsulation of cells prior to scaffold solidification (Lima *et al.* , 2007; Mauck *et al.* , 2000b), making it ideal for certain tissue engineering applications including the repair

of neural tissues (Khaing & Schmidt, 2012), skin (Gaspar *et al.* , 2011), and for bone regeneration (Pandit *et al.* , 2013). Much like native cartilage, agarose displays strain-dependent hydraulic permeability (Buschmann *et al.* , 1995), exhibits 'pre-stress', and contains a network of pores that at once allows for nutrient flux and retains newly synthesized extracellular proteins (Pernodet *et al.* , 1997; Ng *et al.* , 2005).

For these reasons, agarose has been extensively investigated for use in cartilage tissue engineering. Early work on chondrocyte response to mechanical load utilized agarose for long-term suspension cultures (Benya, 1982; Buschmann *et al.* , 1995; Lee & Bader, 1995), as the uncharged material promotes and maintains the chondrocyte phenotype. This work demonstrated the development of the pericellular matrix and, therefore, the ability to transduce mechanical signals to the embedded chondrocytes (Buschmann *et al.* , 1995). Recent efforts in our laboratory have utilized the above properties to develop tissue-engineered cartilage with the most reproducible and robust growth to date (Lima *et al.* , 2007; Roach *et al.* , 2016). Clinically, agarose is being used as a co-polymer with alginate, in combination with autologous chondrocyte implantation, in a cartilage repair product in Europe and has reported good outcomes at a 2-year follow up (Selmi *et al.* , 2007; Selmi *et al.* , 2008).

1.3.3.2 Cell source Early studies in cartilage tissue engineering used primary chondrocytes isolated directly from native cartilage (Buschmann *et al.* , 1995; Benya, 1982). These fully differentiated chondrocytes ensure extracellular matrix synthesis similar to that of native tissue. The number of cells required for cartilage tissue engineering, however, surpasses the level found in available adult or juvenile primary cartilage, thus requiring the expansion *in vitro* of cellular populations. To prevent dedifferentiation (Francioli *et al.* , 2007; Benya, 1982) of these cells during expansion in 2D, a cocktail of growth factors can be added to the culture medium to promote and maintain the chondrocyte phenotype. This is especially critical for adult cells that are inherently less biosynthetically active (Adkisson *et al.* , 2010; Barbero *et al.* , 2003; Barbero *et al.* , 2004; Smeriglio *et al.* , 2015) and therefore must be 'primed' for reintroduction into a 3D scaffold (Sampat *et al.* , 2011) before they can be used effectively at scale.

In addition to their use as primary isolates, a number of studies have expanded juvenile bovine chondrocytes for use in cartilage tissue engineering applications. An ideal candidate for *in vitro*

work, these chondrocytes are plentiful, robust and provide a reliable experimental model for exploring other mechanical and chemical properties of engineered cartilage. Moreover, these chondrocytes synthesize extracellular matrix with near native mechanical and biochemical properties (Lima *et al.* , 2007). For the purposes of our work, these cells allow for stimulation via dynamic compressive loading (Mauck *et al.* , 2000b; Buschmann *et al.* , 1999) as well as stimulation through anabolic and catabolic (Byers *et al.* , 2008; Mauck *et al.* , 2003; Lima *et al.* , 2008a) chemical factors. While suitable for *in vitro* studies, translatability of this approach relies on the use of clinically available cell sources, namely adult chondrocyte or stem cell populations.

As an alternative to adult chondrocytes, adult stem cells are a widely investigated cell source for cartilage tissue engineering (Tuan *et al.* , 2002; Guilak *et al.* , 2004; Caplan, 2007; He *et al.* , 2009). Adult stem cells can be isolated from synovial tissue (Li *et al.* , 2011; Pei & He, 2012), bone marrow aspirates (Pittenger *et al.* , 1999), adipose tissue (Estes *et al.* , 2006a; Estes *et al.* , 2006b; Estes *et al.* , 2008), and other mesenchymal sources. A readily available cell source, adult stem cells can easily be obtained and expanded *in vitro*. Via application of a growth factor cocktail similar to that used for juvenile and adult chondrocytes, adult stem cells can be pushed toward the chondrocyte lineage. While expressing chondrocyte markers, these differentiated cells produce ECM that underperforms native properties.

In this dissertation, for the reasons discussed above, both juvenile bovine chondrocytes, adult canine chondrocytes, and adult human chondrocytes were employed. Juvenile bovine chondrocytes allow us to investigate the impact of chemical cues on the matrix composition of mechanically robust engineered cartilage. The use of canine and human chondrocytes brings clinical application to the fore, resulting in data that is directly translatable to what might be expected *in vivo*.

1.3.3.3 Exogenous cell culture conditions In addition to a chemically defined, serum free culture medium (Bian *et al.* , 2009a; Byers *et al.* , 2008), joint loading is critical for normal maintenance of articular cartilage. This is evidenced by studies demonstrating the impact of mechanical load on the composition of the extracellular matrix and the biosynthetic activity of resident chondrocytes (Gray *et al.* , 1988; Guilak *et al.* , 1994; Buschmann *et al.* , 1999; Torzilli *et al.* , 1997; Lee & Bader, 1997) in cartilage explant cultures. Static compressive loads (0.001-3 MPa) have been shown to cause a decrease in proteoglycan synthesis and increase in release from the ECM to the

medium (Gray *et al.* , 1988), while cyclic loading conditions have been shown to stimulate synthesis and incorporation of proteoglycans (Buschmann *et al.* , 1999; Ng *et al.* , 2009). Similarly, mechanical loading protocols have been applied to tissue-engineered cartilage and have been found to elicit biosynthetic and gene expression changes similar to articular cartilage explants (Buschmann *et al.* , 1995; Davisson *et al.* , 2002; Lo *et al.* , 2001; Lee *et al.* , 2003).

Deformational loading of tissue-engineered cartilage has traditionally employed devices with single actuators that stimulate tissues, in batches, simultaneously and interdependently (Mauck *et al.* , 2000b; Aufderheide & Athanasiou, 2006; Cassino *et al.* , 2007). This allows for physiologic loading (Park *et al.* , 2004), high testing volume, and has proven to aid in the development of tissues with native mechanical properties (Lima *et al.* , 2007).

The alternative to displacement-controlled loading, an approach that may not result in uniform strain (Butler *et al.* , 2009) across a sample population, force-controlled stimulation has been limited by the technical necessity to independently load each sample (Waldman *et al.* , 2006). A recently developed system allows for the continuous, independent, and force-controlled stimulation of up to 6 samples, making use of this approach practical for tissue-engineering studies (Lujan *et al.* , 2011).

Part I

Physiologic Dynamic Loading

Chapter 2 Tissue-engineered articular cartilage exhibits tension-compression nonlinearity reminiscent of the native cartilage

2.1 Abstract

The current set of studies examines the tensile and compressive properties of cylindrical chondrocyte-seeded agarose constructs over different developmental stages through a novel method that combines osmotic loading, video microscopy, and uniaxial unconfined compression testing. This method was previously used to examine tension–compression nonlinearity in native cartilage. Further, this work investigates the impact of dynamic loading (DL) on adult canine chondrocyte cartilage constructs and its ability to better prepare engineered tissues for the harsh mechanical environment *in vivo*.

Engineered cartilage, cultured under free swelling (FS) or dynamically loaded conditions, was tested in unconfined compression in hypertonic and hypotonic salt solutions. The apparent equilibrium modulus decreased with increasing salt concentration, indicating that increasing the bath solution osmolarity shielded the fixed charges within the tissue, shifting the measured moduli along the tension–compression curve and revealing the intrinsic properties of the tissue. With this method, we were able to measure the tensile (401 ± 83 kPa for FS and 678 ± 473 kPa for DL) and compressive (161 ± 33 kPa for FS and 348 ± 203 kPa for DL) moduli of the same engineered cartilage specimens. These moduli are comparable to values obtained from traditional methods, validating this technique for measuring the tensile and compressive properties of hydrogel-based constructs. This study shows that engineered cartilage exhibits tension–compression nonlinearity reminiscent of the native tissue, and that dynamic deformational loading can yield significantly higher tensile properties.

2.2 Introduction

Native articular cartilage exhibits low compressive Young's modulus (E_{-Y}; 0.1–1 MPa) (Wang *et al.* , 2002b; Wang *et al.* , 2002a; Park *et al.* , 2004) relative to its high tensile Young's modulus (E_{+Y}; 3–6 MPa) (Kempson *et al.* , 1968; Williamson *et al.* , 2003a; Williamson *et al.* , 2003b), which regulates the mechanical response of cartilage in unconfined compression (Cohen *et al.* , 1998; Soulhat *et al.* ,

1999; Soltz & Ateshian, 2000; Huang *et al.* , 2001; Huang *et al.* , 2003; Chahine *et al.* , 2004) and in contact configurations (Krishnan *et al.* , 2004). Previous studies indicate that a high E_{+Y} combines with interstitial fluid pressurization to produce an elevated dynamic compressive modulus (G*) at least 6x greater than E_{-Y} (Soltz & Ateshian, 2000; Park *et al.* , 2003; Park & Ateshian, 2006). This mechanism arises because the high E_{+Y} of cartilage restricts lateral expansion of the tissue upon axial compression. Since the interstitial fluid cannot exude rapidly, the initial deformation must be nearly isochoric, occurring only if the interstitial fluid pressurizes considerably to help resist the compressive load. In order to distribute and absorb loads similar to native cartilage, engineered cartilage should exhibit similar tension–compression nonlinearity (TCN). Previous studies have demonstrated that chondrocyte seeded agarose constructs are capable of achieving native values for E_{-Y} and glycosaminoglycan (GAG) content (Kelly *et al.* , 2006; Bian *et al.* , 2009a; Bian *et al.* , 2009b; Bian *et al.* , 2010a; Natoli *et al.* , 2009a; Natoli *et al.* , 2009b). While E_{-Y} and E_{+Y} have been independently analyzed previously, the role of TCN in developing engineered cartilage has not been addressed. Therefore, we adapted a method used previously to examine TCN in native cartilage (Chahine *et al.* , 2004), which permits determination of E_{+Y} and E_{-Y} from a single specimen. Using this technique, E_{+Y} and E_{-Y} were found to be similar to values obtained from direct measurements using more conventional methods (Huang *et al.* , 2001; Huang *et al.* , 2003; Huang *et al.* , 2005; Wang *et al.* , 2002a; Wang *et al.* , 2002b; Williamson *et al.* , 2003b; Williamson *et al.* , 2003a; Park *et al.* , 2004). This technique uses osmotic swelling to place the sample in an initial state of tension. Small compressive displacement increments are then applied and the resultant loads are measured during the tissue's transition from tensile to compressive strains.

The underlying principle behind this technique stems from the fact that hydrated tissues possessing a fixed charge density swell and stiffen under hypotonic loading. Conversely, these tissues shrink and become softer under hypertonic loading via concomitant changes in Donnan osmotic pressure (Maroudas, 1976; Lai *et al.* , 1991; Wang *et al.* , 2002a; Wang *et al.* , 2002b; Lima *et al.* , 2007). Therefore, compressing swollen tissues allows for measurement of E_{+Y} when the applied compressive strain is smaller than the true tensile swelling strain of the solid matrix (Figure 6.5E). As the strain increases, the measured response yields E_{-Y}.

The objective of this study is to determine the TCN in engineered cartilage grown under free swelling (FS) or dynamically loaded (DL) cultures, and we hypothesize that DL will improve both

E_{+Y} and E_{-Y} of engineered cartilage compared to FS controls. Therefore, we acquired a spectrum of engineered cartilage moduli from tension to compression using compressive loading in the presence of osmotic swelling and report for the first time E_{+Y} and E_{-Y} of the same engineered cartilage specimen.

2.3 Materials and methods

2.3.1 Sample preparation and tissue culturing

Articular cartilage was harvested from adult canine knee joints. Three to five joints were used and cells were pooled from all joints, as previously described (Lima *et al.* , 2007; Bian *et al.* , 2010a). Cartilage chunks were digested with 390 U/mL collagenase type VI (Sigma) for 8 h with slight agitation. Isolated chondrocytes were passaged in DMEM containing 10% FBS, 10 ng/mL PDGF, 1 ng/mL TGF-β1, 5 ng/mL FGF-2 and 1% antibiotics/antimycotics. Chondrocytes were seeded in 2% (w/v) agarose at 30 x 10^6 cells/mL and cast between parallel plates.

Cylindrical constructs (⌀ 4.0 2.3 mm) were cored and cultured in DMEM containing 50 μg/mL L-proline, 100μg/mL sodium pyruvate, 1% ITS+ premix (BD Biosciences), 100 nM dexamethasone, 1% antibiotics/antimycotics, 50 μg/mL ascorbic acid, and 10 ng/mL TGF-β3 (R&D Systems). Constructs were maintained in FS culture for 14 days. After day 14, constructs were either cultured under DL conditions or maintained under FS conditions until day 42. For DL, a sinusoidal deformation with a magnitude of 10% peak-to-peak strain at a frequency of 1 Hz (5 days/week, 3 h/day continuous) was applied (Figure 2.1), with an initial 2% tare strain.

2.3.2 Average mechanical properties

A custom unconfined compression device (Mauck *et al.* , 2000a) with rigid-impermeable loading platens and a 250 g load cell (Honeywell Sensotec) was used to assess the E_{-Y} of the whole construct at days 0, 14, 28 and 42 (n=4–11). Before each test, the construct thickness and diameter were measured, specimens were equilibrated under a 0.02 N tare load, and a 10% strain was applied at 0.05% strain/sec. E_{-Y} was calculated from the equilibrium stress and initial cross-sectional area. The average unconfined dynamic modulus (G*) was subsequently measured by superimposing a 2% sinusoidal strain at 1 Hz.

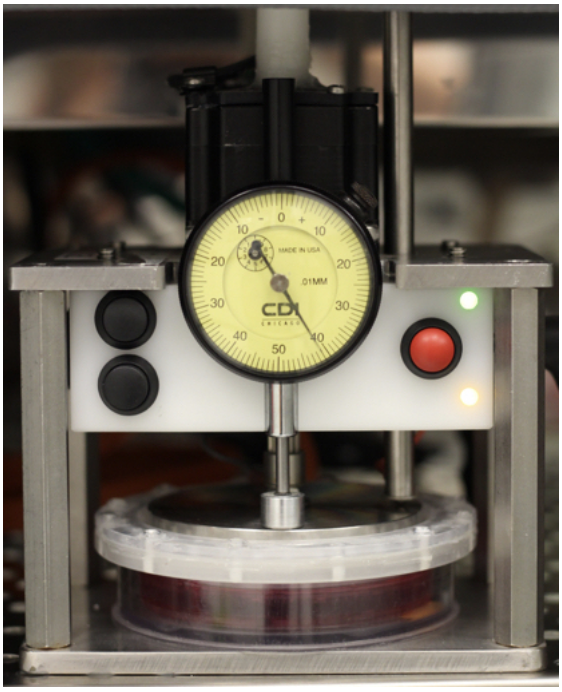

Figure 2.1: Custom device used for dynamic, displacement-controlled deformational loading.

To establish whether E_{-Y} of engineered tissue was dependent on strain, immature bovine articular chondrocytes were harvested and used to create constructs, as described above. On days 0 and 42, these constructs were used in a series of stress-relaxation tests at 5%, 10%, 15%, and 20% strains (n=5). For comparison, freshly harvested explants were also tested.

2.3.3 Direct tensile testing of agarose constructs

Acellular constructs were cast as described above to test the tensile mechanical properties of 2% (w/v) agarose. Rectangular samples were cut from the slab (length=12 mm, width=3 mm, thickness=2.34 mm, n=7). Sandpaper grips were glued to the top and bottom edge of the sample and secured in metal grips that attached to the mechanical testing device (Instron). A quasi-static ramp was applied at a rate of 0.01%/s, and load and displacement data were recorded until failure. The tensile modulus was calculated as the slope of the stress-strain curve.

2.3.4 Tension-compression analysis

A custom glass-bottom device was mounted on the stage of an inverted microscope and used to mechanically test semi-cylindrical specimens (Wang *et al.* , 2002a; Wang *et al.* , 2002b; Wang *et al.*

, 2003; Chahine *et al.* , 2004). Prior to testing, the thickness of each construct was measured, the constructs were halved, and each half was maintained in isotonic saline (Figure 6.5A). At days 0 (n=4) and 42 (n=4–6), the semi-cylindrical samples were tested in 0.015 M NaCl (hypotonic saline) to determine TCN under conditions of maximal osmotic swelling (e.g., expansion of the collagen network) or 2 M NaCl (hypertonic saline) to determine TCN under conditions where the contribution of osmotic swelling is minimal. As an additional control, acellular constructs, cast with dark blue polystyrene microspheres (1 x 10^9 microspheres/mL; 0.88 μm diameter, Bangs Laboratories), were also analyzed in hypotonic saline to measure the TCN of 2% w/v agarose (n=4). The microspheres were used solely in cell-free constructs as fudicial markers to provide optical texture for DIC.

For testing, each semi-cylindrical sample was equilibrated for 1 h in the appropriate saline solution containing LIVE/DEAD dyes (Invitrogen). The equilibrated thickness of the specimen was measured, initial images of the cross-section of the samples were acquired, and the samples were then compressed at nominal 2% strain increments, up to a final compression of 10–12% (Figure 6.5B). After each compression, samples were allowed to equilibrate for 15 min with images being acquired immediately before each subsequent compression (Figure 6.5C, D).

Optimized DIC was used to obtain accurate axial and lateral strains (Wang *et al.* , 2002a; Wang *et al.* , 2002b; Wang *et al.* , 2003; Kelly *et al.* , 2006; Chahine *et al.* , 2004). The equilibrium normal stress was calculated from the measured load and the initial cross-sectional area of the constructs. The effective incremental Young's modulus (E_{Yi}) was calculated for each compression level (Figure 6.5E). E_{+Y} was defined as the highest E_{Yi} measured under initial compression in hypotonic saline, while E_{-Y} was defined as the nearly constant E_{Yi} obtained at higher compressive strains, an average of the values in the range of 8–10% compression. The incremental Poisson's ratio (ν_i) was also calculated as the negative ratio of the axial and lateral strains. After testing, the samples were processed for histology or weighed and stored at -20°C for biochemical analysis.

2.3.5 Biochemical analysis

Samples (n=4–11) were thawed, lyophilized, and weighed dry and digested with 0.5 mg/mL proteinase K (Promega) in 50 mM Tris-buffered saline containing 1 mM EDTA, 1 mM iodoacetamide (Acros Organics). DNA content was quantified using a PicoGreen assay (Invitrogen) (McGowan *et al.* , 2002) with lambda phage DNA standards. GAG was quantified using 1,9-dimethylmethylene

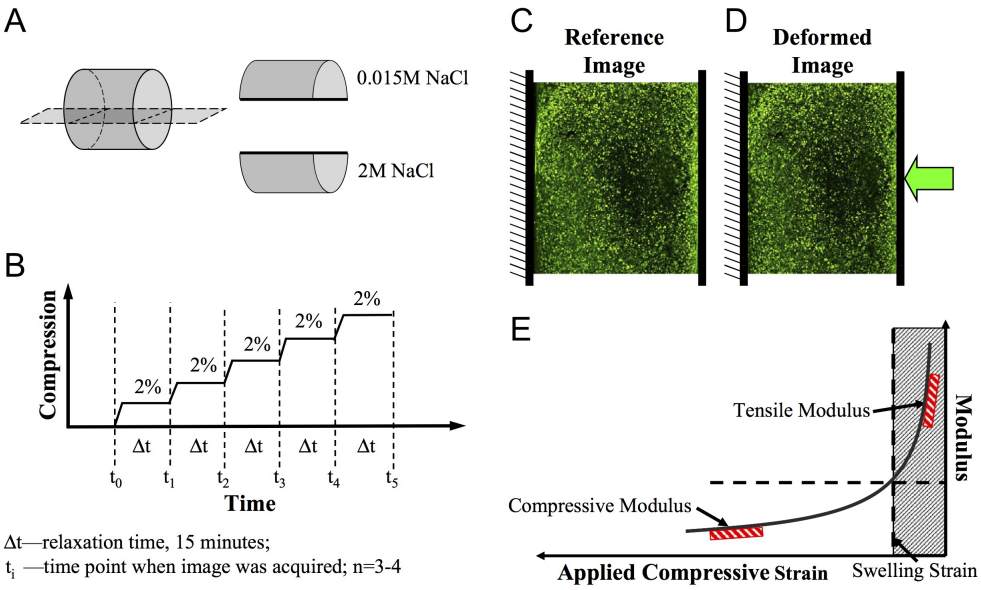

Figure 2.2: (A) Prior to osmotic testing the semi-cylindrical samples were equilibrated in the appropriate saline solution (solution A and solution B). The order of testing was rotated to prevent bias from multiple testing of the same semi-cylindrical sample. (B) For each test, the semi-cylinder was loading into the microscope testing device and compressed at 2% increment to a final compression of 10–12% and allowed to equilibrate for 15 min between each compression. Images were acquired prior to each compression. (C) and (D) Images of typical construct before (C) and after (D) compression. (E) Schematic tension–compression curve: By controlling the osmolarity of the bathing fluid we can swell or shrink a test sample along its tension–compression curve. By then applying a compressive load to a swollen construct and comparing its properties to an unswollen construct we can extract its tensile modulus under compression without special grips. Hatched region represents region where specimen is under tension.

blue (Sigma) dye-binding assay (Farndale *et al.* , 1986), with shark chondroitin-6-sulfate (Sigma) standards. The digests were hydrolyzed in 5 N HCl at 110°C for 16 h and used to quantify the total collagen content via an orthohydroxyproline (OHP) colorimetric assay (Stegemann & Stalder, 1967) with bovine OHP (Sigma) standards. Collagen content was calculated by assuming a 1–10 OHP-to-collagen mass ratio (Stegemann & Stalder, 1967). The collagen and GAG contents were normalized to the construct wet weight, dry weight and DNA content.

2.3.6 Statistical analysis

ANOVA (α=0.05) was used to determine significant differences (n=4–11). If significant changes were noted ($p<0.05$), Fisher's LSD post-hoc test was performed.

2.4 Results

2.4.1 Average tissue properties

At day 0, chondrocyte-seeded constructs exhibited strain-softening behavior between 5% and 20% compression (Figure 2.3A), where E_{-Y} decreased with increasing applied compressive strain. This behavior is typical of agarose hydrogels. By day 42, chondrocyte-seeded constructs (as well as the cartilage explants) exhibited E_{-Y} that remained nearly constant with increasing compressive strain over the tested range, indicative of a stiffer construct due to matrix elaboration and reflective of the diminished contribution of the agarose hydrogel to the overall stiffness.

E_{-Y} increased significantly over time in culture for both FS and DL constructs ($p<0.005$; Figure 2.3B, C). By day 28, E_{-Y} was significantly greater for DL constructs compared to FS controls (Figure 2.3B). DL did not yield significant differences in G* (Figure 2.3C).

The thickness, diameter, wet weight and dry weight of chondrocyte-seeded agarose hydrogels increased significantly over the 6-week culture period for both FS and DL constructs ($p<0.005$; Table 1), with significantly greater increases observed in FS constructs ($p<0.05$). Additionally, the water content decreased significantly over time in culture ($p<0.0005$); however, there were no significant differences with loading.

The biochemical content of the constructs increased significantly over time in culture ($p<0.0005$; Table 1 and Figure 2.4). The DNA content increased significantly over the 42-day culture period

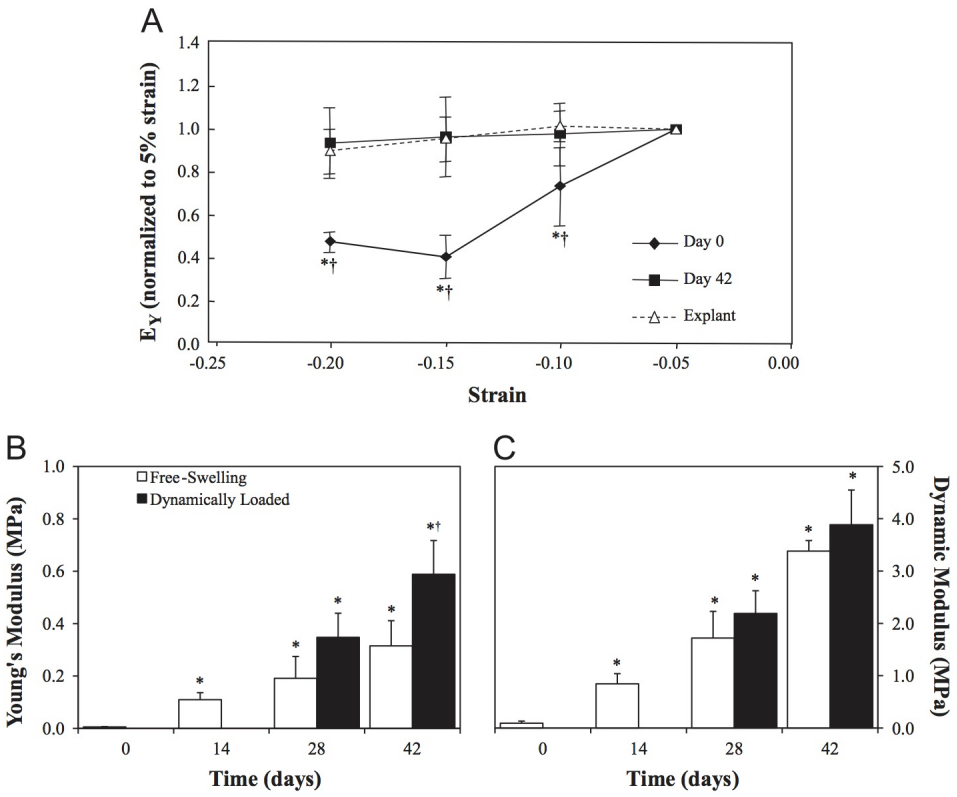

Figure 2.3: (A) The Young's modulus (E_Y) of chondrocyte-seeded constructs tested at days 0 and 42, in isotonic (0.15 M NaCl) saline at 5% strain intervals and normalized to 5% strain values. Immature bovine cartilage explants were tested as an additional control. * $p<0.05$ versus all other strain levels; † po0.05 versus day 42 constructs and cartilage explants (n=5). (B), (C) Young's modulus ((B); E_Y) and dynamic modulus at 1.0 Hz ((C); G*) of free swelling (FS) and dynamically loaded (DL) constructs (n=5–6) over a 42-day culture period. * $p<0.005$ versus day 0; † $p<0.05$ versus FS controls.

($p<0.0005$), however, no significant differences with loading were observed. There were also no significant differences in the GAG content of FS and DL chondrocyte-seeded constructs. The collagen content was significantly higher in DL constructs than in FS constructs by day 42 when normalized to DNA or dry weight ($p<0.05$). No load-dependent differences in collagen content were observed when normalized to the construct wet weight. At day 42, GAG and collagens comprised a significant portion of the solid tissue components compared to day 0 ($p<0.005$; Figure 2.6). By day 42, GAGs and collagens accounted for 54% and 61% of the solid component (i.e., % normalized by dry weight) of FS and DL constructs, respectively.

At day 42, the distribution of GAG was similar in FS and DL constructs (compare Figure 2.4D, E). However, more labeling of collagen was observed in the central regions of DL constructs

	Day 0	Day 42	
		FS	DL
Thickness (mm)	2.34 ± 0.02	$2.72 \pm 0.10^{*}$	$2.59 \pm 0.10^{*\dagger}$
Diameter (mm)	3.76 ± 0.04	$4.12 \pm 0.15^{*}$	$4.09 \pm 0.12^{*}$
Wet weight (mg)	25.3 ± 0.8	$39.5 \pm 10.0^{*}$	$37.4 \pm 6.3^{*\dagger}$
Dry weight (mg)	1.1 ± 0.3	$5.4 \pm 1.6^{*}$	$4.8 \pm 0.5^{*\dagger}$
Water content (%)	95.5 ± 1.2	$86.7 \pm 2.7^{*}$	$86.9 \pm 3.2^{*}$
DNA (% wet weight)	0.016 ± 0.004	$0.024 \pm 0.004^{*}$	$0.022 \pm 0.005^{*}$
GAG (% wet weight)	0.1 ± 0.0	$4.0 \pm 0.8^{*}$	$3.6 \pm 1.1^{*}$
Collagen (% wet weight)	0.1 ± 0.0	$3.4 \pm 0.5^{*}$	$4.8 \pm 1.1^{*}$
GAG/DNA (μg/μg)	7.7 ± 1.8	$17.1 \pm 4.1^{*}$	$15.8 \pm 4.5^{*}$
Collagen/DNA (μg/μg)	7.4 ± 2.3	$12.3 \pm 2.2^{*}$	$18.5 \pm 4.0^{*\dagger}$

Table 1: The bulk morphological and biochemical properties of chondrocyte-seeded agarose hydrogels grown in free swelling (FS) and dynamically loaded (DL) cultures over a 6-week period (for day 0, n=4–5; for day 42, n=6–11; mean ± standard deviation). * Represents significant differences versus day 0 ($p<0.0005$). † Represents significant differences versus FS controls ($p<0.05$). Note that the thickness and diameter presented here were measured prior to any testing.

(Figure 2.4F) compared to FS controls (Figure 2.4G).

2.4.2 Tension-compression nonlinearity

The effects of salt concentration on the thickness and material properties of chondrocyte-seeded constructs are presented in Table 2. The samples were first mechanically tested whole to yield average construct properties, and then allowed to recover for 60 min in the appropriate saline solution prior to testing in the custom built microscope-mounted testing rig (Figure 6.5). Similar intergroup differences in tissue dimensions were observed before bulk testing and after recovery in saline (compare Table 1 and Table 2). Additionally, the thickness of DL constructs increased significantly in hypotonic saline ($p<0.05$), which corresponds to a 3% increase in thickness. There was a 2% increase in thickness observed for the FS controls, however, this difference was not significant. In hypertonic saline, the FS and DL samples shrunk by 4% and 3% ($p<0.05$), respectively. In all cases, DL samples showed significantly lower temporal increases in construct dimensions than FS controls ($p<0.05$).

The effects of salt concentration on the apparent E_{Yi} of acellular and chondrocyte-seeded constructs are shown in Figure 2.5, Figure 2.6, Figure 2.8, and in Table 2. Strain-softening behavior was observed in day 0 and acellular samples. There was no dependence on salt concentration, which is consistent with the uncharged nature of agarose hydrogels. Here, E_{+Y} and E_{-Y} obtained for day 0 and acellular constructs were 28–40 kPa and 8–10 kPa, respectively. Direct measurement of

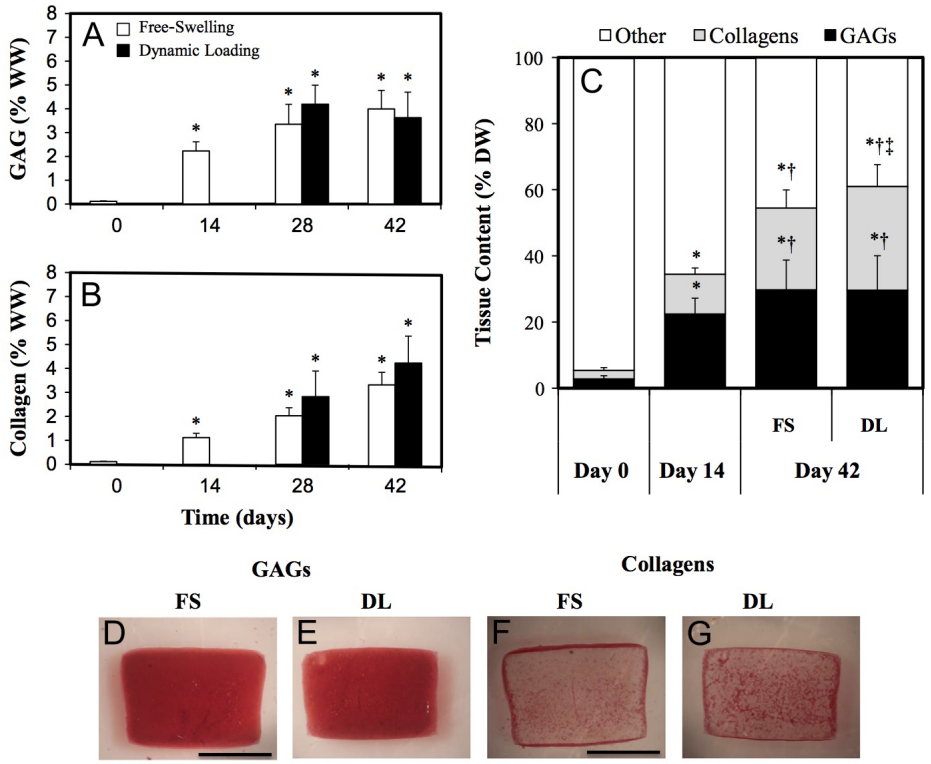

Figure 2.4: (A), (B). GAG (A) and collagen (B) contents (normalized to the wet weight (WW) of the constructs) of free swelling (FS) and dynamically loaded (DL) constructs over a 42-day culture period (n=5–11). * $p<0.005$ versus day 0; † $p<0.05$ versus FS controls. C. Biochemical content normalized to the dry weight (DW) of FS and DL constructs over a 42-day culture period (n=5–11). (D)–(G) Safranin O (GAGs) and Picrosirius Red (collagens) staining of FS and DL constructs at day 42.

		Day 0	Day 42	
			FS	DL
Thickness (mm)	0.015 M NaCl	2.35 ± 0.02	$2.71 \pm 0.05^{*\S}$	$2.65 \pm 0.05^{*\S}$
	2 M NaCl	2.33 ± 0.03	$2.55 \pm 0.08^{*}$	$2.34 \pm 0.06^{*\dagger}$
Diameter (mm)	0.015 M NaCl	4.04 ± 0.04	$4.11 \pm 0.19^{*\ddagger}$	$4.19 \pm 0.10^{*\dagger\S\ddagger}$
	2 M NaCl	3.97 ± 0.10	$3.99 \pm 0.09^{*}$	$3.99 \pm 0.12^{*\dagger}$
Swelling strain (normalized to 0.15 M NaCl)	0.015 M NaCl	0.01 ± 0.01	0.02 ± 0.01	0.03 ± 0.02
	2 M NaCl	-0.01 ± 0.01	-0.04 ± 0.02	-0.03 ± 0.02
Maximum incremental Young's Modulus (kPa)	0.015 M NaCl	39 ± 9	$401 \pm 83^{*\S}$	$678 \pm 473^{*\dagger\S}$
	2 M NaCl	32 ± 8	$115 \pm 15^{*}$	$141 \pm 55^{*}$
Steady-state incremental Young's Modulus (kPa)	0.015 M NaCl	5 ± 2	$161 \pm 33^{*}$	$348 \pm 203^{*\dagger\S}$
	2 M NaCl	5 ± 1	$46 \pm 9^{*\ddagger}$	$35 \pm 16^{*}$

Table 2: The effects of osmotic loading were determined for free swelling (FS) and dynamically loaded (DL) constructs that were tested in 2 M or 0.015 M salt solution (n=4–5, mean± standard deviation). Note that the thickness and diameter presented here were measured after equilibrium in the appropriate saline solution, but prior to macroscopic mechanical testing. * Represents significant differences versus day 0 constructs ($p<0.05$). † Represents significant differences versus FS constructs ($p<0.05$). § Represents significant differences versus 2 M NaCl values ($p<0.05$).

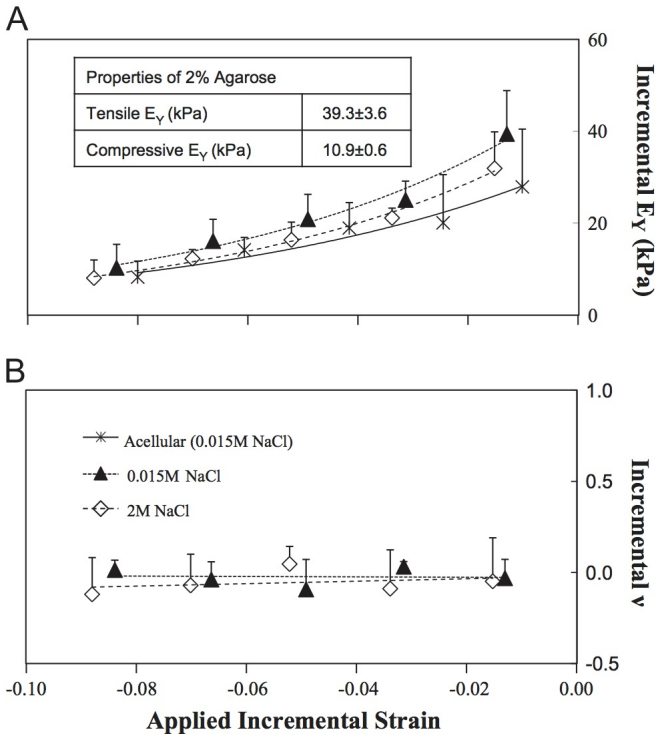

Figure 2.5: (A) Incremental Young's modulus (E_{Yi}) of acellular and day 0 chondrocyte-seeded agarose constructs tested in hypotonic (0.015 M NaCl) and hypertonic (2 M NaCl) saline (n=4). Inset. Compressive and tensile E_Y of 2% agarose obtained from direct measurements (n=7). (B) Incremental Poisson's ratio (ν_i) of day 0 chondrocyte-seeded agarose constructs tested in hypotonic (0.015 M NaCl) and hypertonic (2 M NaCl) saline (n=4).

acellular agarose yielded similar results (E_{+Y} = 39 kPa and E_{-Y} = 11 kPa) (Figure 2.5A inset).

At day 42, FS and DL constructs exhibited similar changes in the apparent E_{Yi} in response to changes in salt concentration and applied strain (Figure 2.6). Here, the constructs are placed in a state of tension via applied hypotonic loading; therefore, E_{Yi} measured at low applied strain (below the swelling strain of the constructs) represents E_{+Y} of the constructs. As the construct is compressed, the tissue transitions from a state of tension to compression, permitting the examination of TCN in these constructs. At both salt concentrations, the apparent E_{Yi} was highest at the lowest applied strain and decreased with increasing applied strain. Overall, the measured apparent E_{Yi} increased with decreasing salt concentration. In the hypotonic state, DL constructs exhibited significantly higher apparent E_{Yi} than FS constructs (Figure 2.7A). No significant differences in the apparent E_{Yi} were observed in hypertonic saline (Figure 2.7B, C).

In hypotonic saline, the apparent E_{+Y} (Table 2) was obtained at the lowest strain increment

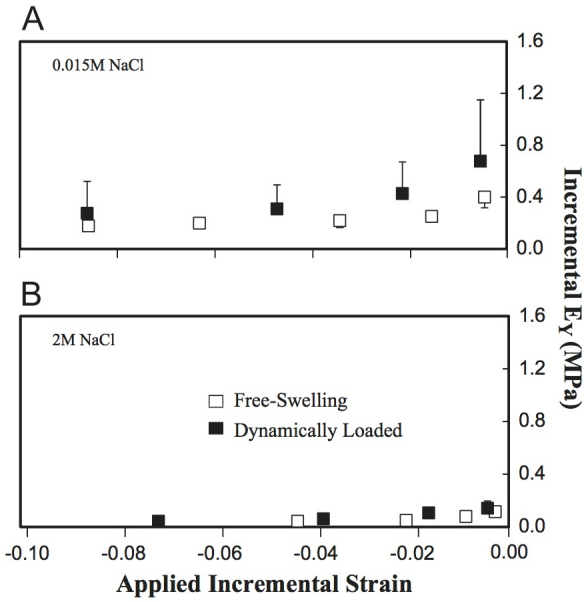

Figure 2.6: Incremental Young's modulus (E_{Yi}) of free swelling (FS) and dynamically loaded (DL) chondrocyte-seeded agarose constructs tested in hypotonic ((A); 0.015 M NaCl) and hypertonic ((B); 2 M NaCl) saline on day 42 (n=4–6). * $p<0.05$ versus free FS, † $p<0.05$ versus higher strain values $p<0.05$; § $p<0.05$ versus >3% strain values.

(401 kPa for FS and 678 kPa for DL), which was significantly higher than hypertonic saline values (46 kPa for FS and 35 kPa for DL; $p<0.05$). Additionally, at each salt concentration, the apparent E_{+Y} of DL constructs was significantly higher than that of the FS controls ($p<0.05$). At high strain, the apparent E_{-Y} of FS constructs was similar in hypotonic and hypertonic saline. However, for DL constructs, the apparent E_{-Y} was significantly greater for constructs in hypotonic saline compared to hypertonic saline ($p<0.05$).

The effects of salt concentration on the apparent ν_i of acellular and chondrocyte-seeded constructs are shown in Figure 2.5, Figure 2.7, and Figure 2.8B. At day 0, ν_i remained constant as the incremental strain was increased and were similar at all saline concentrations (Figure 2.5B). At day 42, FS and DL constructs exhibited disparate changes in ν_i in response to changes in salt concentration and applied strain (Figure 2.7). For FS constructs tested in hypotonic saline, ν_i was high at low strain and decreased at higher applied strain to a steady-state value. In hypertonic saline, ν_i remained constant across all applied strains, similar to the ν_i obtained at higher applied strain in hypotonic saline. For DL, when tested in hypotonic saline, ν_i was initially low, compared to FS controls, but decreased slightly as the applied strain was increased to a steady-state value. In

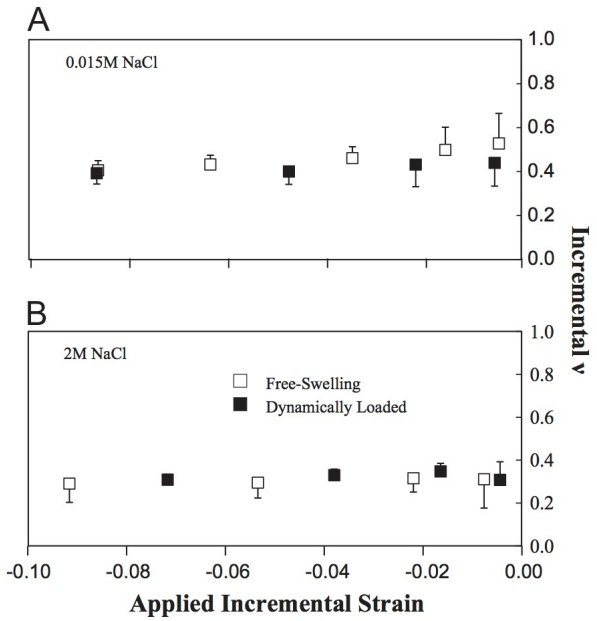

Figure 2.7: Incremental Poisson's ratio (ν_i) of free swelling (FS) and dynamically loaded (DL) chondrocyte-seeded agarose constructs tested in hypotonic ((A); 0.015 M NaCl) and hypertonic ((B); 2 M NaCl) saline on day 42 (n=4-6). * $p<0.05$ versus FS, † $p<0.05$ versus higher strain values $p<0.05$; § $p<0.05$ versus >3% strain values.

hypertonic saline, ν_i did not vary with increased applied strain. Here, ν_i was similar to the values measured in hypotonic saline at higher applied strains. Furthermore, in hypertonic saline, similar ν_i was obtained for both FS and DL constructs.

The data in Figure 2.6 and Figure 2.7 were combined using the construct's swelling strains (Table 2) to generate TCN plots for both E_{Yi} and ν_i (Figure 2.8). Under these conditions, E_{+Y} of both FS and DL constructs were significantly higher in tension, decreasing exponentially as the constructs transition to purely compressive conditions (Figure 2.8A; R^2=0.98–0.99, $p<0.05$). Additionally, DL constructs exhibited significantly higher E_{+Y} compared to FS controls ($p<0.05$). These trends were comparable to those observed for native cartilage (Figure 2.8A inset).

In FS constructs, ν_i was significantly higher when the constructs were in tension but decreased exponentially as the constructs transitioned into purely compressive conditions (Figure 2.8B; R^2=0.87; p=0.05). For DL constructs, ν_i exhibited a slight but exponential decrease as the tissue transitioned from tensile to compressive conditions (R^2=0.60). Additionally, ν_i of DL constructs was significantly lower than FS controls when the constructs were placed in tension (p=0.05). νi showed similar trends to native cartilage (Figure 2.8B inset), i.e., decreased nonlinearly with increased strain, however un-

der tensile strain, ν_i was higher than in native tissue.

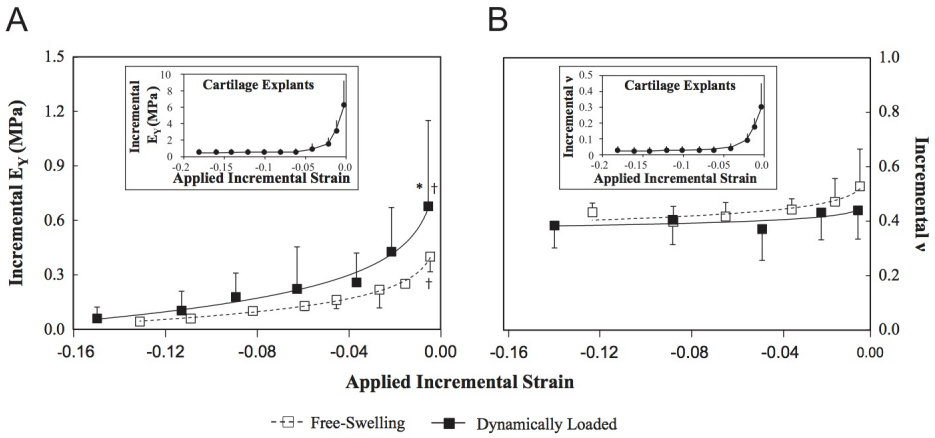

Figure 2.8: (A), (B). Tension–compression nonlinearity plots highlighting differences in the incremental Young's modulus ((A); E_{Yi}) and incremental Poisson's ratio ((B); ν_i) of free swelling (FS) and dynamically loaded (DL) chondrocyte-seeded agarose constructs tested in hypotonic (0.015 M NaCl) and hypertonic (2 M NaCl) saline on day 42 (n=4–6). * $p<0.05$ versus FS, † $p<0.05$ versus higher strain values; § $p<0.05$ versus 43% strain values. The data was curve fitted to show the overall trends. In all cases exponential functions yielded best-fits (E_{Yi} FS R^2=0.99; E_{Yi} DL R^2=0.98; ν FS R^2=0.87; ν DL R^2=0.60). Insets. Tension–compression nonlinearity plots illustrating Young's modulus ((A); E_{Yi}) and incremental Poisson's ratio ((B); ν_i) of cartilage explants (in the depth direction; n=8).

2.5 Discussion

In this study, osmotic swelling and uniaxial compressive loading were used to determine tensile and compressive responses within the same chondrocyte-seeded agarose constructs. Using the general framework of porous media mechanics and Donnan equilibrium theory (Overbeek, 1956; Grodzinsky, 1982; Lanir, 1986; Lai *et al.* , 1991; Basser *et al.* , 1998; Wang *et al.* , 2002a; Wang *et al.* , 2002b; Ateshian *et al.* , 2004; Wilson *et al.* , 2007; Maroudas, 1976; Chahine *et al.* , 2004), it is apparent that bathing native or engineered cartilage in solutions of greater salt concentration will result in a decreased contribution of osmotic pressure to the effective tissue material responses (due to increased shielding of the fixed charge density arising from GAGs). Likewise, bathing native or engineered cartilage in hypotonic solution results in tissue swelling (relative to isotonic dimensions) and stiffening. Tissue swelling is a manifestation of the expansion of the fibrillar collagen network (e.g., recruitment of collagen fibers extended beyond their toe-region) to balance the increase in Donnan osmotic pressure resulting from the fixed charge density associated with the

GAGs (Maroudas, 1976).

While the E_{-Y} of 2% agarose is in a typical range of 5–15 kPa (Figure 2.5, Inset), tensile testing yielded E_{+Y} of 39 kPa, similar to previously reported values (Huang *et al.* , 2008). Although agarose does not exhibit swelling or shrinking in response to salt solutions, there is observable strain-softening in response to greater levels of applied compression. The initially higher E_{Yi} at very low applied compression, similar to the measured E_{+Y} determined from conventional testing, is thought to arise from residual stresses of the polymer that place the hydrogel in a swollen state during gelation (Amici *et al.* , 2000; Normand *et al.* , 2000). As this swollen state is overcome, compressive properties are exhibited. Since E_{-Y} and E_{+Y} of mature engineered tissues are more than an order of magnitude greater than agarose, the hydrogel scaffold contributes minimally to the mechanical behavior of the mature engineered tissues.

The results of this study showed that testing of mature (day 42) engineered cartilage in hypertonic saline significantly reduced the apparent E_{Yi} of constructs relative to hypertonic conditions but not to day 0 levels, which were consistent with data obtained for native cartilage (Chahine *et al.* , 2005). In contrast, for immature (day 0) and acellular constructs, no differences were observed at various salt concentrations (Figure 2.5A). These results confirm that the observed effects of salt concentration can be attributed to the charged GAG species accumulated in the mature engineered cartilage over time (Ehrlich *et al.* , 1998; Chahine *et al.* , 2005). Cell swelling may contribute to the tensing of the fibrillar collagen network, however previous results indicate the ECM acts to limit cell expansion (Lee & Bader, 1995; Knight *et al.* , 1998). As such, the measured properties with hypertonic saline reflect the intrinsic material properties of the engineered cartilage without the contribution of Donnan osmotic pressure.

When the matrix is in a state of tension the measured stiffness represents E_{+Y}, the highest modulus measured under initial compression in hypotonic saline. The results of this study indicate that tissue growth of chondrocyte-seeded agarose constructs leads to an increase in E_{+Y}. At day 42, E_{+Y} measured in hypotonic saline ranged from an average of 0.40 MPa for FS constructs to 0.68 MPa for DL constructs. E_{+Y} ranging from 0.2 to 5 MPa has been reported for engineered cartilage (Gemmiti & Guldberg, 2006; Gemmiti & Guldberg, 2009; Huang *et al.* , 2008; Huang *et al.* , 2012; Bian *et al.* , 2009a; Bian *et al.* , 2009b; Natoli *et al.* , 2009a; Natoli *et al.* , 2009b; Natoli *et al.* , 2010; Moutos & Guilak, 2009; Eleswarapu *et al.* , 2011; Eleswarapu & Athanasiou,

2013). In fact, previous data from our laboratory for constructs cultured under similar conditions found similar tensile properties (0.2 MPa for Bian's CONT versus 0.4 MPa for FS) (Bian *et al.* , 2009a; Bian *et al.* , 2009b). Those values are consistent with E_{+Y} observed in this study at day 42. As with native cartilage, the measured E_{Yi} decreased with increasing salt concentration, since the concomitant reduction in swelling pressure also reduced the swelling strain, thereby shifting the FS initial configuration on the TCN curve to the left (Figure 2.6; (Chahine *et al.* , 2005)). Furthermore, increasing the swelling strain by further decreasing the bathing media osmolarity would be anticipated to yield a higher measured E_{Yi}, thereby shifting the TCN curve to the right. We chose 0.015 M NaCl, because it allows for sufficient tissue swelling without causing the tissue to burst apart.

This method allows for the analysis of local material properties of the constructs (data not shown). Spatial variation in E_{+Y} was similar to those previously reported for E_{-Y}, that is the edges of the constructs (i.e., axial faces) were stiffer compared to the middle with DL exhibiting a stiffer central region compared to FS controls (Kelly *et al.* , 2006).

The results of this study confirmed our previous observation that DL yielded lower ν than FS culture, which is expected if DL constructs have higher E_{+Y} than FS controls (Kelly *et al.* , 2006). The observed increases in tensile ν_i of FS constructs over native values emphasize the importance of E_{+Y} on proper functioning of cartilaginous tissues (Figure 2.8B). For DL constructs, ν_i was in the range observed for native cartilage. Higher swelling strains may be required to fully elucidate the effects of tensile strain on ν_i.

When comparing FS and DL cultures, it is found that the biochemical composition evolves similarly for both groups at most time points, except for day 42, where the collagen content is greater in DL group when normalized to the DNA or dry weight (Figure 2.4C and Table 1). The mechanical response of the tissues exhibit significant differences on day 42 for E_{-Y} (Figure 2.3 B); however, no significant difference in G* was observed (Figure 2.3C). E_{+Y} measured from the osmotic swelling experiments shows a significantly higher value in DL group (Figure 2.5C). We have previously shown that DL produces constructs with a more organized matrix than those grown in FS culture. More specifically, in DL constructs, the collagen fibers were shown to be aligned transversely to the direction of loading with increased type II and IX collagen (Kelly *et al.* , 2004; Kelly *et al.* , 2006), which may have contributed to the increased E_{+Y}.

The best results from these studies reveal engineered cartilage with E_{-Y} and GAG content similar to those of native cartilage; however, G* (∼10–30% of native), E_{+Y} (∼15–25%) and collagen (∼24–48%) are a fraction of the native values (Huang *et al.* , 2005; Chahine *et al.* , 2004). Low collagen content and its effect on engineered cartilage material properties remains a major challenge in cartilage tissue engineering (Riesle *et al.* , 1998; Mauck *et al.* , 2000a; Mauck *et al.* , 2002; Williamson *et al.* , 2003b; Williamson *et al.* , 2003a; Kelly *et al.* , 2004; Kelly *et al.* , 2006; Gemmiti & Guldberg, 2006).

Here, hypotonic and hypertonic conditions were used as a methodological tool to examine TCN in these constructs. For the first time, we are able to determine E_{-Y} and E_{+Y} of engineered cartilage using applied compressive loading without the need to prepare multiple specimens or conduct multiple experiments. The resolution of optical strain measurements makes it possible to examine the transition from tension to compression, producing a clearer understanding of the disparate material properties of DL and FS constructs. More complete characterizations of the material properties of engineered cartilage can improve critical assessments of the efficacy of tissue engineering approaches for producing functional tissues for articular cartilage repair and replacement.

2.6 Conclusion

TCN is a phenomenon that describes articular cartilage's complex response to tensile and compressive forces. A higher stiffness in tension versus compression allows cartilage to resist radial expansion under axial compressive loading, resulting in increased fluid pressurization, dynamic stiffness and improved performance under dynamic loads *in vivo*. The studies described in this dissertation are complementary to previous work with cartilage explants, characterizing TCN in engineered tissues and demonstrating the ability to use osmotic swelling to measure both compressive and tensile properties in a single cartilage sample. Uniquely, this approach may allow for more rigorous investigation into the quantification of tissue swelling as an early indicator of cartilage pathology in OA, with important implications for the clinical diagnosis of cartilage matrix damage.

In addition to the characterization of TCN, these studies demonstrate the beneficial effect of displacement-controlled dynamic compressive loading in engineered cartilage. Developed from an adult chondrocyte cell source, these tissues reached near-native compressive mechanical properties, with dynamic loading producing significant improvements in both E_Y and collagen content. As

a strategy for preparing engineered tissues for mechanical loading *in vivo*, displacement-controlled compressive loading is an attractive approach.

2.7 Acknowledgements

This research was supported by the National Institutes of Health under Award Numbers AR046568 (CTH), EB014382 (CTH), AR060361 (GAA, CTH), as well as graduate and postdoctoral research supplements (TNK). The content is solely the responsibility of the authors and does not necessarily represent the official views of the National Institutes of Health.

Chapter 3 Application of a Turn-Key Bioreactor for Functional Tissue Engineering of Articular Cartilage

3.1 Introduction

As discussed in Chapter 2, dynamic compressive loading *in vitro* is a promising strategy for preparing tissue-engineered cartilage for the harsh mechanical environment experienced *in vivo* (Hung *et al.* , 2004; Lima *et al.* , 2007; Cassino *et al.* , 2007). To this end, deformational loading of tissue-engineered cartilage has traditionally employed devices with single actuators that stimulate tissues, in batches, simultaneously and interdependently (Aufderheide & Athanasiou, 2006; Cassino *et al.* , 2007; Mauck *et al.* , 2003). While this approach allows for physiologic loading patterns (Park *et al.* , 2004), high testing volume, and has proven to aid in the development of tissues with native mechanical properties (Lima *et al.* , 2007), this approach ignores the reality that not all tissues are of equal thickness or stage of development (Davisson *et al.* , 2002; Park *et al.* , 2004). '10%' strain applied uniformly by the actuator, therefore, may not result in uniform strain across a sample population, with some being strained less and some strained more than the target deformation. The resulting divergences in real tissue strain can negatively impact cartilage development (Butler *et al.* , 2009).

Similar to previous designs that account for differences in construct thickness (Butler *et al.* , 2009), the Mechanoactive Tissue Engineering bioreactor (MATE), a commercially available unit (APEX Biomedical, LLC), was developed to allow for sample specific dynamic loading patterns and analysis (Lujan *et al.* , 2011). With 6 independent voice coil motors, the MATE is able to use both displacement- and force-controlled protocols to stimulate samples individually. While displacement-controlled loading protocols have previously been used to generate reproducible results for batch loading (Ng *et al.* , 2006; Waldman *et al.* , 2004; Kisiday *et al.* , 2009; Kisiday *et al.* , 2004; Aufderheide & Athanasiou, 2006; Lima *et al.* , 2007), and was utilized in Chapter 2 of this dissertation, the MATE allows for stimulation of individual samples with reproducible force-controlled regimens, ensuring tissue quality across a population. Both approaches will be investigated here in the context of the MATE.

The following studies aim to do two things: 1) Characterize and optimize the MATE for cartilage

tissue engineering applications and 2) investigate the utility of the bioreactor to stimulate tissue growth in explants and constructs from a variety of cell sources.

3.2 Materials and methods

3.2.1 Bioreactor characterization and optimization for tissue engineering strategies

3.2.1.1 Characterization of MATE analysis protocols To evaluate the ability of the MATE to analyze samples of variable equilibrium moduli, agarose hydrogels of multiple concentrations (2%, 4%, and 6%) were used. Each sample was cored from an agarose slab via biopsy punch (Ø 4.0 x 2.34 mm) immediately prior to analysis. Analysis was conducted using the MATE software from test strains of 1% to 10%. Additionally, accuracy of the MATE was compared against values obtained via established material testing methodologies (Roach *et al.* , 2016).

To investigate the impact of structural properties on the performance of the MATE system, agarose hydrogels of variable diameters and consistent equilibrium moduli were used. Each sample was cored from an agarose (2%) slab via biopsy punch (Ø 4.0, 6.0, 8.0 x 2.34 mm) immediately prior to analysis. Analysis parameters were held constant for this evaluation, applying a 2% pre-strain and 3% test strain.

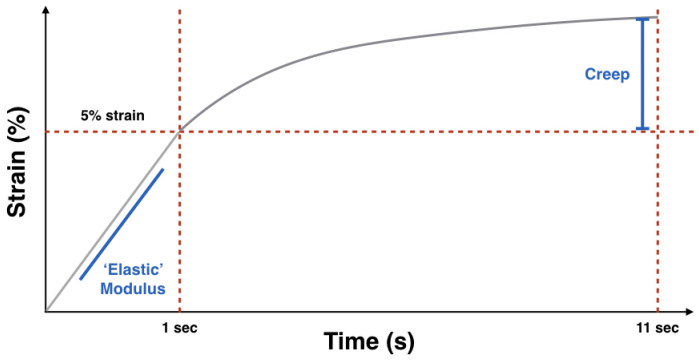

Figure 3.1: MATE bioreactor analysis protocol. The slope of the curve over the first second determines the 'elastic' modulus of the tissue. After 1 second, the load is held constant and the tissue is allowed to creep for 10 seconds. The change in strain required to maintain this load is recorded as creep.

For all analysis protocols, samples were submerged in a PBS bath within individual sample wells and mounted in the loading dish. The testing strain was applied over a pre-determined 1 second interval (indicating 'elastic' modulus), and the hydrogel was allowed to relax under constant load

for 10 seconds (indicating viscosity of the tissue) (Figure 3.1).

3.2.1.2 Optimization of MATE stimulation protocols Initial stimulation with the MATE was done in an effort to mimic, as closely as possible, the loading pattern used by our lab previously (Mauck *et al.* , 2000b; Lima *et al.* , 2007). This established loading pattern provides a sinusoidal deformation with a magnitude of 10% peak-to-peak strain at a frequency of 1 Hz (5 days/week, 3 h/day continuous, 2% tare strain), and has been shown to be effective in yielding superior compressive mechanical properties compared to unloaded free-swelling controls (Lima *et al.* , 2007; Bian *et al.* , 2010a). For this reason, the investigation described here first utilized a strain-controlled approach. The initial protocol produced a 2.0% pre strain and 3.0% test strain (1 Hz, 60 cycles). The strain amplitude was adjusted as appropriate for optimization. Following exhaustion of strain-controlled loading parameters, a force-controlled stimulation protocol was evaluated, unique to the capabilities of the MATE (Lujan *et al.* , 2011), beginning with a 2 N pre load and a 3 N test load (1 Hz, 10 cycles). This protocol was iteratively adjusted to optimize results.

The protocols described above were applied to engineered and explanted cartilage tissues of varying maturity levels in an effort to identify a single loading protocol suitable for a range of cartilage stiffnesses. When a broadly applicable stimulation protocol was found, it was then applied for subsequent cell-based studies.

3.2.2 Sample preparation and tissue culturing

Following identification of an optimal loading protocol, and to investigate the general applicability of the MATE (Figure 3.2b) to cartilage tissue engineering, two different chondrocyte cell sources were used for subsequent studies: juvenile bovine and adult human tissues.

As described previously (Lima *et al.* , 2007) and in Chapter 2.3.1, articular cartilage was harvested from knees of freshly deceased donor specimens. At least three joints were used for experimentation and cells were pooled from all joints. Chondrocytes were isolated from cartilage chunks via digestion overnight with agitation in 390 U/mL collagenase type II (Worthington). For isolated adult human chondrocytes, as described in Chapter 1.3.3.2, the use of a growth factor cocktail maintained and promoted the chondrocyte phenotype while priming the cell for biosynthetic activity when reintroduced in a 3D environment (Adkisson *et al.* , 2010; Barbero *et al.* , 2003; Barbero

et al. , 2004; Sampat *et al.* , 2011). Following two passages, cells were prepared for encapsulation in an agarose hydrogel (type VII, Sigma). For both cell sources, chondrocytes were seeded at 30 x 10^6 cells/mL in 2% agarose. Cylindrical constructs (Ø 8.0 x 2.34 mm) were cored and cultured in chondrogenic medium (detailed in Chapter 2.3.1). For juvenile chondrocytes, 10 ng/mL TGF-β3 (R&D Systems) was supplemented for the first 2 weeks of culture (Lima *et al.* , 2007). For adult human chondrocytes, TGF-β3 was supplemented for the entirety of the study. Culture media was exchanged 3x per week.

Following five weeks of culture, juvenile bovine chondrocyte-based tissues were stimulated via MATE (Figure 3.2a) with optimized protocol for the next two weeks. For adult human chondrocyte-based tissues, stimulation was initiated following six weeks of culture and was maintained for the subsequent three weeks. Once begun, the stimulation protocol was active 24 hours a day and 7 days a week. This force-controlled protocol applied a 0 N pre load and 5 N test load for 3 cycles at 10 Hz (20 minute rest between cycles). For the duration of stimulation, samples were maintained inside individual wells (Figure 3.2b). Free-swelling control samples were maintained in equal volumetric ratios of chondrogenic medium.

3.2.2.1 Impact of fluid flow on tissue growth

Because the optimized stimulation protocol is in contrast to previously used protocols (Mauck *et al.* , 2000b), the source of tissue growth (tissue deformation or fluid flow) needed to be isolated for accurate interpretation of results. A subset of juvenile bovine chondrocyte tissues was isolated and cultured in the MATE system with protective rubber cylinders. These rubber cylinders provided clearance between the surface of the culture medium and the surface of the construct, allowing for the same loading protocol to be applied to the fluid but not the constructs. These wells were loaded in tandem with the study described above.

3.2.3 Average mechanical properties

Evaluation of mechanical properties was performed in the MATE via the protocol described earlier (Figure 2.3). Analysis was performed on these samples every 10 cycles. At the onset and end of the stimulation window, engineered tissues were evaluated via established material testing methodology (Roach *et al.* , 2016). This custom unconfined compression device (MT), with rigid-impermeable loading platens and a 250 gram load cell (Honeywell), was used to assess compressive dynamic (G*)

Figure 3.2: (a) Image of the MATE, assembled, and ready for culture in the incubator. A 6-sample tray (b) sits on top of the unit and voice coil motors drive each sample dish up into the polysulfone lid to create compress. Plastic guards surround the sample and create a guide for platens while keeping the sample safely underneath.

and equilibrium moduli (E_Y) (n=6). Before testing, the construct thickness and diameter were measured. The specific testing protocol is described in Chapter s2.3.1. Following testing, samples were halved and then frozen for biochemical analysis.

3.2.4 Biochemical analysis

For juvenile bovine chondrocyte based tissues, samples (n=6) were thawed, lyophilized, and weighted dry. Proteinase K digestion, as well as biochemical assays for DNA, GAG, and OHP were completed as described (Chapter 2.3.5).

3.2.5 Statistical analysis

Because of the limited time points and groups associated with this study, a Student's t-test (α=0.05) was satisfactory to determine significant differences (n=6).

3.3 Results and discussion

3.3.1 Bioreactor characterization and optimization for tissue engineering strategies

3.3.1.1 Characterization of MATE analysis protocols The MATE was able to discern differences in 'elastic' modulus measured across agarose samples of different concentrations (Table e3). 'Elastic' modulus was positively correlated, however, with the magnitude of applied strain in each sample. The 'elastic' modulus of a 4% agarose hydrogel at 1% test strain measured ~3x

Strain		1%	2%	3%	4%	5%	6%	7%	8%	9%	10%	Lab Testers
Agarose %w/v	2	27.9	42.3	54.2	62.0	72.2	74.9	86.5	84.5	71.4	N/A	10.81
	4	83.3	124.1	103.9	140.5	158.5	172.4	183.6	185.4	199.1	216.2	66.22
	6	224.2	300.3	347.7	368.2	374.6	383.4	380.8	416.8	414.0	419.8	114.36

Table 3: Equilibrium compressive moduli of agarose constructs at different concentrations was measured via 'Lab Testers' (MT). The 'elastic' modulus, as measured by the MATE, is shown to the left at each strain interval.

lower than did the same gel at 10% testing strain. The same trend was observed in 2% and 6% agarose hydrogels. As a direct comparison, the same gels were evaluated using MT. These values are significantly lower than those measured at any strain level by the MATE.

Differences in measurement of 'elastic' moduli between MATE and MT can be attributed to the manner in which this value is determined. For MT, full equilibrium is reached prior to determination of the equilibrium load and thus, the equilibrium modulus. The MATE compresses the tissue to the desired test strain in 1 second and records the force response of the gel at this point (Figure 3.1). Because this strain occurs over a pre-determined 1 second interval, water is not able to exude instantly to the surrounding bath and is trapped inside the agarose core. This trapped water is pressurized within the agarose and the resulting 'elastic' modulus value reflects this. As the test strain is increased from 1% to 10%, the strain rate also increases, leading to elevated levels of fluid pressurization and thus higher 'elastic' moduli. As such, the 'elastic' modulus measured with the MATE is more accurately described as an 'instantaneous' modulus. It it is recommended that a technique more representative of the material properties of the tissue be used in future work to allow for comparison with the work of colleagues and collaborators. For intergroup comparisons within a single study, however, a consistent test strain may be used for the duration of the study to allow the MATE to discern differences in tissue growth relative to baseline properties.

Comparing 2% agarose cores of varying diameters, the mechanical properties determined by the MATE ranged from 74 kPa to 135 kPa. These results can be compared to the E_Y measured by MT ($\sim$10 kPa). Interestingly, the 'elastic' modulus of 2% agarose cores decreased with increasing diameter (Table 4), while the thickness, as measured by the MATE, increased. Further, the creep response of 4 mm diameter hydrogels was significantly different from other geometries, registering nearly 6x more creep than 8 mm diameter samples prepared from the same gel.

2% agarose	4 mm	6 mm	8 mm
Thickness (mm)	1.96	2.07	2.17
Elastic Modulus (kPa)	135.67	87.17	74.50
Creep (%)	6.75	2.63	1.18

Table 4: MATE bioreactor output as determined across 2% agarose hydrogels from 4 mm to 8 mm in diameter. The thickness of all samples was identical (2.34 mm)

These results, together with those from Table 3, bring to light complications inherent in the analysis mode of the MATE. For example, although the samples analyzed in Table 4 are of identical thickness, the measured thickness decreases with decreasing diameter. This inaccuracy is due to the sensing mechanism of the MATE. In order to determine contact, each station of the MATE compresses their respective sample until 10 grams of load are sensed. This point becomes the thickness of each sample. In reality, in samples of equal E_Y and thickness, 10 grams applied to a 4 mm diameter sample results in more displacement than does 10 grams applied to an 8 mm diameter sample. In the case of Table 4, this may result in compaction of the pore structure with decreasing diameter samples, increased fluid pressures, and thus elevated 'elastic' modulus. Because of the elevated load following application of the test strain, creep is elevated in the 4 mm diameter sample compared with larger diameter samples, as it is unable to withstand the elevated load.

Our characterization of the MATE suggests the utility of this system lies in the use of consistent analysis protocols and samples of equal diameter. If these parameters are tightly controlled, then study results may be used to draw conclusions on tissue growth and comparisons between groups. Biological studies rarely allow this level of control, however, making external validation of MATE results critical.

3.3.1.2 Optimization of MATE stimulation protocols In an effort to identify the ideal stimulation protocol, a variety of parameters were evaluated with immature and mature engineered cartilage as well as immature explant cartilage tissue. Being consistent with previous work in the laboratory demonstrating beneficial effects of strain-controlled dynamic loading (Mauck *et al.* , 2000a; Lima *et al.* , 2007; Bian *et al.* , 2010a), initial efforts at stimulation via MATE used this approach.

To evaluate the ability of MATE to stimulate tissues with E_Y near day 0 values, soft tissue

engineered constructs (Ø 4 mm, E_Y = ~10 kPa) were stimulated with a 3% test strain for 60 cycles (1.0 Hz, 2% pre strain). These parameters were informed by manufacturer guidelines. Within 4 cycles (Figure 3.3), on average, the strain differential (maximum strain - minimum strain) reached an infinitesimal strain, at which point the system disengaged the voice coil motors (VCMs) as a protective measure.

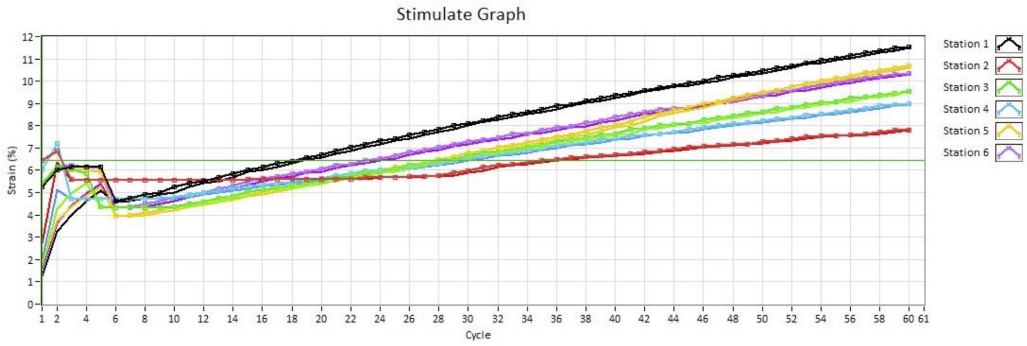

Figure 3.3: Stimulation of immature tissue-engineered cartilage constructs at 3% test strain resulted in system power down within 4 cycles. The solid line indicates the minimum strain at each cycle. The line with symbols at each cycle indicates the maximum strain.

The response seen from immature tissues is the combined result of creep within the tissue and thickness measurements acquired by the MATE. At each cycle, the MATE reevaluates the thickness of the tissue using a 10 gram load to determine the load strain required for subsequent cycles. An extension of previous characterization results (Chapter 4), this 10 gram pre-load is prohibitively high in the context of small diameter, soft hydrogels.

To determine if this outcome can be remedied by an increase in sample diameter, a sample of similar stiffness (E_Y = ~10 kPa) but larger diameter (Ø 6 mm) was submitted to the same stimulation regimen (2% pre strain, 3% test strain, 1.0 Hz for 60 cycles) (Figure 3.4). As understood from mechanics, and demonstrated in Chapter 4, a constant load applied to a larger cross-sectional area will reduce the strain experienced in the sample.

Following 10 cycles, on average, the strain differential neared zero and the VCMs were disengaged. This improvement in loading duration, compared with a 4 mm diameter sample of similar E_Y, indicates that a successful loading protocol for relatively soft hydrogels should consider using larger sample geometries.

To evaluate the applicability of MATE stimulation for mature samples, cartilage explants (Ø

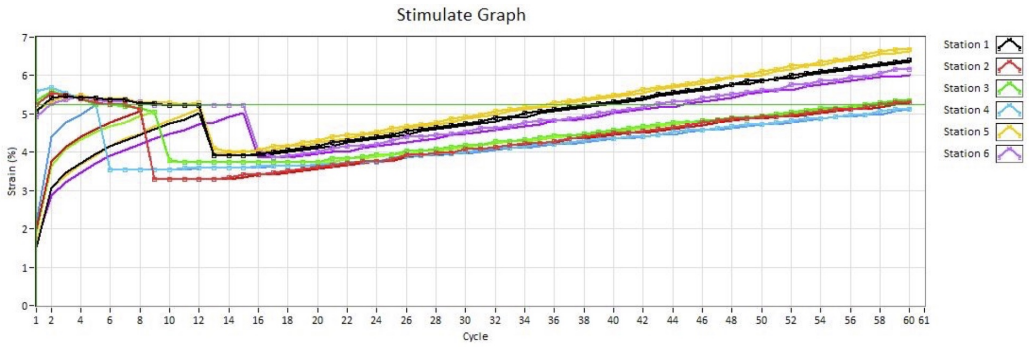

Figure 3.4: Stimulation of 6 mm diameter, acellular 2% agarose constructs at 3% test strain resulted in system power down within 10 cycles. The solid line indicates the minimum strain at each cycle. The line with symbols at each cycle indicates the maximum strain.

3 mm, E_Y = ~500 kPa) isolated from juvenile calf knees were subjected to the identical protocol as above (2% pre strain, 3% test strain, 1.0 Hz for 60 cycles) (Figure 3.5). Following 15 cycles, on average, the strain differential neared zero and the VCMs were disengaged. These results, however, indicate that the mechanical properties of the tissue play a substantial role in success of the loading protocol and suggests that mature samples improve chances for successful, continuous stimulation.

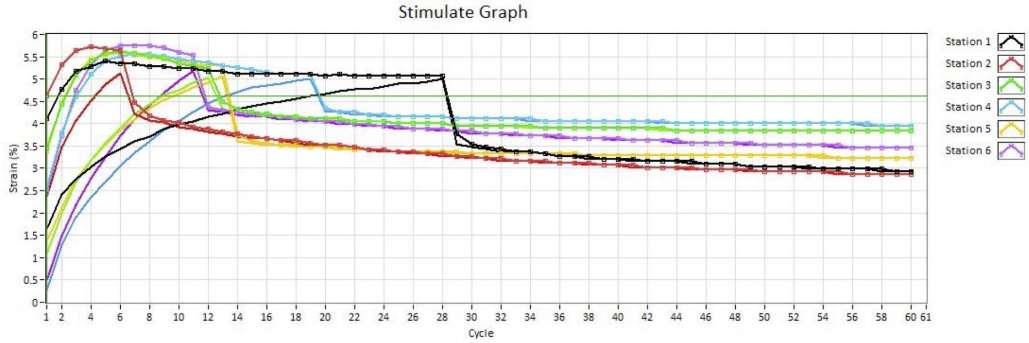

Figure 3.5: Stimulation of 3 mm diameter, juvenile bovine explant at 3% test strain resulted in system power down within 15 cycles. The solid line indicates the minimum strain at each cycle. The line with symbols at each cycle indicates the maximum strain.

Building on the results discovered with both large, soft hydrogels and small, stiff hydrogels, the final evaluation of strain-controlled stimulation involved a mature (~75 kPa), large diameter (Ø 6 mm) engineered cartilage construct. Stimulation of these samples was similar to previous efforts.

Unlike previous attempts with softer and smaller samples, stimulation of mature, large diameter constructs was able to proceed for nearly 4 minutes (Figure 3.6). Like previous attempts, however, strain-controlled stimulation resulted in a shortened loading program (compared with 3 hours for

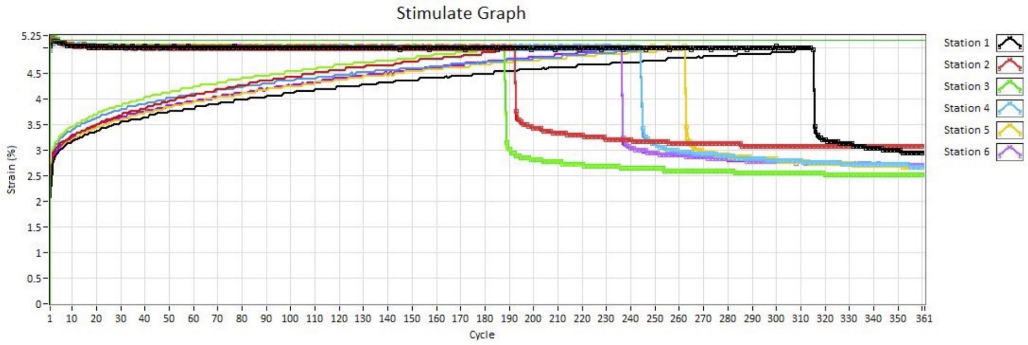

Figure 3.6: Stimulation of 6 mm diameter, mature tissue-engineered cartilage constructs at 3% test strain resulted system power down following 240 cycles. The solid line indicates the minimum strain at each cycle. The line with symbols at each cycle indicates the maximum strain.

established protocols (Lima *et al.* , 2007; Mauck *et al.* , 2000b)) and a diminished tissue thickness. Prior to subsequent stimulation, complete relaxation of the sample must occur. Because of this, a strain-controlled loading approach to tissue-engineered or explant cartilage becomes impractical, as the time necessary for full equilibration of the sample results in a maximum of 12 daily sequences. This fact, along with conclusions regarding tissue diameter and stiffness, formed the baseline for evaluation of the MATE via force-controlled stimulation.

Beginning with a 6 mm diameter sample of sufficient stiffness (∼75 kPa), force parameters (0 N pre load, 0 N → 10 N test load), loading frequency (1 Hz → 10 Hz), and cycle duration were modified to optimize the force-controlled stimulation protocol. Working within the limitations of the MATE (each station can only apply 10 N), the determination was made to select the loading frequency that allowed for the largest force to be applied without disengaging the VCMs. The use of a 5 N test load applied at 10 Hz for 3 cycles allowed for near 'elastic' tissue deformation that was able to recover within a 20 minute rest period. Moreover, the real strain observed in the tissue with these parameters was ∼10%, similar to the strain applied in our previously established dynamic loading model (Mauck *et al.* , 2000b). Using the MATE, this force-controlled protocol can be employed for continuous loading of engineered tissues, 24 hours a day, with no input from the user.

3.4 Application

Now optimized, this force-controlled protocol was applied to our cartilage tissue engineering system to evaluate its potential to produce mechanically superior tissues when compared to free-swelling controls. As described above (Chapter 3.2.2), two different cell sources were used in this work.

Initial application of the MATE utilized juvenile bovine chondrocytes. Following 35 days of culture, the average proteoglycan content of the engineered tissues was 3.59 ± 0.27% GAG/ww. Following 21 days of force-controlled stimulation, the proteoglycan content of both free-swelling (FS) and dynamically stimulated (DS) tissues reached near-native values (4.97 ± 0.57% for FS, 5.93 ± 0.39% for DS), showing a significant improvement in the proteoglycan content of DS tissues ($p<0.01$) (Figure 3.7a). As verification that tissue growth was a function of direct tissue deformation and not fluid flow, MATE tissues not directly stimulated contained biochemical properties statistically similar to FS controls ($p=0.21$ for GAG, $p=0.32$ for DNA, $p=0.61$ for collagen). This increase in proteoglycan content in DS tissues was reflected in the 'elastic' modulus as measured by the MATE. Following 3 weeks of stimulation, the 'elastic' modulus of DS tissues was significantly higher than FS tissues, reaching 825.21 ± 139.19 kPa compared with 640.53 ± 60.44 kPa ($p<0.05$). As a validation measure, this increasing trend in 'elastic' modulus was preserved in E_Y of DS and FS tissues, with DS tissues reaching nearly 160 kPa by the final time point. While there was no change in the collagen content of these tissues, as was seen in previous studies of strain-controlled samples (Chapter 2), a significant change in cellularity was observed in response to dynamic stimulation. Following stimulation, DS tissues contained significantly more chondrocytes than did FS controls, proliferating to 1.5x the cellular content of FS tissues by day 56 in culture ($p<0.05$). As a proof of concept, these results demonstrated that MATE stimulated tissues can, under an optimized loading protocol, cultivate mechanically superior engineered tissues.

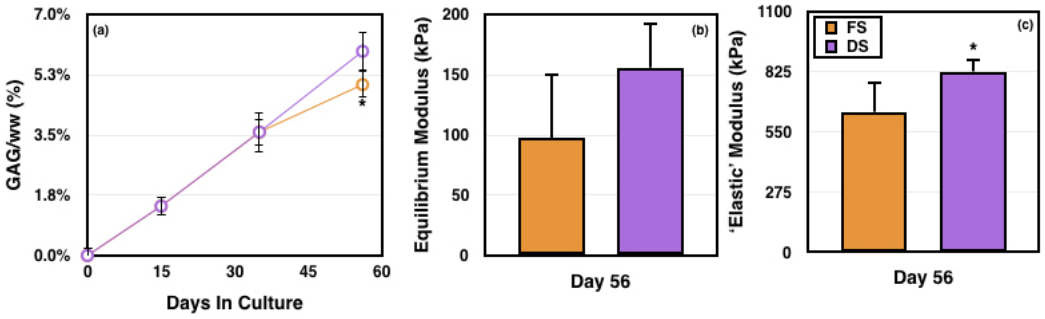

Figure 3.7: Analysis of juvenile bovine chondrocyte engineered tissues following MATE stimulation. GAG concentration (a) was significantly increased in DS tissues by day 56 in culture ($p<0.01$). While the 'elastic' modulus of DS tissues was significantly higher than FS controls ($p<0.05$), substantial sample variance during testing resulted in only trending differences in E_Y of these tissues.

Following successful application of MATE to a juvenile population of cells, this DS protocol was extended to a clinically relevant cell source, adult human chondrocytes. Following culture for 35 days, a subset of these tissues was dynamically stimulated for the following 4 weeks. At the onset of DS, the MT-measured equilibrium modulus of all tissues was 54.15 ± 16.65 kPa. Significant growth ($p<0.05$) occurred over the next 4 weeks in both FS and DS tissues. By day 64, the GAG content in all groups developed to nearly 4% GAG/ww. Notably, the GAG content of dynamically stimulated tissues was significantly higher than the GAG content of free-swelling tissues ($p<0.05$) (Figure 3.8a).

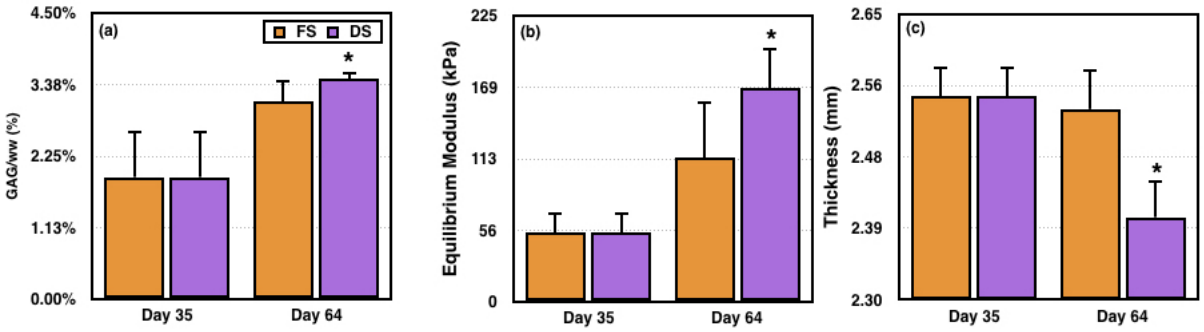

Figure 3.8: Analysis of adult human chondrocyte engineered tissues following MATE stimulation. GAG concentration (a) was significantly higher in DS tissue by day 64 in culture ($p<0.05$). Likewise, there was a significant increase ($p<0.05$) in E_Y (b) measured in DS samples at the final time point. Of note, the thickness (c) of stimulated tissues was significantly reduced following 4 weeks of force-controlled loading.

This relationship in GAG content was preserved in the mechanical properties of the tissue. By day 64, dynamically stimulated tissues measured 167.96 ± 31.56 kPa compared with 113.13 ± 44.31

kPa for free-swelling tissues, a significant increase in E_Y ($p<0.05$). This robust response in adult human engineered cartilage is promising for future applications of the MATE for clinically-relevant cartilage tissue engineering applications.

3.5 Conclusion

The results of this work demonstrate the potential benefits of the MATE bioreactor for tissue engineering applications.

Because of the specifications of the device, however, there are important factors to consider when using the MATE. If a strain-controlled protocol is desired, the sample being stimulated must be of sufficient stiffness and diameter (Figure 3.6) to prevent substantial compression following application of load for thickness measurement. Even so, as cartilage is viscoelastic, the tissue will creep away from the loading surface as stimulation is applied. This reduction in sample height, along with sample diameter, should be considered in determining the time allowed between loading sequences. Modifications of the loading chamber itself may allow for continuous strain-controlled stimulation similar to established protocols (Mauck *et al.* , 2000b; Kelly *et al.* , 2006; Lima *et al.* , 2007), producing a sinusoidal loading pattern (10% peak-to-peak strain) that operates within the load and travel limitations of the device (Figure 3.9). The use of an elastic spring obviates the complication of thickness measurement, as the spring returns instantaneously to its original length following the release of load. The use of a spring is not practical in all cases, however, and requires maximum effort from the MATE, leading to excess heat production and potentially negative impacts on chondrocyte viability. More investigation should be performed prior to implementing this strategy for cellular work.

While the use of an elastic spring would produce an effective 10% strain in tissue-engineered samples, the merits of a global zero, strain-controlled approach are debated. Stimulation of cartilage, a viscoelastic material, will result in creep upon continued stimulation. In certain situations, this may lead to compaction of the tissue, as illustrated in this work (Figure 3.8c). This may improve mechanical and normalized biochemical properties of the tissue, as the same biochemical constituents are now occupying a smaller volume. Concurrent with compaction, the use of a global zero leads to lift-off (Mauck *et al.* , 2000b) from the surface during unloading, a phenomenon sometimes experienced *in vivo* in the lateral compartment of patients with OA (Kumar *et al.* , 2013).

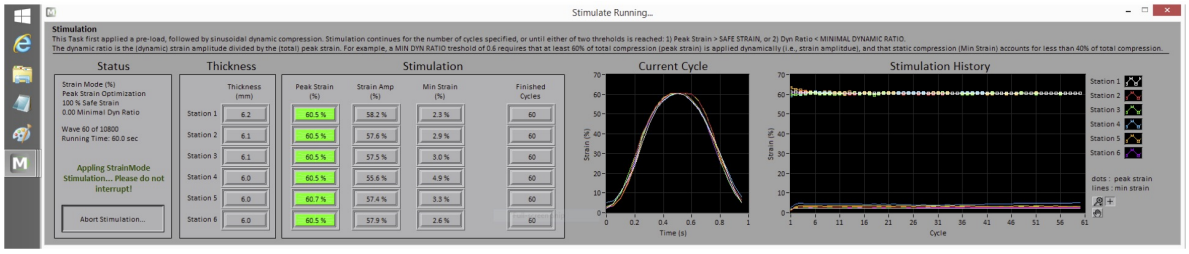

Figure 3.9: Following the addition of a spring, displacement could be controlled so that the force response in the spring was the primary driver of VCM action. Matching the length with the correct spring constant, the tissue sample is compressed to 90% of the original thickness. The waveform under 'Current Cycle' indicates the shape of each cycle. The two sets of lines under 'Stimulation History' indicate the measured maximum and minimum strain values for each cycle it has completed.

In contrast, the MATE provides continuous monitoring of tissue geometry, ensuring sample contact throughout stimulation. The advantages and disadvantages of both approaches merit further investigation.

Using the MATE in force-controlled mode offers a more broadly applicable approach. In contrast to strain-controlled loading, a force-controlled approach allows the tissue to strain as much or as little as necessary, and is not constrained by peak strain optimization during stimulation. Importantly, the optimized force-controlled approach used in the tissue engineering studies described above (Figure 3.7, 3.8) improved the mechanical and biochemical properties of these tissues. Moreover, this is the first report, to our knowledge, of clinically-sized (Ø 8 mm) engineered cartilage, developed from primary adult human chondrocytes, to achieve near native E_Y values.

As a bioreactor, the MATE provides the opportunity to continuously, and independently, stimulate and monitor tissue growth *in vitro*. Unlike standard tissue culture practices, this eliminates the need for tissue sacrifice at study time points. Further, the ability to analyze and stimulate tissues within the same device may allow for bioreactor cultivation of clinical tissues prior to implantation, using the MATE to assess individual tissue properties and select tissues best suited for *in vivo* application. Together with the work presented in Parts II and III of this dissertation, the MATE may one day allow for cultivation of the ideal osteochondral plug, impregnated with chondroprotective dexamethasone-loaded MS, and exhibiting anatomically-shaped, patient-specific contours optimized for clinical success.

3.6 Acknowledgments

The MATE bioreactor was used in collaboration with APEX Biomedical, LLC. This research was supported by the Musculoskeletal Transplant Foundation Established Investigator Grant (C.T.H.), National Institutes of Health (AR060361 [C.T.H., G.A.A.], AR068133 [C.T.H.], 5T32AR059038 [B.L.R.]), and National Science Foundation Graduate Research Fellowship Program under Grant No. DGE-11-44155 (B.L.R.).

Part II

Dexamethasone-Loaded PLGA Microspheres

Chapter 4 Fabrication and Characterization of Dexamethasone-Loaded Poly(lactic-*co*-glycolic acid) Microspheres

4.1 Introduction

Poly(lactic-*co*-glycolic acid) (PLGA) was first introduced in the 1970s as a material for bioresorbable sutures. Comprised of poly(lactic acid) and poly(glycolic acid) linked by a hydrolyzable ester bond (Figure 4.1), this physically strong and biocompatible material is currently employed clinically in a number of FDA-approved products. *In vitro*, PLGA has been extensively explored as a vehicle for drug delivery and as a scaffold for tissue engineering, having been used to encapsulate a variety of drugs, proteins and other macromolecules such as DNA, RNA, and peptides (Bouissou *et al.* , 2006; Jain, 2000; Ruhe *et al.* , 2003). The ability to optimize loading efficiency and the rate of payload release via modification of manufacturing parameters (e.g., microsphere size, copolymer composition, polymer molecular weight, excipients) make PLGA an attractive material for drug delivery applications. Therapeutic strategies using PLGA as a drug-delivery system are currently being developed for osteoarthritis (Elsaid *et al.* , 2016; Kumar *et al.* , 2015), eye disorders such as a age-related macular degeneration (Rodríguez Villanueva *et al.* , 2016), neurodegenerative disorders (Kim & Martin, 2006), and malignant lymphomas (Alimohammadi & Joo, 2014), among others.

Exploiting the tunability of this system, PLGA-based micro- and nanoparticles have been devel-

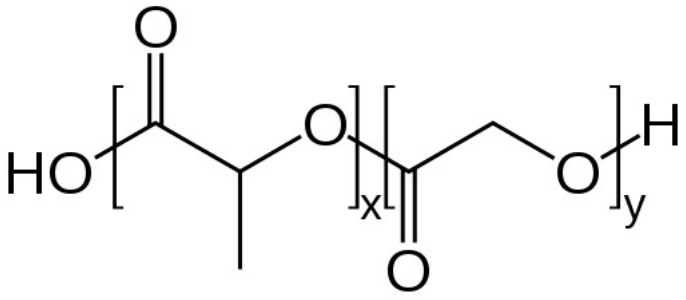

Figure 4.1: The chemical structure of PLGA. Hydrolyzed via water penetration at the ester linkage, the rate of degradation of PLGA is governed fundamentally by the ratio of the co-polymer, PLA:PGA. The higher the percentage of PLA in the copolymer (PLA contains a hydrophobic methyl side group), the less rapid the rate of degradation.

oped to encapsulate anti-inflammatory compounds for a variety of applications (Dang *et al.* , 2011; Galeska *et al.* , 2005; Tang *et al.* , 2010; Bae *et al.* , 2010; Hickey *et al.* , 2002b; Hickey *et al.* , 2002a; Rubin *et al.* , 2009; Kelmendi-Doko *et al.* , 2014; Elsaid *et al.* , 2016). Hickey et al. employed PLGA microspheres for continuous delivery of dexamethasone to inhibit the inflammatory host response to implantable medical devices (Hickey *et al.* , 2002a; Dawes *et al.* , 2010; Dang *et al.* , 2011; Galeska *et al.* , 2005). Addressing the issue of inflammation in the myocardium, Fargnoli et al. employed PLGA nanoparticles for the delivery of aspirin and prednisolone, a synthetic glucocorticoid, offering a potential clinical approach to maximize cardiac gene therapy while minimizing the risk of host response (Fargnoli *et al.* , 2014). Gu, et al. evaluated the *in vivo* and *in vitro* performance of dexamethasone-loaded PLGA microspheres as a strategy for mitigation of the foreign body reaction. In this study, dex-loaded microspheres demonstrated 4.5 months of anti-inflammatory efficacy *in vivo*, ameliorating a major cause of dysfunction and extending the usable lifetime of implanted glucose biosensors (Gu & Burgess, 2015; Gu *et al.* , 2015).

In the context of the knee joint, sustained delivery systems are an attractive alternative to intra-articular (IA) injections of corticosteroids. While shown effective in reducing pain in some patients for up to 2 years (Raynauld *et al.* , 2003), rapid clearance from the joint space necessitates highly concentrated injections, upwards of 2 mg/mL (MacMahon *et al.* , 2009). This dosage increases the risk of local cartilage damage (Wernecke *et al.* , 2015), can negatively impact gastrointestinal function (Singh, 1996), and reduces the body's ability to respond to infection (Singh, 1996; Glaser & Kiecolt-Glaser, 2005). To this end, PLGA-based delivery systems have been employed in articular cartilage applications to deliver anti-inflammatory molecules at safe but effective doses. Interleukin 1 receptor antagonist (IL-1ra) (Morisset *et al.* , 2007), an FDA-approved therapy for the treatment of rheumatoid arthritis (Kimmerling *et al.* , 2015), has been encapsulated in PLGA microspheres and shown to inhibit lymphocyte activity and cartilage degeneration (Elsaid *et al.* , 2016). Higaki et al. demonstrated that the continuous administration of betamethasone sodium phosphate via PLGA nanoparticles inhibited inflammation in an experimental model of osteoarthritis (Higaki *et al.* , 2005).

While glucocorticoids, and dexamethasone specifically, demonstrate anti-catabolic effects *in vitro (Lima* et al. *, 2008a)* and *in vivo* (DeRijk *et al.* , 1997), these steroids are also employed in cartilage tissue engineering for their prochondrogenic and proanabolic effects (Florine *et al.* , 2012; Bian

et al. , 2010b; Lima *et al.* , 2004; Lima *et al.* , 2008a; Huang *et al.* , 2016b; Wang *et al.* , 2005). Dexamethasone has been used in the differentiation of adipose derived stem cells and mesenchymal stem cells (Diekman *et al.* , 2010; Johnstone *et al.* , 1998; Yoon *et al.* , 2012), has been implicated in the integrity of collagen crosslinks (Roach *et al.* , 2016; Athens *et al.* , 2013; Bian *et al.* , 2010b), and is instrumental for the development and maturation of functional tissue-engineered cartilage (Lima *et al.* , 2008a; Henderson *et al.* , 2007; Ng *et al.* , 2010; Tan *et al.* , 2015; Bian *et al.* , 2009a; Huang *et al.* , 2016b). Used in our laboratory for the culture of tissue-engineered cartilage derived from human chondrocytes, dexamethasone catalyzes tissue growth, with constructs reaching near-native values of mechanical properties and proteoglycan content by only 4 weeks in culture (Cigan *et al.* , 2016).

Informed by the combined benefits of PLGA MS and dexamethasone, and work performed by the Adipose Stem Cell Research Laboratory at the University of Pittsburgh (Kelmendi-Doko *et al.* , 2014; Rubin *et al.* , 2009), led by Dr. Kacey Marra, the following methodologies describe the fabrication of dexamethasone-loaded PLGA microspheres for cartilage tissue engineering applications.

4.2 Methods

4.2.1 Dexamethasone 21-phosphate phosphate disodium salt encapsulation

Dexamethasone-loaded PLGA microspheres (MS) were prepared using a double emulsion (water-oil-water) technique. First, a 0.2% poly(vinyl alcohol) (PVA; Sigma 360627), 150 mM sodium chloride (NaCl, Sigma S6191) solution was prepared in 700 mL distilled, de-ionized water (ddH_20) and stirred at 550 rpm. 100 mg of PLGA (75:25) (Sigma P1941), under vigorous vortexing, was dissolved in 4.5 mL dichloromethane. Dexamethasone 21-phosphate disodium salt (dex; Sigma D1159) was dissolved in 0.5 mL methanol and added to the PLGA solution. Following vortex of the PLGA-dex mixture, the resulting emulsion was slowly added to the stirring PVA/NaCl bath.

Following 3 hours of stirring, the microspheres were collected by centrifugation (3,000 rpm for 5 minutes) and frozen at -20°C overnight. Following freezing, collected microspheres were freeze-dried for at least 48 hours prior to use. Unloaded MS were prepared similarly, omitting the addition of dex.

4.2.2 Dexamethasone release and loading capacity measurement

The release of dex from the MS was analyzed both as free-floating MS and as encapsulated within an acellular agarose hydrogel. In both cases, releasates were analyzed spectrophotometrically at 242 nm, a natural absorbance wavelength for most compounds, dex included. The amount of dex released was determined via comparison with standard curve. Preparation of standards is described in Appendix A.2.

For free-floating MS, microspheres (10 mg) were placed in a microcentrifuge tube containing 1 mL phosphate buffered saline (PBS) (n=5). At various time points the tubes were centrifuged, the supernatant collected, and then frozen at -20°C until analysis. The samples were refreshed with 1 mL PBS and vortexed.

For encapsulated MS, acellular agarose hydrogel constructs (Ø 6.0 x 2.34 mm) were produced by preparing a 2% agarose (Sigma A9414) hydrogel containing 5.33 mg MS/mL agarose. Constructs were isolated in a microcentrifuge tube in 1 mL (PBS) (n=4). At various time points the supernatant collected and then frozen at -20°C until analysis.

Loading capacity was determined via complete polymer hydrolysis. Briefly, 1 mL dimethyl-sulfoxide (DMSO) was added to 5 mg MS. The mixture was briefly vortexed and allowed to rest for 1 hour. Following rest, the mixture was vortexed again for 30 seconds and then 5 mL of 0.05 NaOH containing 0.05% w/v sodium dodecyl sulfate was added. The mixture was vortexed and allowed to rest for an additional hour. Following rest, aliquots of this mixture were assessed via spectrophotometry at 242 nm and results were compared to a standard curve.

Discussed in more detail in Appendix A.1, high pressure liquid chromatography, not necessary for these *in vitro* release studies, is ideal for assessing small concentrations (<100 ng) of dexamethasone.

4.2.3 Microsphere characterization

Morphological characterization of the MS was performed using scanning electron microscopy (SEM). MS were were coated for 45 seconds with gold-paladium using a Cressington 108auto (Cressington). MS were then viewed using an EVO LS SEM (Zeiss) operated at 2 kV extra high tension voltage level. Images were acquired from 250 X-1.5k X for morphological analysis and to allow for particle sizing during post-processing.

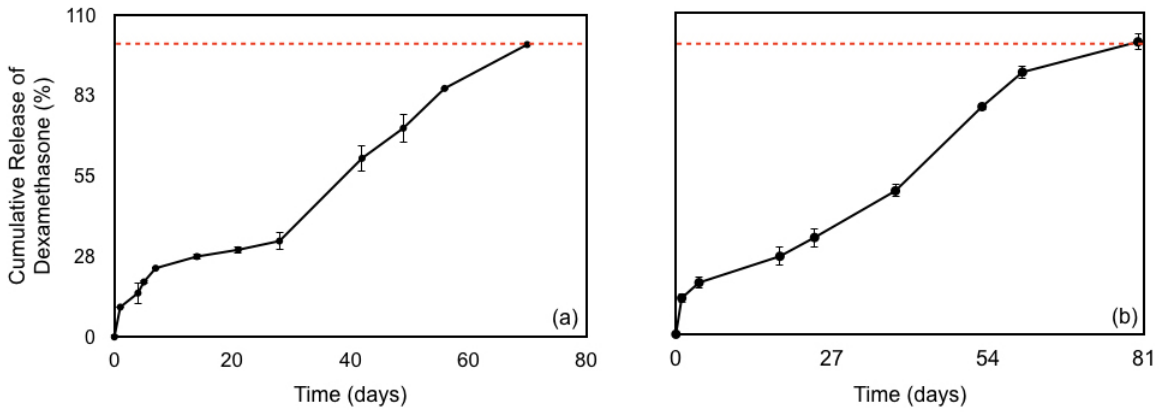

Figure 4.2: Dexamethasone release curves for (a) free-floating and (b) agarose encapsulated dex PLGA MS. The red hyphenated line indicates 100% release.

4.3 Results

4.3.1 Dexamethasone release and loading capacity measurement

Dexamethasone release was similar between free-floating and agarose encapsulated MS. For free-floating MS (Figure 4.2a), a burst release of 10.2% was observed after 24 hours. A linear fit of subsequent release data (R^2=0.97) yielded a daily release rate of 250 ng dex per mg MS. After 28 days in culture, 32.8% of dex had been released. The loading capacity was 19.9 mg dex per mg MS. For agarose encapsulated MS (Figure 4.2b), a minimal burst release of 12.37% was observed in the first 24 hours. Fitting the subsequent release data to a line (R^2=0.97) over the next 90 days, a daily release rate of 284 ng dex per mg MS, equivalent to 46.24 ng dex/construct/day (for a Ø 4 mm construct), was measured. The loading capacity of the agarose encapsulated MS, determined via DMSO hydrolysis, was measured to be 63.31 µg dex/mg MS.

4.3.2 Microsphere characterization

Morphological characterization of dex MS can be seen in Figure 4.3. The average diameter of dex-loaded microspheres was 46.03 ± 16.67 µm (n=543). The average diameter for unloaded microspheres was 25.02 ± 15.39 µm (n=411).

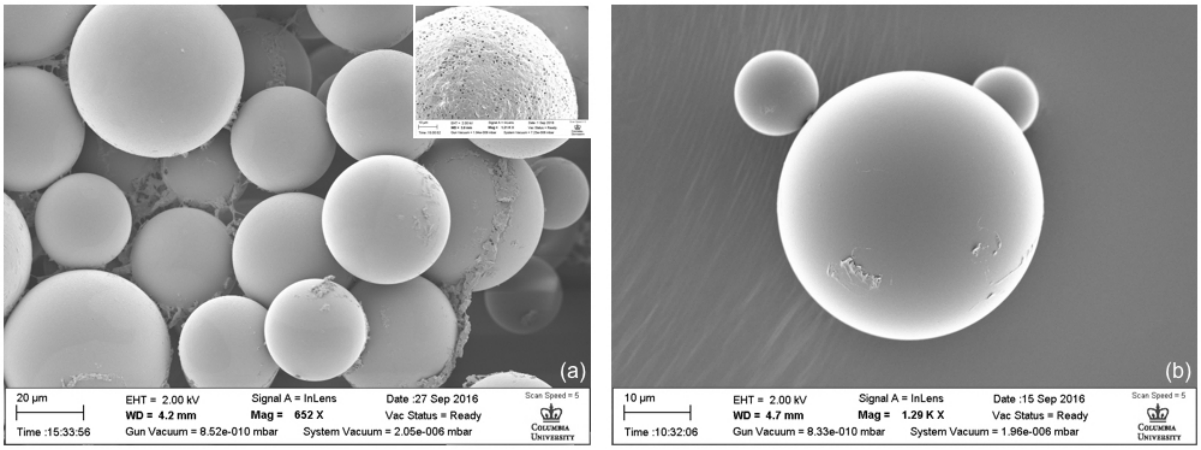

Figure 4.3: Scanning electron micrograph of (a) dex-loaded and (b) unloaded PLGA MS. Inset: PLGA MS prepared with 0 mM NaCl.

4.4 Conclusions

4.4.1 Manufacturing parameters

As alluded to in the introduction, there are many parameters that affect PLGA MS fabrication. The potential pharmacokinetic impact of a change in even one parameter can be significant. Several studies have illustrated the impact of these parameters (e.g., drug hydrophilicity, surfactant concentration, bath osmolarity, molecular weight of PLGA, viscosity of PLGA) on the resulting paricle size, loading efficiency, and release kinetics of PLGA MS (Ito *et al.* , 2007; Gasparini *et al.* , 2008; Mao *et al.* , 2007; Siegel *et al.* , 2006; Gu & Burgess, 2015; Rodríguez Villanueva *et al.* , 2016). In our investigations, changing the osmolarity of the bath from 0 mM NaCl to 150 mM NaCl improved the loading efficiency of dexamethasone by 50%. This change in bath osmolarity improved the salt balance inside and outside the PLGA MS, preventing the rapid osmotic flux that can result in pitting (Figure 4.3, Inset). A function of stirring speed and polymer addition rate, particle size, along with previously mentioned parameters, greatly influences degradation rate and drug release kinetics. While slowing the stirring speed of the bath may allow for increased loading efficiency of the drug in some cases, the resulting size increase of the particle will likely lead to expedited release of the drug, as carboxylic acid end groups, a result of biodegradation, accumulate inside the particle and create an acidic environment that autocatalyses the degradation process.

Because of the many parameters involved, it is critical, especially for cellular-based studies, that

MS fabrication be consistent and reliable. In this investigation, the current parameters allow for fabrication of MS of a controlled size with zero-order release kinetics to nearly 100 days. A controlled, linear release makes it possible to use dex-loaded MS at concentrations within the hydrogel that are equivalent to those used via exogenous supplementation (100 nM, (Lima *et al.* , 2008a)). Reliable fabrication makes direct comparisons of tissue growth possible and allows for improved accuracy in modeling of dex release kinetics.

4.4.2 Clinical relevance

A controlled release approach to steroid administration is advantageous in the context of current therapies for early intervention in OA. The inherently short duration of therapeutic action for corticosteroids (Goodman, 1996), and dex (6–8 days (Wernecke *et al.* , 2015)) in particular, suggest that more frequent injections may improve joint pain. The accumulated availability of glucocorticoids through repeated injections, however, has been shown to lead to gross morphological cartilage changes (Breuner & Orchinik, 2002) along with lowered viability and biosynthetic activity of chondrocytes (Song *et al.* , 2012). Successively elevated systemic levels of glucocorticoid can also impact the hypothalamus–pituitary–adrenal axis, (Habib, 2009) inhibiting the immune system's ability to respond to infection. Low dose, sustained delivery of glucocorticoids, as presented in this work, provides a forward thinking strategy for improving cartilage repair while minimizing negative systemic effects. The fabrication protocol described here produces dex-loaded MS with narrowly-distributed particle sizes (∼45 µm) and a sustained release profile of up to 90 days (Figure 4.2b), maintaining a consistent level of drug release throughout. Daily release of the drug is measured at only ∼46 ng per construct, a level 17.5x lower than the amount used in standard tissue culture (Lima *et al.* , 2008a) and 5.5x lower than commonly used triamcinolone acetonide IA injection dosages (Wilusz *et al.* , 2008; Wernecke *et al.* , 2015; Shepherd & Seedhom, 1999; Parma *et al.* , 1988). While the dex-loaded MS detailed here are meant for incorporation into tissue-engineered cartilage, Flexion Therapeutics, a specialty pharmaceutical company, has recently completed a Phase III clinical trial evaluating the pain reduction potential of FX006 (Zilretta^{TM}), a PLGA-based delivery system for the sustained release of low levels of triamcinolone acetonide (Kumar *et al.* , 2015). Early results have shown clinically significant improvement of pain, stiffness, and function in patients with moderate to severe osteoarthritis, suggesting that our approach to tissue-engineered cartilage has

therapeutic translatability in a human population.

In addition, as an alternative to strategies that target specific pro-inflammatory cytokines, dex has broad potential to mitigate the deleterious effects of IL-1, TNF-α, and other cytokines associated with inflammation. Once internalized, dex acts directly and indirectly by activating anti-inflammatory proteins (Hafezi-Moghadam *et al.* , 2002; Cato *et al.* , 2002), upregulating their production through glucocorticoid-responsive elements on DNA (Nagaich *et al.* , 2004; McKay & Cidlowski, 1999), and by interfering with the translocation of other transcriptional factors, such as nuclear factor-kappa B (McKay & Cidlowski, 1999; McKay & Cidlowski, 1998; De Bosscher *et al.* , 2003). These cell-independent mechanisms of action allow this strategy for dex delivery to be considered as a therapeutic approach for inflammation in other tissues and organ systems.

4.4.3 Future work

4.4.3.1 Modeling drug release It is important to know and be able to control the rate of drug release, and thus local drug concentration, from PLGA MS. Nearly fitting a simple zero-order model of release (Hines & Kaplan, 2013), the current MS can be used and a linear rate of drug release can be expected. Changes to any number of the manufacturing parameters, however, may alter these drug release kinetics and lead to temporally unpredictable local drug concentrations. In the case of cartilage tissue engineering applications, this may lead lower than expected doses of dex, and thus an inability to provide chondroprotection in the face of inflammatory cytokines.

Drug release assays, which can last up to 3 months (Figure 4.3), make continuous modification and improvement of the PLGA MS system impractical. For this reason, drug release models should be investigated and incorporated into PLGA MS design so that improvements in MS fabrication can be made concurrently with advances in cartilage tissue engineering.

4.4.3.2 Cartilage tissue engineering The parameters selected for dex-loaded MS fabrication provide a drug release profile appropriate for cartilage tissue engineering applications (Lima *et al.* , 2008a). Initial studies using these MS will confirm the activity and ability of internally released dex to foster tissue growth at a rate comparable to exogenously supplemented dex. Moreover, the internal delivery of dex allows for consideration of *in vivo* applications. One component of the knee's harsh environment, chemical insult via pro-inflammatory cytokines can be detrimental to

the biochemical and mechanical properties of tissue-engineered cartilage. This, in turn, decreases the chances for implant survival *in vivo*. Capitalizing on the anti-inflammatory properties of dex described above and in work from our lab (Lima *et al.* , 2008a), dex-loaded MS may be considered as a strategy to provide chondroprotection to engineered cartilage following implantation. Continued dex delivery *in vivo*, an approach discussed further in Chapter 5, may increase the chances for implant survival via chondroprotection, improved integration with host tissue (Djouad *et al.* , 2009), and maintain mechanical sufficiency of the implanted tissue.

4.5 Acknowledgments

This research was supported by the National Institute of Arthritis and Musculoskeletal and Skin Diseases of the National Institutes of Health under Award Number R01 AR60361 and T32 AR059038. The content is solely the responsibility of the authors and does not necessarily represent the official views of the National Institutes of Health. Funding support from the Coulter Foundation, the Musculoskeletal Transplant Foundation, and a NSF Graduate Fellowship (BLR) is also acknowledged.

Chapter 5 Dexamethasone Release from Within Engineered Cartilage as a Chondroprotective Strategy Against Interleukin-1α

5.1 Abstract

While significant progress has been made toward engineering functional cartilage constructs with mechanical properties suitable for *in vivo* loading (see Chapters 2 and 3), the impact on these grafts of inflammatory cytokines, chemical factors that are elevated with trauma or osteoarthritis, is poorly understood. Previous work has shown dexamethasone to be a critical compound for cultivating cartilage with functional properties, while also providing chondroprotection from pro-inflammatory cytokines. This study tested the hypothesis that the incorporation of poly(lactic-*co*-glycolic acid) (PLGA) (75:25) microspheres that release dexamethasone from within chondrocyte-seeded agarose hydrogel constructs would promote development of constructs with functional properties and protect constructs from the deleterious effects of interleukin-1α (IL-1α). After 28 days of growth culture, experimental groups were treated with IL-1α (10 ng/mL) for 7 days. Reaching native equilibrium moduli and proteoglycan levels, dexamethasone-loaded microsphere constructs exhibited tissue properties similar to microsphere-free control constructs cultured in dexamethasone-supplemented culture media and were insensitive to IL-1α exposure. These findings are in stark contrast to constructs containing dexamethasone-free microspheres or no microspheres, cultured without dexamethasone, where IL-1α exposure led to significant tissue degradation. These results support the use of dexamethasone delivery from within engineered cartilage, through biodegradable microspheres, as a strategy to produce mechanically functional tissues that can also combat the deleterious effects of local pro-inflammatory cytokine exposure.

5.2 Introduction

Joint injury, especially in younger patients, dramatically increases the risk of developing OA (Roos *et al.* , 1995; Gelber *et al.* , 2000; Roos, 2005) and has been shown to produce radiological evidence of cartilage degeneration in 50–78% of patients within 20 years of the event (von Porat, 2004; Lohmander *et al.* , 2007). Restoration of damaged cartilage is performed in an effort to arrest or slow

the progression of joint degeneration. Living osteochondral allografts represent the gold standard for repair of joint defects greater than 2–3 cm^2 (Williams *et al.* , 2007). As the availability of suitable allografts is insufficient to meet the clinical demand, intensive research efforts are focused on the development of strategies to grow living replacement cartilage tissues. Our laboratory has focused on growing tissues appropriate for repair of focal defects and entire articular surfaces (Ateshian & Hung, 2005; Hung *et al.* , 2003; Hung *et al.* , 2004; Ng *et al.* , 2010; Roach *et al.* , 2015). The impacts of cytokines that contribute to joint inflammation and pain, however, which are elevated with iatrogenic injury (Amin *et al.* , 2009; Amin *et al.* , 2010; Houston *et al.* , 2013; Lotz & Kraus, 2010; Patwari *et al.* , 2003; D'Lima *et al.* , 2006; Goldring & Goldring, 2004), trauma, or OA, on joint repair are not often considered.

In clinical patients following acute ACL injury (Irie *et al.* , 2003), cytokines such as tumor necrosis factor α (TNF-α) and interleukin-1β (IL-1β) were significantly elevated from baseline 24 hours after injury. At 1 week, while reduced, these cytokines remained elevated above chronic levels. Tsuchida et al. analyzed the synovial cytokine profiles of patients undergoing microfracture or autologous cell implantation (ACI) for focal defect repair (Tsuchida *et al.* , 2014) and observed increased concentrations of inflammatory cytokines in the synovial fluid of injured as compared with healthy joints. The increased presence of cytokines in injured joints may contribute to the inferior clinical results observed for ACI in some patients (Vanlauwe *et al.* , 2011; Filardo *et al.* , 2013; Saris *et al.* , 2003; Ozsoy *et al.* , 2009), as elevated levels of inflammatory mediators have previously been shown to hamper cartilage regeneration (Yang *et al.* , 2006; Beekhuizen *et al.* , 2013; Rodrigo *et al.* , 1995). To this end, data from animal studies and early clinical trials suggest that early inhibition of the IA inflammatory response (e.g., 4 weeks) and posttraumatic injury of the knee may improve clinical outcomes (Olson *et al.* , 2014). Morisset et al. reported an improvement in cartilage repair following IA injection of an adenoviral vector carrying an IL-1ra gene (Morisset *et al.* , 2007), indicating that modulation of the joint's chemical environment may be beneficial for chondrocyte and tissue health (Elsaid *et al.* , 2015).

Palliative strategies for managing joint pain include anti-inflammatory analgesics such as non-steroidal anti-inflammatory drugs alongside IA injections of glucocorticoids or hyaluronan (Zhang *et al.* , 2008). IA glucocorticoid injections have proven effective in reducing pain in patients for up to 2 years with no deleterious effects to joint morphology (Raynauld *et al.* , 2003). A residence time

of only 36–72 hours, however, mandates that the concentration of injected solutions and suspensions be high, upwards of 2 mg/mL (MacMahon *et al.* , 2009). Rapid clearance from the joint space results in excess circulating glucocorticoids, which leads to increased susceptibility to viral infections and delayed wound healing (Glaser & Kiecolt-Glaser, 2005; Singh *et al.* , 1996) systemically, as glucocorticoids are effective in suppressing IL-β and TNF production by leukocytes (DeRijk *et al.* , 1997).

Complementary to its use in IA injections, dex, a synthetic glucocorticoid, has been reported to inhibit collagen degradation of cultured cartilage explants in response to interleukin-1α (IL-1α) (Saito *et al.* , 1999). Work in our laboratory has found that engineered bovine cartilage constructs with native properties can be protected from the deleterious effects of IL-1α by culture supplementation with dex, in a manner similar to native cartilage explants (Lima *et al.* , 2008a; Lima *et al.* , 2008b; Lu *et al.* , 2011). Additionally, preexposure to dex has been reported to prevent proteoglycan degradation and restore biosynthesis of cartilage explants exposed to TNF-α and mechanical injury (Lu *et al.* , 2011). Several in vivo studies have demonstrated the chondroprotective effects of dex as well. Repeated IA injection of high-dose dex, for instance, was observed to protect cartilage from damage in a lapine posttraumatic model of OA (Huebner *et al.* , 2014; Huebner *et al.* , 2013). Malfait et al. have demonstrated that dex inhibited proteoglycan degradation induced by IA injection of TNF-α (Malfait *et al.* , 2009). While effective, the continuous administration of drug through IA injection is not recommended, as this increases the risk of infection and patient discomfort, emphasizing the need for sustained release formulations (Gerwin *et al.* , 2006).

Recent work has exploited poly(lactic-*co*-glycolic acid) (PLGA) systems for the delivery of anti-inflammatory drugs (Dang *et al.* , 2011; Galeska *et al.* , 2005; Tang *et al.* , 2010; Bae *et al.* , 2010; Hickey *et al.* , 2002a; Hickey *et al.* , 2002b; Rubin *et al.* , 2009; Kelmendi-Doko *et al.* , 2014; Defail *et al.* , 2006). Higaki et al. demonstrated that the continuous administration of betamethasone sodium phosphate through PLGA nanoparticles provided increased inhibition of inflammation in an experimental model of OA when compared with the same dosage of betamethasone sodium phosphate delivered three times through IA injection (Higaki *et al.* , 2005). Dang et al. demonstrated that dex releasing PLGA microparticles are capable of suppressing the host response to implanted polymer materials in a mouse model. Notably, animals that received a higher drug loading treatment suffered an increased incidence of death within 7–10 days after administration, while a low

drug loading group maintained healthy body conditions, but still benefited from the drug's anti-inflammatory properties (Dang *et al.* , 2011). These studies demonstrate that locally delivered, low concentrations of anti-inflammatory steroids are capable of suppressing the local host response without the systemic impact observed with higher drug concentrations.

In the context of cartilage tissue engineering, our laboratory has broadly employed dex for its proanabolic and anticatabolic effects in cartilage tissue engineering systems (Florine *et al.* , 2012), its proven importance for cultivation of tissues with native properties, and its ability to confer chondroprotection against inflammatory cytokines (Lima *et al.* , 2008a; Lima *et al.* , 2008b; Dvorak *et al.* , 2002; Kuroki *et al.* , 2005). As these factors can impact clinical success of cartilage tissue engineering strategies, we sought to develop a more clinically focused cartilage tissue engineering approach utilizing the FDA-approved steroid dex. An ideal therapy would retain the benefits of dex on engineered cartilage without the requirement for its exogenous supplementation, obviating the systemic (Neustadt, 2006) and joint level complications associated with clinical injections of steroids (Backes *et al.* , 2013; Ikeuchi *et al.* , 2013). As such, the current study tested the hypothesis that the incorporation of PLGA microspheres (MS), with the ability to release dex from within chondrocyte-seeded agarose hydrogel constructs, would promote development of constructs with native mechanical properties and protect constructs from the deleterious effects of IL-1α, laying the foundation for future, clinically focused studies.

5.3 Materials and methods

5.3.1 Experimental design

To assess the potential for chondroprotection through internally released dex, PLGA MS, loaded with the steroid, were embedded in the tissue construct during gelation (Figure 5.1). Tissues were cultured in chondrogenic medium for 4 weeks before cytokine exposure to allow for sufficient tissue maturation (Miot *et al.* , 2012).

Following 4 weeks of culture in a chondrogenic medium, a subset of these tissues were treated with supraphysiological levels of inflammatory cytokine for 1 week (Figure 5.2). Following 1 week of treatment, tissues were evaluated for their mechanical and biochemical properties.

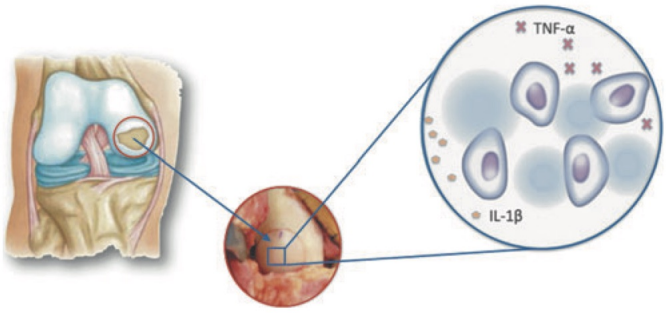

Figure 5.1: Representative schematic of the dex-loaded microsphere strategy employed in this study. PLGA microspheres are embedded alongside chondrocytes in an agarose hydrogel. In this way, dexamethasone is available locally to the cell to optimize the chondroprotective effects of the glucocorticoid against pro-inflammatory cytokines, such as interleukin-1 and tumor necrosis factor α. dex, dexamethasone; PLGA, poly(lactic-co-glycolic acid).

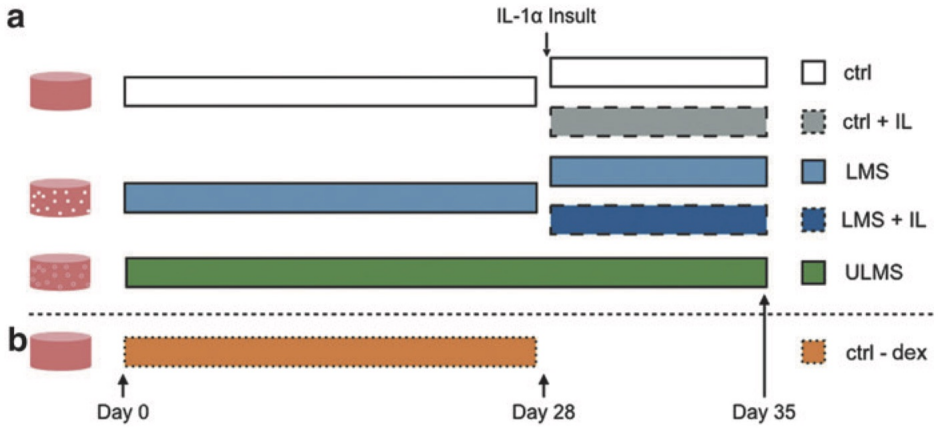

Figure 5.2: (a) Schematic of experimental design. ctrl and dex-loaded microsphere (LMS) tissues were treated with interleukin-1α (10 ng/ mL) after 4 weeks of culture. Unloaded microsphere (ULMS) samples, untreated, were cultured as a negative control for the duration of the study. (b) ctrl–dex tissues were cultured for the first 28 days of culture as a microsphere-free, dex-free control.

5.3.2 Microsphere fabrication and preparation

Dex-loaded PLGA MS were fabricated and characterized as described previously (Rubin *et al.* , 2009) and in detail in Chapter 4. Prior to use in the experiment, 8 mg of dex-loaded and empty MS were weighed and sterilized through ultraviolet light. Quantification of dex was performed as described for free-floating MS in Chapter 4.2.2.

5.3.3 Cell culture and sample preparation

As described previously (Lima *et al.* , 2007) and in Chapter 2.3.1, articular cartilage was harvested from stifles of freshly slaughtered 2- to 4-week-old calves. Three joints were used for the experiment and cells were pooled from all joints. Cartilage chunks were digested in 390 U/mL collagenase type IV (Worthington) for 11h with agitation. Isolated chondrocytes were passaged in Dulbecco's modified Eagle's medium (DMEM) containing 10% fetal bovine serum, 1 ng/mL TGF-β1, 5 ng/mL FGF-2, and 1% antibiotics/antimycotics. Following two passages, cells were prepared for encapsulation in an agarose (type VII; Sigma) hydrogel. For MS-free controls (ctrl, ctrl+IL, ctrl-dex), chondrocytes were seeded at 30 x 10^6 cells/mL in 2% agarose. For MS-containing samples (dex-loaded (LMS), LMS+IL, and empty microspheres (ULMS)), 1.5 mL of concentrated cell solution was combined with previously prepared MS. This cell/MS suspension was combined with 1.5 mL agarose and cast between glass slides for a final concentration of 2.66 mg MS per milliliter and 30 x 10^6 cells/mL in a 2% agarose hydrogel. This concentration of MS was selected as it has been previously shown to positively impact biosynthetic activity of human adipose stem cells (Rubin *et al.* , 2009). Cylindrical constructs (Ø 4.0 x 2.34 mm) were cored and cultured in chondrogenic medium as described previously (Chapter 2.3.1). MS-loaded tissues effectively received 21.9 ng dex/construct/day. MS-free controls received 100 nM dex at each media change (26.9 ng dex/ construct/day). MS-containing samples received no exogenous dex. A subset of MS-free tissues was cultured without dex for the first 28 days of culture to determine any adverse or beneficial effects of the PLGA on tissue development.

5.3.4 Cytokine insult

Following 28 days in growth culture, a subset of ctrl and LMS samples were subjected to 10 ng/mL IL-1α. IL-1α was added at each media change for 7 days. During this period, MS-free samples were starved of dex so as to isolate the potential impact of internally released dex in MS-loaded samples.

5.3.5 Mechanical characterization

A custom unconfined compression device was used to determine the equilibrium compressive modulus (E_Y) of whole samples at days 0, 14, 28, and 35 (n = 5), as described in Chapter 2.3.2. A custom glass-bottom device mounted on the stage of an inverted microscope (Wang *et al.* , 2001; Chahine *et al.* , 2004) was used to determine depth-dependent properties of ctrl and LMS samples on day 35. Before testing, samples were halved and maintained in a sterile PBS solution containing calcein-AM (Life Technologies). Following staining, samples were positioned with the cross-section facing the objective and initial measurements of thickness were performed digitally. As described in detail in Chapter 2.3.4, initial images of the cross-section were acquired followed by compression of the samples at nominal 5% strain increments to a final compression of 15%. Digital image correlation was used to obtain accurate axial and lateral strains (Wang *et al.* , 2001; Chahine *et al.* , 2004), which were combined with incremental compressive loading data to determine depth-dependent mechanical properties.

5.3.6 Biochemical characterization

Samples were thawed, lyophilized, weighted dry, and digested with 0.5 mg/mL proteinase K in 50 mM Tris-buffered saline containing 1 mM EDTA and 1 mM iodoacetamide. Biochemical assessement of GAG, DNA, and collagen, as well as histology for the same, were performed via established protocols (Stegemann & Stalder, 1967; Farndale *et al.* , 1986), as described in Chapter 2.3.5. The swelling ratio was also determined from tissue volumes at each time point normalized to average day 0 tissue volumes. Tissue maturity was assessed qualitatively and quantitatively (ImageJ) through histology, before freezing, and day 35 samples were fixed in acid formalin ethanol for histological staining.

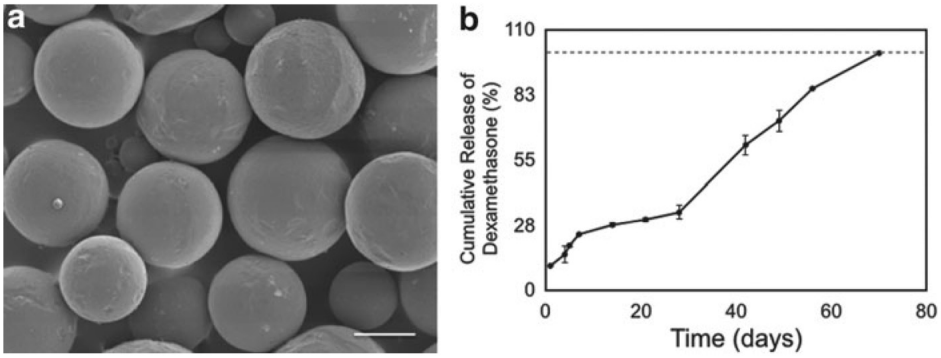

Figure 5.3: (a) SEM image. This image demonstrates consistent shape and size of the PLGA microspheres used in this study. Scale bar = 10 mm. (b) Cumulative release curve of dexamethasone released from 10 mg PLGA microspheres. By 70 days in culture, all dexamethasone had been released from within the microspheres. Dotted line indicates 100% release.

5.4 Results

5.4.1 Microsphere fabrication and preparation

MS were observed through scanning electron microscopy (Figure 5.3a) and determined to have an average diameter of 10 µm. A burst release of 10.2% ± 0.8% of initial dex content was observed after 24h. A linear fit of subsequent release data (R^2=0.97) yielded a daily release rate of 250 ng dex per milligram MS (Figure 5.3b). After 28 days in culture, 32.8% ± 1.1% of dex had been released. The loading capacity was 19.9 ± 1.9 mg dex per milligram MS. These results have been confirmed through high-performance liquid chromatography (Hickey *et al.* , 2002b; Lamiable *et al.* , 1986).

5.4.2 Bulk mechanical characterization

At day 0, there were no significant differences between MS and ctrl samples (4.8 ± 2.5 kPa vs. 2.7 ± 1.7 kPa). All groups displayed significant growth from day 0 to 28 ($p<0.05$) (Figure 5.4). By day 28, E_Y of all groups achieved ∼200 kPa (Figure 5.4a). ULMS and ctrl-dex samples developed similarly to this time point, indicating minimal negative or positive impact from PLGA degradation. Following treatment with IL-1α, the equilibrium modulus of ctrl+IL tissues dropped significantly ($p<0.05$). At day 35, ctrl tissues reached 527 ± 74 kPa, whereas ctrl+IL tissues dropped to 194 ± 98 kPa from 297 ± 101 kPa at day 28 (Figure 5.4d). LMS tissues reached 387 ± 80 kPa at day 28. Following cytokine exposure, LMS+IL tissues continued to mature to 645 ± 136 kPa, similar to

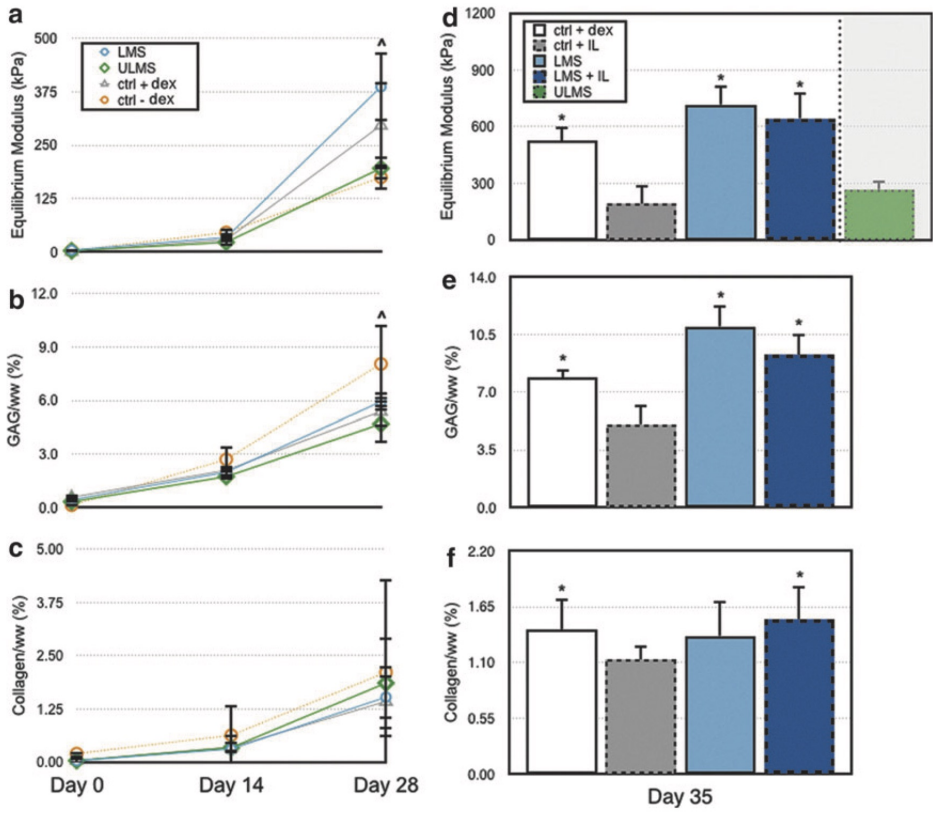

Figure 5.4: Mechanical and biochemical development of tissue-engineered cartilage throughout culture. ctrl-dex is provided as a reference for the first 28 days of growth. ULMS tissues exhibited poor growth at day 35 and were not included in other metrics. (a, d) Illustrate equilibrium moduli. (b, e) Illustrate the GAG content of engineered tissues throughout the study. (c, f) Illustrate the collagen content of engineered tissues throughout the study. * Indicates $p<0.05$ when compared with ctrl+IL at the same time point. ^ Indicates $p<0.05$ between LMS and ULMS. GAG, glycosaminoglycan; IL, interleukin.

LMS tissues that grew to 717 $\pm$ 99 kPa at the same time point. ULMS tissues, those that received neither dex nor IL-1α, reached 269 $\pm$ 49 kPa by day 35. As a result of its inferior mechanical properties at day 35, ULMS tissues were excluded from analysis in Figure 5.4e and Figure 5.4f.

5.4.3 Depth-dependent mechanical characterization

MS remained visible in the tissue at day 35 (Figure 5.5a). At day 35, strain distributions from both ctrl and LMS samples displayed tissue inhomogeneity consistent with previous work (Kelly *et al.* , 2006; Kelly *et al.* , 2013) (Figure 5.5b). While LMS tissues displayed a significantly higher ($p<0.05$) local equilibrium modulus than ctrl in 67% of the thickness of the tissue, tissue inhomogeneity does not appear to be impacted by the local delivery of dex.

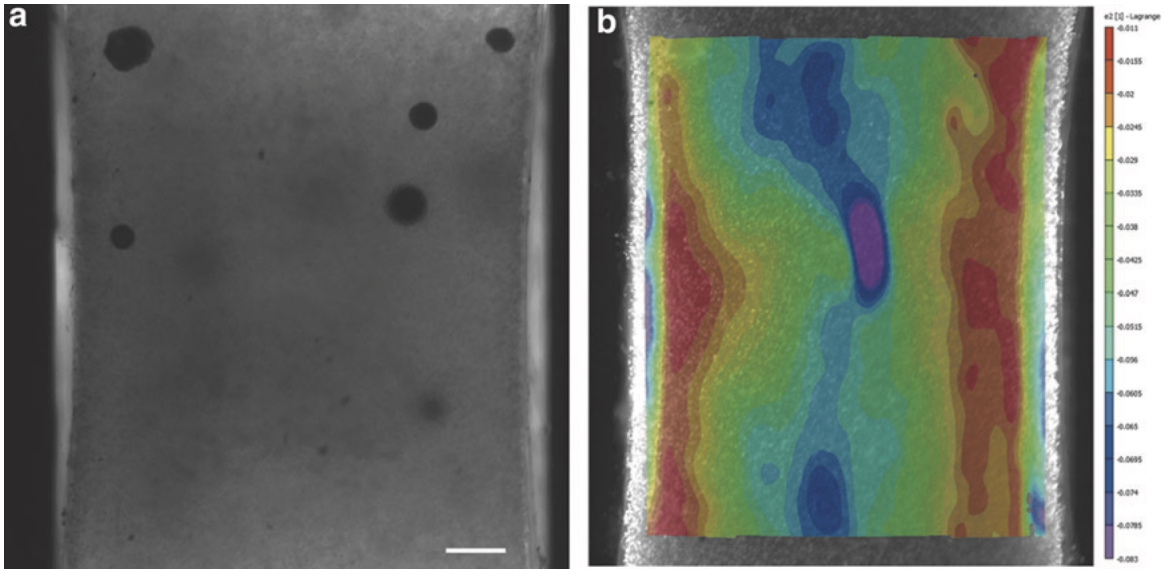

Figure 5.5: Cross-section of samples prepared for depth-dependent mechanical testing using a custom designed microscope testing device. (a) Transmitted light image of the cross-sectional area of LMS tissues at day 35. The amorphous shape of certain microspheres indicates the degradation of the polymer. Scale bar = 250 mm. (b) Following testing, digital image correlation was performed to determine strain patterns throughout the tissue. A gradient along the horizontal axis indicates higher strain in the central region of the tissue and lower strain at the edges, indicating depth-dependent changes in stiffness.

5.4.4 Biochemical characterization

5.4.4.1 ***Cellularity.*** The DNA content of all tissues increased throughout time in culture (Fig. 6a). At day 28, ctrl tissues contained 2.04 ± 0.20 million cells per construct. Following IL-1α treatment, the number of cells in ctrl+IL tissues was significantly lower (1.53 ± 0.19 million) compared to ctrl tissues (1.96 ± 0.23 million cells, $p < 0.05$). Similarly, LMS tissues contained 2.09 ± 0.17 million cells at day 28. Unlike ctrl+IL tissues, the cellularity of LMS+IL tissues was pre- served at day 35 (1.92 ± 0.15 million cells) as compared to LMS samples (2.01 ± 0.10 million cells). Uniquely, by day 35, the number of cells in ULMS tissues increased to 3.49 ± 0.52 million cells per construct, a 2.76-fold increase above day 0 values.

5.4.4.2 ***GAG incorporation.*** At day 28 in culture, all tissues contained at least 4.69% ± 1.07% GAG per wet weight (GAG/ww) (Figure 5.4b). Following IL-1α treatment, GAG content of ctrl+IL samples (5.07% ± 1.15% GAG/ww) was significantly lower than respective controls (7.91% ± 0.46% GAG/ww, $p<0.05$) (Figure 5.4e). In contrast, LMS+IL tissues continued to grow following

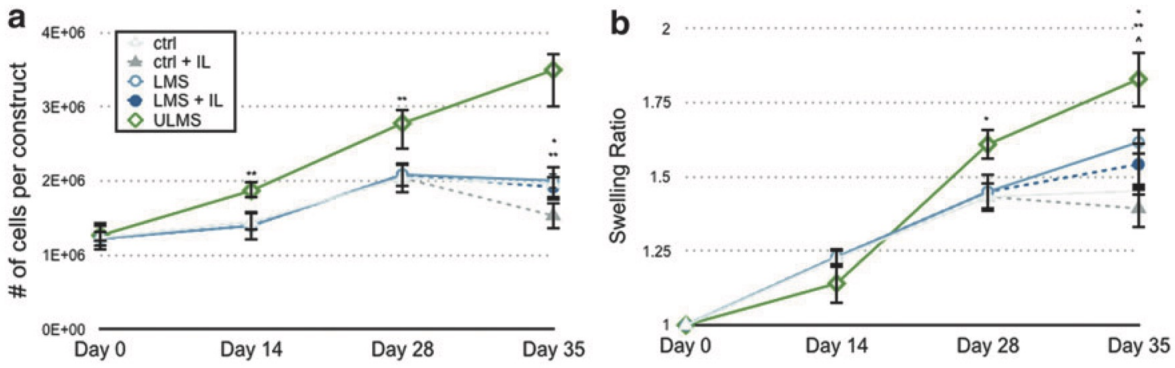

Figure 5.6: Cellular proliferation and tissue swelling throughout the entire culture period. (a) Cellular proliferation was experienced in all groups. Samples cultured without dex (ULMS) experienced significant cellular proliferation by day 35 in culture. * Indicates $p < 0.05$ for all samples compared with ctrl+IL at the same time point. ** Indicates $p < 0.05$ for ULMS samples compared to all others at the same time point. (b) As expected, all samples swelled to day 35. Samples cultured without dex (ULMS) swelled significantly compared to all other groups at day 35. * Indicates $p < 0.05$ for ULMS samples compared with all other groups at the same time point. ** Indicates $p < 0.05$ for LMS samples compared to ctrl, ctrl+IL at the same time point. ^ Indicates $p < 0.05$ for LMS+IL samples compared with ctrl+IL at the same time point.

the initiation of cytokine treatment, reaching 9.29% ± 1.26% GAG/ww by day 35, similar to LMS controls that achieved 10.99% ± 1.32% GAG/ww at the same time point. ULMS tissues reached 7.65% ± 1.17% GAG/ww by day 35 in culture.

5.4.4.3 ***Collagen content.*** Collagen content of ctrl and LMS tissues reached 1.43% ± 0.33% collagen normalized to wet weight (collagen/ww) and 1.53% ± 0.34% collagen/ww, respectively, at day 28 (Figure 5.4c). ULMS tissues contained 1.86% ± 0.18% collagen/ww at the same time point. Following cytokine insult, collagen content significantly decreased in ctrl+IL tissues ($p<0.05$) when compared with ctrl, LMS+IL (Figure 5.4f), and ULMS tissues.

5.4.4.4 ***Swelling ratio.*** All tissues exhibited significant swelling by day 35 in culture (Figure 5.6b). ULMS displayed a significantly greater ($p<0.05$) swelling ratio at day 35 when compared with all other groups, swelling to nearly 2x its original volume.

5.4.5 Histological/morphological characterization

Histology (Figure 5.7a–i), through ImageJ analysis, indicates weaker staining for GAGs in ctrl+IL samples (Figure 5.7b) when compared with other groups at day 35. Weaker intercellular staining

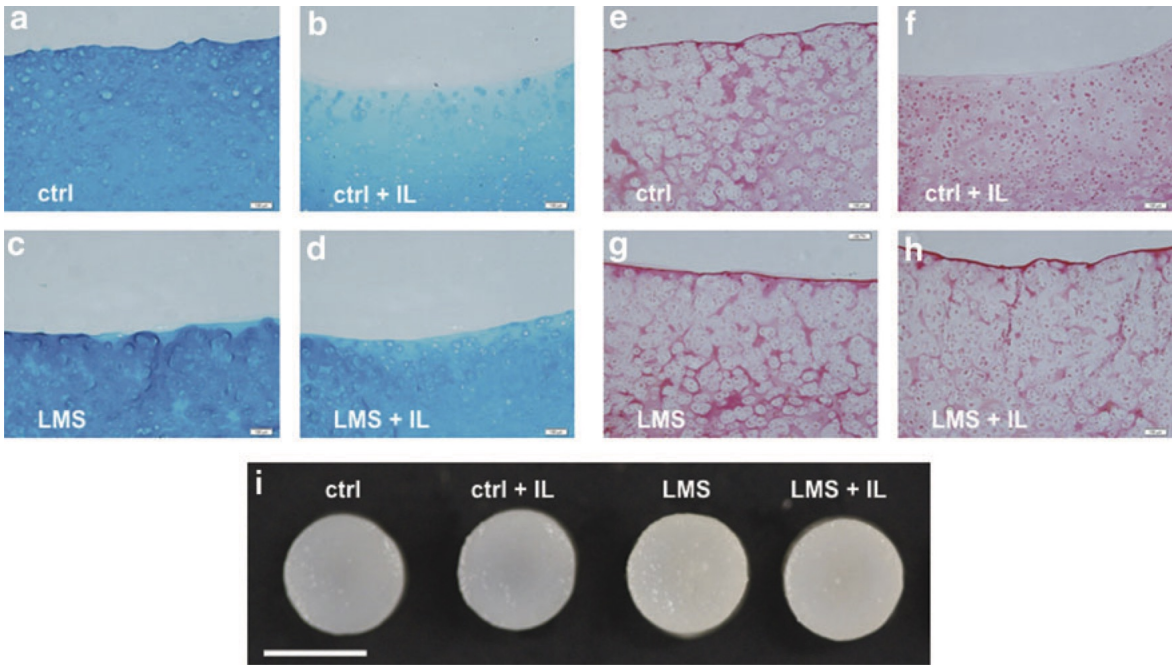

Figure 5.7: Histological sections from day 35. Alcian Blue staining indicates loss of GAGs following treatment with IL (b). Picrosirius Red displays inferior intercellular staining for collagen in controls treated with IL (f). In LMS tissues treated with IL, the same decrease in proteoglycan and collagen intensity is not observed (d, h). (a, e) Correspond to control. (b, f) Correspond to control+IL. (c, g) Correspond to LMS. (d, h) Correspond to LMS+IL. (i) Illustrates the gross differences at day 35 between samples cultured ± LMS and ±IL. Opacity is conserved between LMS and LMS+IL groups at this time point. Scale bar = 4 mm.

was observed in ctrl+IL samples (Figure 5.7f) at the same time point when compared with other groups. This response is contrasted with LMS+IL samples (Figure 5.7d, h), which maintain the intensity of their staining following treatment with IL-1α.

5.5 Discussion

This study demonstrated that dex-loaded PLGA MS embedded in chondrocyte-seeded agarose hydrogels promote development of mechanically functional cartilage tissue in culture. This local dex-delivery system also provides chondroprotection against the deleterious effects of IL-1α, a ubiquitous cytokine known to play a major role in the innate immune response and articular cartilage degeneration.

By releasing dex from within engineered cartilage, our therapeutic strategy targets the complicated autocrine control system of chondrolysis, through which cartilage damage is triggered by pro-inflammatory cytokines produced from leukocytes and the synovium (Shinmei *et al.* , 1989;

Shinmei *et al.* , 1991). Compared to strategies that target specific pro-inflammatory cytokines, such as IL-1 receptor antagonist (Kimmerling *et al.* , 2015; Olson *et al.* , 2015), dex has been shown to mitigate the deleterious effects of IL, TNF-α, and other cytokines associated with inflammation.

As a culture supplement, dex is known to perform a variety of roles, including as a promoter of chondrogenesis in mesenchymal stem cell populations (Mackay *et al.* , 1998; Sekiya *et al.* , 2002; Wang *et al.* , 2005). Additionally, as reiterated in this study, dex is a critical element in the development and maturation of tissue-engineered cartilage. Here, all tissues developed similarly for the first 2 weeks of culture (Figure 5.4a), regardless of dex supplementation. Tissues receiving dex achieved an E_Y within the native range (Kiviranta *et al.* , 2008) by the end of culture and were ~2-fold higher than tissues receiving no dex (ULMS) (Figure 5.4d). Moreover, dex-loaded MS expedited this tissue development (day 35).

While delivery of dex from within constructs cultivates tissues with E_Y in the range of native values, the internal delivery of dex from homogeneously distributed MS was not observed to modulate the axial inhomogeneity of tissue properties reported in chondrocyte-seeded agarose constructs of similar dimensions (Kelly *et al.* , 2006). This inhomogeneity, described in Chapter 2, resembles a U-shape, with stiffer regions of tissue located at the periphery (Kelly *et al.* , 2009; Nims *et al.* , 2015). (Figure 5.5b), and is thought to reflect nutrient gradients associated with free swelling culture. This finding suggests that dex is not responsible for the nonuniform tissue development observed in our current study. Recent work suggests that other media components, such as insulin and glucose, may play a role in this phenomenon (Cigan *et al.* , 2013; Nims *et al.* , 2014). The high binding affinity of active TGF-β3, an ~25kDa molecule (compared with 400 Da for dex), to agarose and cartilage matrix has also been implicated in contributing some part to the development of tissue heterogeneity (Albro *et al.* , 2016).

The E_Y values observed here are interestingly in tandem with cellular density and swelling ratio. With respect to cellularity, tissues that received no dex throughout the study (ULMS) proliferated to a cellular density ~2.75-fold higher than those that did (ctrl, LMS) (Figure 5.6a). The antiproliferative effects of dex seen here are consistent with work in 2D chondrocyte cultures (Hainque *et al.* , 1987). While a higher cellularity yielded near-native GAG levels (~7% GAG/ww, data not shown) and GAG levels comparable to those in ctrl tissues, E_Y remained significantly lower at the final time point (Figure 5.4d), despite minimal variation in collagen content across tissue

groups. Furthermore, ULMS tissues experience greater swelling and inferior mechanical properties compared to LMS, attributed to the absence of dex. We speculate that dex influences the biosynthetic behavior of chondrocytes that dictates the structural organization of the collagen network and collagen–proteoglycan interactions that serve to combat tissue swelling (Williams *et al.* , 2007; Olson & Guilak, 2015; Bastiaansen-Jenniskens *et al.* , 2008).

In addition to the physical demands of the joint, its harsh inflammatory environment will likely impact the performance of engineered cartilage. The presence of IL-1β upregulates the expression of aggrecanases, the primary proteases identified in pathological aggrecan degradation in human OA (Song *et al.* , 2007), and has a predominant effect on the GAG content of engineered cartilage. Previous studies have shown that GAG content of IL-1-treated engineered cartilage is depleted ~4-fold as compared with controls (Lima *et al.* , 2008a). It is also known, however, that dex supplementation reduces sulfated GAG loss and rescues proteoglycan synthesis in cartilage explants exposed to inflammatory cytokines (Lu *et al.* , 2011). In the study presented here, LMS and ctrl tissues were treated with IL-1α beginning at day 28 in culture. The time point selected for cytokine insult was informed by work in our laboratory and others suggesting that construct maturity plays an important role in the tissue's response to cytokine and in vivo outcomes (Lima *et al.* , 2008a; Miot *et al.* , 2012; Francioli *et al.* , 2011), with delayed exposure to insult being beneficial to tissue health. Following 7-day treatment of IL-1α, ctrl+IL tissues contained ~36% less GAG than their respective controls (Figure 5.4e), resulting in an inferior tissue with equilibrium moduli measuring ~2.75-fold lower than ctrl tissues. LMS tissues, however, did not experience a similar depletion of GAGs. In fact, LMS tissues exposed to cytokine continued to elaborate their extracellular matrix beyond day 28, increasing GAG content nearly 2-fold by day 35 (Figure 5.4d). The continued biosynthetic activity of LMS tissues in the presence of a supraphysiological dose of IL-1α (10ng/mL vs. 0.288ng/mL (McNulty *et al.* , 2013) in moderate OA joints), compared with the significant decline in synthesis by ctrl+IL tissues, is encouraging in the context of using dex-loaded MS as a strategy to promote cartilage repair *in vivo* (Miot *et al.* , 2012).

Recent work demonstrates the successful translation of this dex microsphere strategy to engineered constructs seeded with adult human chondrocytes (O'Connell *et al.* , 2015) from three donors (Figure 5.8), supporting the need for continued research efforts pursuing dex-loaded MS. Similar to constructs derived from juvenile bovine chondrocytes, co-encapsulation of adult human

chondrocytes and dex-loaded MS were able to promote cartilaginous tissue development similar to exogenous dex supplementation of the culture media and afforded chondroprotection against IL-1α.

While simplistic, the use of a single pro-inflammatory cytokine, IL-1α, is a well-established culture model for OA (Lima *et al.* , 2008a; Lu *et al.* , 2011; Shinmei *et al.* , 1989; Kimmerling *et al.* , 2015; Kumar *et al.* , 2015; Wilusz *et al.* , 2008; McNulty *et al.* , 2007) proven to provide valuable insight on the impact of cytokines on articular cartilage. The use of IL-1, specifically, exploits the cytokine's importance in inflammation (Rhen & Cidlowski, 2005). IL-1, along with TNF-α, is responsible for the majority of degradation of the extracellular matrix in vivo (Wojdasiewicz *et al.* , 2014) and both cytokines share a common set of pathways, including the activation of nuclear factor-kappa B (NF-kB) (Kawai & Akira, 2006). The utilization of dex is therefore unique, as glucocorticoids have been shown to physically interact with the p65 sub-unit of NF-kB and transrepress its function (McKay & Cidlowski, 1998). While anti-inflammatory cytokines such as IL-4 and IL-13 are known to directly regulate IL-1 function in the joint (Joosten *et al.* , 1999; Cleaver, 2001; Joosten *et al.* , 1997), the use of dex in the context of cartilage tissue engineering is critical for functional maturation of the tissue (as shown in this work) and has been demonstrated to confer chondroprotection against both IL-1α and TNF-α (Lu *et al.* , 2011).

This study demonstrates the ability of dex-loaded MS to cultivate tissues that are mechanically viable (within native levels of compressive modulus) while simultaneously providing chondroprotection. In addition to the benefits of dex-loaded MS in culture, a controlled release approach to steroid administration is particularly advantageous in the context of current therapies for early intervention in OA. While it has been reported that IA injections lead to improved outcomes at 2-year follow-ups (Raynauld *et al.* , 2003), the inherently short duration of therapeutic action for corticosteroids (Goodman, 1996) and dex (6–8 days (Wernecke *et al.* , 2015)), in particular, the result of rapid systemic absorption suggests that more frequent injections may obtain ideal joint pain outcomes. The accumulated availability of glucocorticoids through repeated injections, however, has been shown to lead to gross morphological cartilage changes (Breuner & Orchinik, 2002) alongside lowered viability and biosynthetic activity of chondrocytes (Song *et al.* , 2012). Successively elevated systemic levels of glucocorticoid also impact the hypothalamus–pituitary–adrenal (HPA) axis (Habib, 2009), inhibiting the immune system's ability to respond to infection. The dual impact of rapid systemic absorption, both inside and outside the joint, suggests that sustained delivery of

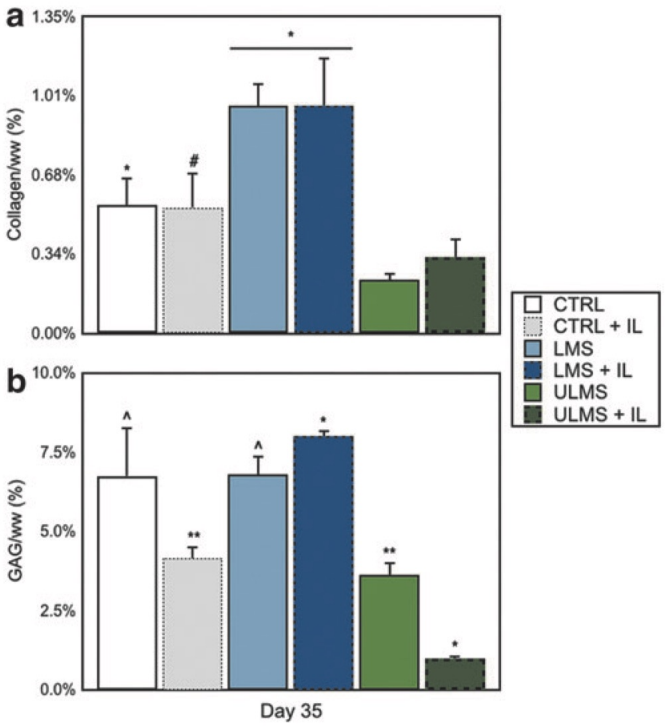

Figure 5.8: GAG content from preliminary study using adult human chondrocytes. Chondrocytes were isolated from the femoral articular cartilage of three donors. Following casting at 40 million cells per milliliter in 2% agarose hydrogels, tissues were cultured as described previously. At day 28, samples were divided and a portion was treated with 0.1 ng/mL IL-1. (a) As expected, there was no change in collagen content among treatment groups following cytokine insult. (b) It was observed, however, that GAG levels in LMS+IL tissues increased from ∼5% at day 28 to ∼8% GAG/ww at day 35, a value within the range of native tissues and significantly higher than all other groups ($p<0.05$). At the same time, ctrl tissues experienced a significant decrease in GAG content ($p<0.05$) from ∼6% GAG/ww at day 28 to ∼4% GAG/ww at day 35. This biochemical profile suggests that the chondroprotective effect of dex-loaded microspheres observed in juvenile bovine chondrocyte constructs is applicable to adult human chondrocyte constructs, as well, providing motivation for further investigation into the role that dex-loaded microspheres may play clinically. * Indicates $p<0.05$ when compared with all other tissues. ** Indicates $p<0.05$ when compared with ctrl, LMS, LMS+IL, and ULMS+IL. ^ Indicates $p<0.05$ when compared with ctrl+IL, LMS+IL, ULMS, and ULMS+IL. # Indicates $p<0.05$ when compared with ctrl, LMS, LMS+IL, and ULMS. GAG/ww, GAG per wet weight.

low levels of glucocorticoids may address these concerns while improving patient outcomes.

Low dose, sustained delivery of glucocorticoids, as presented in this work, provides a forward thinking strategy for improved cartilage repair and healing. The MS used in this study have been shown to release drug for up to 70 days (Figure 5.2b), maintaining a consistent level of drug release throughout culture and ensuring local availability of the steroid beyond the 5 weeks observed in this study. Daily release of the drug is measured at only ∼19 ng per construct. This amount is 35x lower than the amount used in standard tissue culture (Lima *et al.* , 2008a) and 11x lower than commonly used triamcinolone acetonide IA injection dosages (Wilusz *et al.* , 2008; Wernecke *et al.* , 2015; Shepherd & Seedhom, 1999; Parma *et al.* , 1988). Additionally, this strategy has been shown to minimize the potential effects on the HPA axis, having been employed in vivo and shown to promote tissue formation with minimal systemic impact (Kelmendi-Doko *et al.* , 2014).

We further anticipate a strategy of chondroprotection where a glucocorticoid, administered from the locale of the injury/repair site in a manner that provides its sustained release at much lower levels than clinical injections, can also impact tissue healing and repair of the engineered graft upon implantation (Huebner *et al.* , 2014; Huebner *et al.* , 2013). While future plans are aimed at further optimization of the dex microsphere strategy, including the testing of other pro-inflammatory cytokines such as TNF-α and the evaluation of tissue integrative repair in a cartilage explant ring model (Theodoropoulos *et al.* , 2011; Gilbert *et al.* , 2009; Hunter & Levenston, 2004), the efficacy of our approach on cartilage repair will necessarily have to be evaluated in vivo.

5.6 Conclusion

In this study, we have demonstrated that the internal release of dexamethasone, an anti-inflammatory and FDA-approved synthetic glucocorticoid, can promote the development of mechanically functional engineered cartilage and simultaneously provide protection against a supraphysiologic dosage of the pro-inflammatory cytokine IL-1α. As such, this study presents a strategy for delivery of dexamethasone from within engineered cartilage as a potential strategy for improving the success of cartilage repair *in vivo*.

5.7 Acknowledgments

This research was supported by the Musculoskeletal Transplant Foundation Established Investigator Grant (C.T.H.), National Institutes of Health (AR060361 [C.T.H., G.A.A.], AR068133 [C.T.H.], 5T32AR059038 [B.L.R.]), and National Science Foundation Graduate Research Fellowship Program under Grant No. DGE-11-44155 (B.L.R.).

Part III

Fabrication Process for Anatomical Resurfacing

Chapter 6 Fabrication of tissue engineered osteochondral grafts for restoring the articular surface of diarthrodial joints

6.1 Abstract

Osteochondral allograft implantation is an effective cartilage restoration technique for large defects (>10 cm^2), though the demand far exceeds the supply of available quality donor tissue. Large bilayered engineered cartilage tissue constructs with accurate anatomical features (i.e. contours, thickness, architecture) could be beneficial in replacing damaged tissue. While progress has been made in improving the mechanical and biochemical properties of engineered cartilage (see Chapters 2, 3, and 5), it is pertinent to also maintain biofidelity to restore full functionality. Here, we describe a step-by-step framework for the fabrication of a large osteochondral construct with correct anatomical architecture and topology through a combination of high-resolution imaging, rapid prototyping, impression molding, and injection molding.

6.2 Introduction

Articular cartilage, a white, dense connective tissue that lines diarthrodial joints, serves as the load-bearing material of joints, and is characterized by excellent friction, lubrication, and wear properties (Mow & Lai, 1990). When damaged due to injury or osteoarthritis, the tissue undergoes degeneration resulting in pain and dysfunction. Upon becoming symptomatic, this discomfort necessitates surgical intervention. Treatment options, however, are dependent on the joint involved, the location, size and severity of the defect, and patient-related factors.

Endstage, global joint pathology often warrants total joint arthroplasty to replace the articulating surfaces and underlying bone. Total joint arthroplasty is associated with a relatively high need for revision surgery due to implant wear, subsidence, and/or loosening (Ayers, 1997; Bradley *et al.* , 1993; Mowery *et al.* , 1987; Whiteside, 1989). For focal articular cartilage lesions (<2 cm^2), minimally invasive reconstructive surgical approaches including microfracture (Steadman *et al.* , 2001), autograft cell/tissue transfer via periosteal grafts (O'Driscoll *et al.* , 2001), autologous osteochondral grafting such as mosaicplasty (Hangody *et al.* , 1997), and autologous chondrocyte implantation (Brittberg *et al.* , 1994) are currently utilized. While these surgical treatment options

can address symptoms of pain and improve function, they have not shown long-term durability and are associated with a number of limitations and potential complications. Cell-based therapies and osteochondral autograft harvesting are limited by the availability of healthy cartilage from which to harvest tissue or cells. Furthermore, autologous osteochondral grafts are harvested from non load-bearing regions that may provide tissue of sub-optimal material properties for use in load-bearing recipient sites (Ahmad *et al.* , 2001). Additionally, the harvest procedure itself can induce significant donor site morbidity (Lee *et al.* , 2000a; Lee *et al.* , 2000b), leading to further structural and biochemical breakdown in the joint.

For larger lesions, greater than 10 cm^2, when articular cartilage loss has distorted the morphology of the condyle, fresh osteochondral allografts may be indicated (Bugbee, 2002). The technical demands associated with this procedure and the limited supply of suitable grafts to meet clinical demand have prompted pursuit of cell-based therapies for cartilage repair, including tissue-engineered constructs of cultured cells on three-dimensional scaffolds (Lima *et al.* , 2004; Mauck *et al.* , 2000a; Pazzano *et al.* , 2000; Vunjak-Novakovic *et al.* , 1999).

For engineered constructs to functionally bear the loads experienced *in vivo*, it is necessary to recreate the natural topology of the articular surface to fully recapitulate the normal contact geometry and load distribution across the joint (Cooney & Chao, 1977; Ateshian *et al.* , 1992; Ateshian *et al.* , 1995; Eberhardt *et al.* , 1990; Huberti & Hayes, 1984; Hung *et al.* , 2003). To capture the complete 3D geometry of articular cartilage, the topography of the cartilage surface as well as the underlying subchondral bone must be quantified. A number of models derived directly from the target tissue have been used for the purpose of quantifying the articular joint surface. These include mechanical as well as optical techniques; the geometry of the articular layer of cartilage surfaces has been quantified using cryosectioning (Stäubli *et al.* , 1999), stereophotogrammetry (Ateshian *et al.* , 1991; Ghosh, 1983; Huiskes *et al.* , 1985), A-mode ultrasound (Adam *et al.* , 1998), and magnetic resonance imaging (MRI) (Cohen *et al.* , 1999; Eckstein *et al.* , 1994). Many of these same techniques, in addition to computed tomography (CT), can be used to quantify the subchondral bone. Once acquired, these data are used to create negative templates for the desired tissue via computer aided design (CAD) and stereolithography, such as for the temporomandibular joint (TMJ) (Undt *et al.* , 2000; Weng *et al.* , 2001), the auricular cartilage of human ear (Cao *et al.* , 1997), or to recreate iatrogenic defects on the articular surface of the femur (Koo *et al.* ,

2010). Through the combination of CAD and injection molding, our previous work has created entire articular layers, successfully replicating the human patellar articular layer and trapeziocarpal articular layer of the thumb joint (Hung *et al.* , 2003). These large, full surface replications need only to integrate with the underlying subchondral bone and can be exposed to a milieu of chemical and physical stimuli (Vunjak-Novakovic *et al.* , 1999; Gooch *et al.* , 2001; Kaysen *et al.* , 1999; Freed *et al.* , 1997; Ateshian *et al.* , 2003; Mauck *et al.* , 2002; Byers, 2006; Mauck, 2003; Bian *et al.* , 2010b) in vitro to optimize the functional properties of developing constructs.

While the replication of full articular surfaces highlights one potential application of this technology, for clinical management of cartilage injuries, it may be more relevant to fabricate osteochondral constructs for large defects that exhibit anatomically defined surfaces matching the native architecture of both the cartilage surface and subchondral bone. As such, in this paper, we follow a general protocol for generating tissues with biofidelic shape (Figure 6.1a), and detail how this principle may be applied to a specific embodiment, the fabrication of an osteochondral graft (Figure 6.1b).

6.3 Materials and methods

For proof of concept, we performed this technique to generate a graft suitable for restoring a large femoral condyle defect in the dog. The use of adult canine tissue represents a large preclinical animal model with clinically relevant similarities to humans, notably in anatomy of the knee joint, pathology, and treatment. Surgical interventions such as arthroplasty, autologous chondrocyte transplantation, and osteochondral grafting, as well as postoperative care including bandages, braces, and physical rehabilitation, can be readily performed. Here, we created a large osteochondral implant for the medial femoral condyle. An intact canine stifle joint from a 2–5 year-old mongrel canine was dissected via removal of integument, fascia, muscle, and excision of capsular ligaments to expose the joint surface of the distal femur for 3D data acquisition.

6.3.1 3D laser scanning

Surface morphology was acquired with a NextEngine^{TM} HD Desktop 3D Scanner (NextEngine, Inc., California, USA), a portable device equipped with twin 3.0 megapixel CMOS image sensors. First, a transverse cut was made through the thickness of the femur 4 cm proximal to the patellofemoral joint to allow for mounting of the joint to a 6 cm x 6 cm 1 cm block supplemented with an alignment

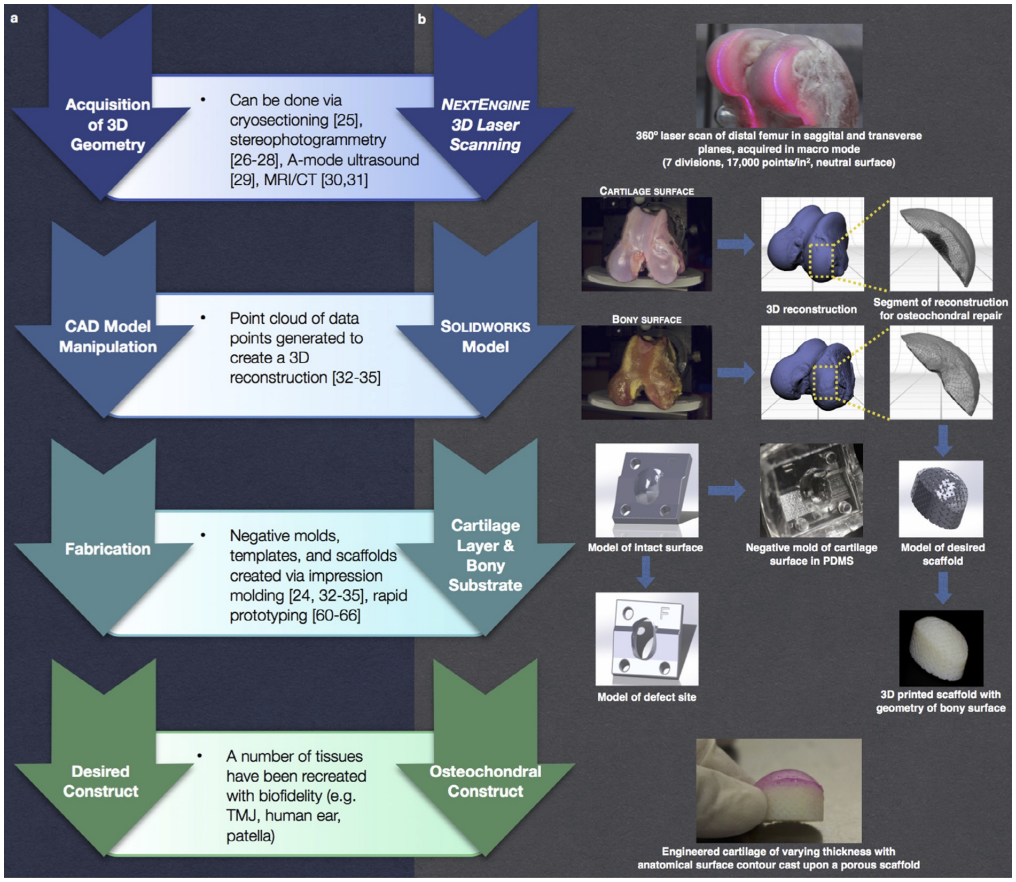

Figure 6.1: Schematic of (a) general design protocol and (b) detailed implementation of steps for fabrication of an anatomical osteochondral graft.

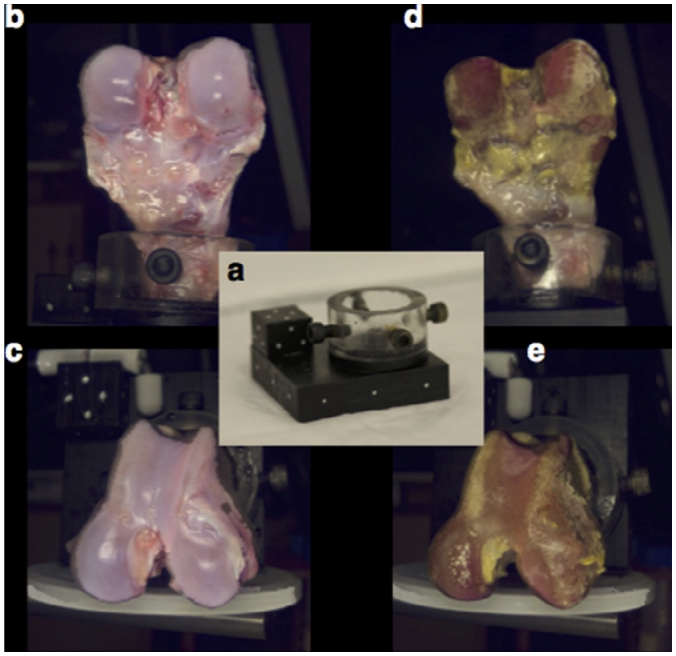

Figure 6.2: (a) A mounting setup was used for 360° imaging of the intact articular surface and subchondral bone in the sagittal (b and d) and transverse (c and e) planes. A matrix of fiduciary markers, including an alignment cube positioned on the surface of the mounting block, was used to globally align scans of the two surfaces during image processing.

cube for proper positioning of the joint in three axes (Figure 6.2a). A matrix of fiduciary markers on the mount was created using a white paint pen. Both joint and mounting block were placed within the field of view for image acquisition to allow for digitization of the joint surface over 360° with simultaneous fiduciary marker capture. Utilizing the NextEngine^{TM} 3D ScanStudio^{TM} HD software package, 3D scans were acquired in macro mode with optimized settings (360°, 7 divisions, 17,000 points/in.^{2}, neutral surface). To obtain the full curvature of the surface, 2 panels of images were acquired from varying angles in both the sagittal (Figure 6.2b) and transverse plane (Figure 6.2c). During imaging, phosphate buffered saline was administered to the cartilage as necessary to maintain tissue hydration. Following capture of the articular cartilage surface, while still secured to the mounting jig, the distal femur was submerged in bleach (5–10% sodium hypochlorite) for 45 minutes to expose the subchondral bone. The same 2 panels of images were then acquired in a similar manner as the articular cartilage surface (Figure 6.2d and Figure 6.2e).

The ScanStudio^{TM} HD software package was then used to process the acquired point clouds, aligning and trimming the reconstruction. Articular cartilage surface and subchondral bone layers were aligned relative to their global markers to ensure that any model manipulations were confidently

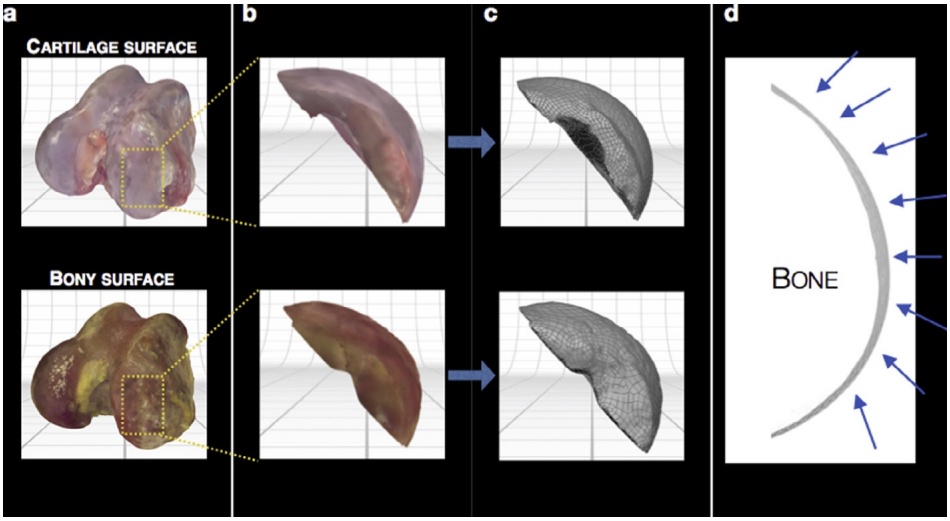

Figure 6.3: Manipulation of reconstructed models to isolate desired region. (a) Both cartilage and bony reconstructed surfaces were rendered in color, (b) trimmed to expose only the medial femoral condyle, and (c) modeled by 2001 surfaces for CAD manipulation. (d) A representative silhouette of the articular cartilage thickness following subtraction of the subchondral bone from the intact articular cartilage model (changing thickness marked by arrows).

consistent. For this proof of concept, we focused on creating a large osteochondral construct on the medial condyle, the most common site of unicompartmental osteoarthritis in the joint; accordingly, the models (Figure 6.3a) were trimmed to expose only this region (Figure 6.3b). Once the desired surface was isolated, a water-tight model was fused, simplifying the point cloud where advantageous without losing accuracy (63.5 μm tolerance), resulting in a 38,980 point model. Before the models could be manipulated via CAD, surfaces were created from the fused models using ScanStudio^{TM} HD CAD Tools (Figure 6.3c), and when superimposed upon one another, resulted in the identification of the articular cartilage layer alone (Figure 6.3d). Each model was approximated by 2001 surfaces. Once complete, these surfaces were exported as SolidWorks (Dassault Systemes, France) compatible IGES files.

6.3.2 CAD modeling

The solid surface models for the intact articular cartilage layer and underlying subchondral bone were then manipulated to produce three pieces: (1) an intact articular cartilage model for a negative mold, suitable for biological contact; (2) a defect template that allows for scaffold delivery, and (3) a scaffold model with the contour of the subchondral bone (Figure 6.3a). To create an artificial defect

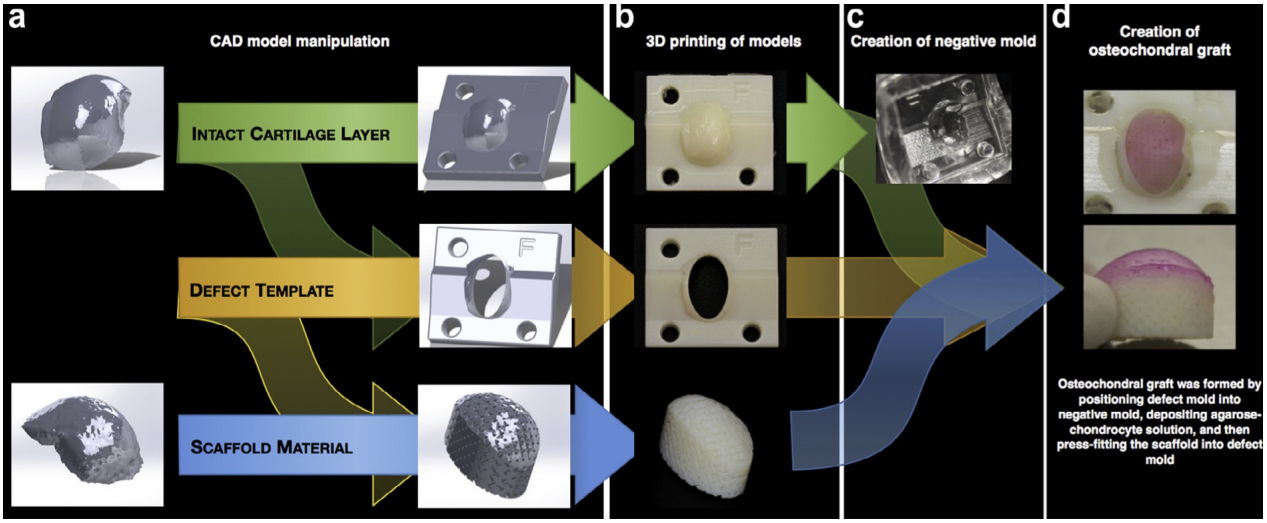

Figure 6.4: Fabrication process for creating a large anatomical osteochondral construct. (a) Solid surface models were manipulated to create three pieces (intact articular layer, defect mold, subchondral bone) that were (b) rapid prototyped via 3D printing. (c) A PDMS negative mold was formed from the intact cartilage mold and (d) all components were positioned together to create an osteochondral graft with anatomical topology and architecture.

on the medial condyle, a large ellipsoid covering 70% of the cartilage surface was imposed on the intact articular cartilage model to produce the defect template. This large defect size on the canine condyle was chosen to reflect a critical size defect when scaled up for the size of the human medial condyle (Parma *et al.* , 1988). Following completion of the defect template, the same defect geometry was mirrored on the subchondral bone model, creating an implant geometry identical to the defect site and with the surface topology of the underlying bone. This scaffold model was then modified with a multi-axis series of channels (Figure 6.4a; 500 μm diameter, 1250 μm center-to-center) to mimic the networked trabecular structure of the subchondral bone. Following CAD modeling of these three pieces, the models were converted to rapid-prototyping ready stereolithography (.stl) files and imported into Objet Studio^{TM} for transformation into 3D modeling slices.

6.3.3 Rapid prototyping

An Objet24 (Stratasys, Ltd., USA) desktop 3D printing system was used for rapid prototyping (Figure 6.4b). In particular, the 28 μm print layers allowed for modeling and implementation of precision design features, including the accurate modeling of articular cartilage thickness. Following 3D fabrication, support material was removed from the models with a high-pressure water pick,

which was further facilitated by submerging the pieces in an ultrasonic 1% alkali detergent bath for 1 hour.

6.3.4 Negative mold fabrication

In order to recapitulate the morphology of the articular surface in a tissue-engineered osteochondral implant, a mold was created from the intact articular cartilage model. To allow for contact with biological tissues, a biocompatible silicone elastomer (Sylgard 184, Corning, USA) was selected for the mold material. 80 mL of polydimethylsiloxane (PDMS) mixture was produced according to the manufacturers instructions in 2–50mL conical tubes and centrifuged to remove air pockets. A polyoxymethylene cylinder (1" OD; 3/4" ID), used to stabilize the intact articular cartilage model once submerged in PDMS, was placed in the bottom of a hollow plastic rectangular container (with one face removed). Cylinder- and container-size was dependent on the size of the model. PDMS was added to the cylinder until cresting. The intact articular cartilage model was then inserted, allowing the base to rest on the polyoxymethylene cylinder. The remainder of the PDMS was added, ensuring the model was completely submerged. This container was then placed in a vacuum chamber for 20 minutes to remove any remaining air pockets. Once a homogenous mixture was achieved, the container was transferred to a 60°C oven overnight (16 hours) to ensure complete curing. Once cured, the plastic container was removed with a band saw, taking care not to damage the PDMS. The mold was then trimmed as necessary to expose the base of the intact articular cartilage model, which was removed from the PDMS mold (Figure 6.4c), leaving behind a negative mold of the medial condyle.

6.3.5 Osteochondral implant fabrication

As described previously (Ng *et al.* , 2010) and in Chapter 2.3.1, chondrocytes were isolated from the femoral condyles of canine stifles, passaged twice, and suspended in chondrogenic medium at a concentration of 60 million cells/mL for implant fabrication. Concurrently, agarose (4%, Type VII, Sigma, USA), was prepared and maintained in molten state at 40°C until use. Equal parts cell solution and agarose were then mixed in a separate conical tube and 500 µL of this mixture (30 million cells/mL; 2% agarose) was deposited into the defect. Using the directional aids, the scaffold was then placed into the defect and pressed until flush with the base of the defect template, ensuring

proper cartilage thickness. After allowing 10 minutes for gelation, both the defect template and osteochondral implant were removed from the negative mold. Using the easy access ports in the rear of the defect template, the osteochondral implant was carefully removed to reveal an anatomically shaped construct with accurate cartilage thickness (Figure 6.4d) and placed into chondrogenic medium (CM) at a ratio of 10 mL CM per OC implant. This well-established agarose-based system has been shown to encourage favorable cell morphology and foster tissue growth over time (Knight *et al.* , 1998; Lee *et al.* , 1998; Lee *et al.* , 2000c; Bian *et al.* , 2009a; Kelly *et al.* , 2013; Mauck *et al.* , 2000a; Vacanti *et al.* , 2001).

6.4 Conlusion

The process described here represents the integration of several established techniques in an innovative manner to produce a large clinically relevant osteochondral graft with appropriate surface topologies and cartilage thickness.

Maintaining biofidelity of anatomical surfaces has long been a goal of tissue engineering, with impression molds of cadaveric tissues used as models to produce negative molds of curved tissues. To date, extensive work has been done to replicate complex geometries such as a human ear (Cao *et al.* , 1997), mandibular joint (Weng *et al.* , 2001), and avulsed phalanx (Vacanti *et al.* , 2001). Stereophotogrammetry, in combination with CNC milling and injection molding, has been used to quantify, model, and replicate the articular surface of the human patella (Hung *et al.* , 2003; Ateshian *et al.* , 1991; Ghosh, 1983; Huiskes *et al.* , 1985). CAD-based injection molds have been used for a variety of applications including cardiovascular (Baudis *et al.* , 2011; Neidert & Tranquillo, 2006) and musculoskeletal tissues (Hung *et al.* , 2003; Ballyns *et al.* , 2008). With a focus on clinical feasibility, the field has recently shifted to the utilization of medical imaging modalities to inform the creation of anatomically shaped engineered tissues. These imaging modalities, such as fluoroscopy, MRI, CT, and ultrasound enable the replication of patient specific architectures and have greatly facilitated the use of additive manufacturing in the biomedical sciences. In the time since, medical imagining modalities have been used to partially or fully recreate the specific geometries of the tissue of interest. MRI and μCT of bovine knees have been used to inform CAD models of meniscal architecture (Ballyns *et al.* , 2008; Ballyns & Bonassar, 2011). Rapid prototyping (solid free form fabrication, 3D printing, etc.) has allowed the widespread realization

of digital models. First introduced in the early 2000s as researchers looked for a way to create 3D organs with shape fidelity (Mironov *et al.* , 2003), new advances in 3D printing have been applied to osteochondral composites, allowing for spatial control of material and chemical properties through the depth of a tissue (Sherwood *et al.* , 2002; Schek *et al.* , 2004; Zhang *et al.* , 2014), as well as TMJ reconstruction (Feinberg *et al.* , 2001; Grayson *et al.* , 2010), humeral head regeneration (Lee *et al.* , 2010), and tissue-engineered epiglottis (Brown *et al.* , 2013). Recent advances include hybrid printing, allowing the simultaneous deposition of electrospun fibers with cell-seeded hydrogels to provide optimal mechanical and biological properties layer by layer (Xu *et al.* , 2013).

The protocol outlined herein exploits several of these established technologies to provide a blueprint for tissue reconstruction and replacement as it pertains to the knee joint (Figure 6.1). While we have shown utility of this protocol through 3D data acquisition from an *ex vivo* knee joint, similar patient-specific information acquired through clinically used medical imaging (e.g. MRI, CT (Cohen *et al.* , 1999; Eckstein *et al.* , 1994; Ateshian & Hung, 2005)) can be incorporated via commercially available and open-sourced software platforms (via Mimics®, TurtleSeg, Geomagic, etc.). Further, the framework of this process can be tailored to the equipment available, however, the ability to capture the anatomical geometry of the articular cartilage layer and underlying subchondral bone [57] is critical, as the success of osteochondral graft replacement is heavily dependent on the surgeon's ability to restore native joint congruency (Cooney & Chao, 1977; Ateshian *et al.* , 1992; Ateshian *et al.* , 1995; Eberhardt *et al.* , 1990; Huberti & Hayes, 1984; Hung *et al.* , 2003), which inherently includes cartilage thickness. Additionally, once the articular geometry is obtained for the entire diarthrodial joint (Figure 6.5a), any sub-region of interest (e.g., distal femoral condyle, trochlear groove, etc.) can be generated. For comparison, we have illustrated this by producing engineered constructs in the form of a cylindrical osteochondral plug suitable for repair of focal defects (Figure 6.5b) and, as described here, as a larger construct able to replace an entire condyle (Figure 6.5c).

The choice of method of acquisition of 3D data, from laser scanning technologies in the laboratory to clinical MRI or CT scans, is dictated by the goal at hand (modeling purposes vs. creation of tissue engineered constructs) and perhaps by the desired resolution. For the current application of replacing damaged cartilage, anatomically shaped osteochondral constructs could be personalized for an individual by acquiring pertinent 3D geometry data to create a custom mold, or obtained

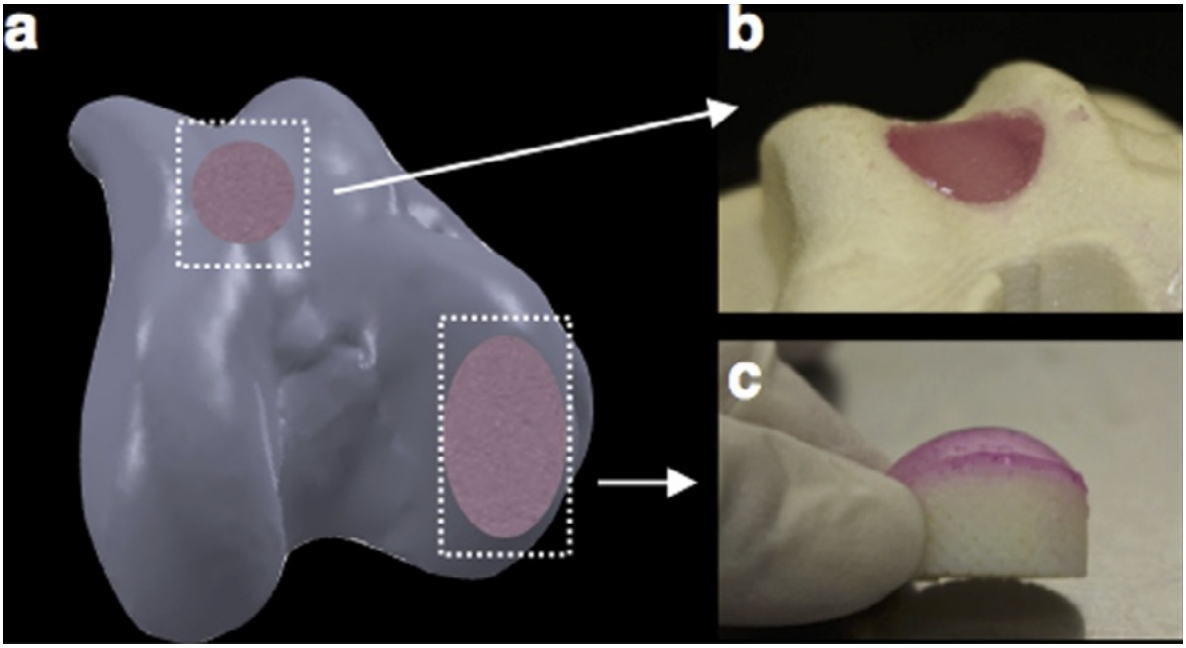

Figure 6.5: Example of how (a) 3D reconstruction of the articular surface can be used to generate osteochondral constructs for a range of defect sites: (b) focal defects and (c) large surface defects.

from a plurality of a population for a given set of biometrics (e.g. height, weight, gender). For the former, the accuracy of currently available clinical imaging modalities may pose a limitation in the near future. Accuracy of the cartilage thickness derived from a cartilage model from 1.5 Tesla MR images (B-spline snake method for segmentation) has been shown to be to be affected by the actual thickness of the tissue; thin cartilage is overestimated while thick cartilage is underestimated (Koo *et al.* , 2009). The use of 3.0 Tesla magnets capable of higher in-plane resolution (0.31 mm or less (Eckstein *et al.* , 2007)) along with additional segmentation techniques may provide for more accurate cartilage thicknesses. With this in mind, it may be more useful to produce a variety of available sizes and shapes based on a plurality of the population, providing the possibility for an off-the-shelf graft.

The osteochondral constructs created here not only demonstrate a process for digitizing, modeling, and fabricating accurate scaffolds for cartilage repair, but also the cultivation of biofidelic living engineered cartilage grafts. In combination with our laboratory's experience in the fabrication and storage of osteochondral grafts (Nover *et al.* , 2015; Nover *et al.* , 2016), these anatomically-shaped engineered tissues can be further improved via mechanical and chemical stimulation, as described in Chapters 2, 3, and 5. Using the surfaces already modeled from acquired 3D data, loading platens

can be developed to apply mechanical loading across the entire articular surface *in vitro* (Figure 6.6). Together with the incorporation of dex-loaded PLGA microspheres, these osteochondral constructs will be prepared for the harsh mechanochemical environment of the knee.

Figure 6.6: Platen fabricated from 3D acquisition of articular surface and used for mechanical stimulation of osteochondral construct.

The work presented herein provides a framework for fabrication of a complex, multi-layered construct through a combination of high-resolution imaging, rapid prototyping, impression molding, and injection molding. Our approach has accurately recreated, for the first time, a large, anatomically shaped osteochondral graft to meet the rapidly increasing demand of allografts for large area cartilage repair.

6.5 Acknowledgements

Research reported in this publication was supported by the National Institute of Arthritis and Musculoskeletal and Skin Diseases of the National Institutes of Health under Award Number R01 AR60361 and T32 AR059038. The content is solely the responsibility of the authors and does not necessarily represent the official views of the National Institutes of Health. Funding support from the Coulter Foundation and a NSF Graduate Fellowship (BLR) is also acknowledged.

Part IV

Conclusions and Future Directions

Chapter 7 Conclusions and Future Directions

This dissertation is built on several key underpinnings of cartilage functional tissue engineering adopted by the Cellular Engineering Laboratory. The use of the clinically-relevant agarose hydrogel scaffold, chondrogenic media supplemented with TGF-β, as well as native chondrocytes provides a robust platform in which to develop a chondroprotection strategy against the inflammatory cytokine environment of the injured or diseased diarthrodial joint. To confer this new dimension of function to our engineered cartilage, established protocols for drug delivery via polymer microspheres were incorporated. As a consequence, the collective work described in this dissertation has provided a holistic strategy for functional tissue engineering of articular cartilage. Moving forward, there are several avenues that should be explored to further this work in regard to optimization and clinical translation. Future studies will include those aimed at providing a more comprehensive understanding of the benefits of local dexamethasone delivery from within engineered cartilage constructs on tissue development and chondroprotection against pro-inflammatory cytokines. Complementary studies will look to better understand the underlying cellular mechanisms that mediate the beneficial effects of dexamethasone, including dexamethasone transport behavior in tissue as well as ligand-receptor interactions within cells.

First, the key findings for each major study of this dissertation are summarized in the context of the tissue engineering paradigm adopted by our laboratory (Figure 7.1). A brief overview of the complementary research areas described above follows.

7.1 Conclusions

Each Part of this dissertation is intended to address an aspect of the imperative our lab subscribes to. In doing so, we evaluate the global hypothesis of this work, that a combination of 1) optimized dynamic compressive loading and the 2) incorporation of polymer microspheres that release dexamethasone from within cell-seeded hydrogel constructs will prepare and protect constructs from the deleterious effects of mechanical and chemical exposure in the diarthrodial joint.

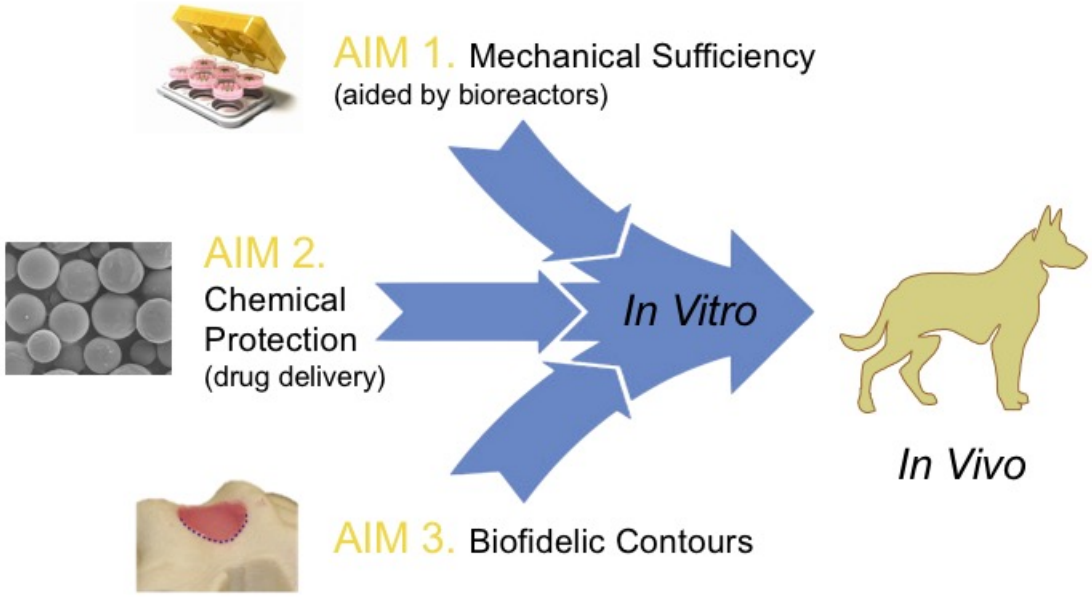

Figure 7.1: Schematic of work described in this thesis in the context of the larger tissue engineering paradigm, with the intent to employ these combined approaches in an *in vivo* model.

7.1.1 Characterizing and optimizing physiologic application of dynamic loading

We begin this dissertation in Part I, by examining the role of mechanical stimulation in the functional maturation of engineered cartilage, specifically evaluating tension-compression nonlinearity in tissue-engineered cartilage (Chapter 2) and demonstrating the utility of a commercially available bioreactor to dynamically stimulate and evaluate engineered tissues (Chapter 3). Tension-compression nonlinearity is the phenomenon used to describe articular cartilage's varied response to tensile and compressive forces. Critical to its function as a dynamic load bearing surface, this phenomenon is characterized by a higher stiffness in tension versus compression, allowing cartilage to resist radial expansion under axial compressive loading and resulting in increased fluid pressurization and dynamic stiffness (Huang *et al.* , 2001; Soltz & Ateshian, 2000; Soulhat *et al.* , 1999). While this phenomenon had previously been investigated in native explant cartilage tissues (Chahine *et al.* , 2004; Huang *et al.* , 2001; Huang *et al.* , 2003; Huang *et al.* , 2005; Huang & Gu, 2006), our findings reveal, for the first time, the presence of tension compression nonlinearity in tissue-

engineered cartilage. Similar to native explants, the mechanical properties of engineered cartilage are significantly higher in tension than compression, decreasing exponentially as the transition from tensile loading (during osmotic swelling) to compressive loading occurs. Further quantification of the proteoglycan-collagen interactions responsible for this varied response may also be indicative of cartilage health *in vivo* and be used as a diagnostic model to investigate tissue degradation. The utility of dynamic compressive loading for cartilage tissue engineering was further investigated in the context of the Mechanoactive Tissue Engineering bioreactor (MATE), a commercially available bioreactor system. In contrast to traditional single actuator, batch loading approaches ((Aufderheide & Athanasiou, 2006; Cassino *et al.* , 2007; Mauck *et al.* , 2000b; Lima *et al.* , 2007)), the MATE allows for simultaneous stimulation of 6 samples, independently, and the subsequent analysis thereof. In this way, the MATE makes possible continuous mechanical stimulation of engineered cartilage with active monitoring of sample mechanical properties. Chapter 3 characterized and optimized MATE stimulation for engineered cartilage, identifying a loading protocol suitable for nascent and mature tissues. Subsequent application of this protocol demonstrate the beneficial effects of force-controlled deformational loading on the functional development of tissue-engineered cartilage. Following four weeks of MATE stimulation, clinically sized engineered cartilage derived from adult human chondrocytes achieved near native levels of compressive equilibrium moduli (∼175 kPa), the highest properties reported to date. Together, we've confirmed the benefits of dynamic compressive loading *in vitro* and provided an avenue for clinical translation of large diameter, adult human chondrocyte based tissues via MATE bioreactor cultivation.

7.1.2 Chondroprotection via internal delivery of dexamethasone

In Part II, we sought an approach to prepare tissue-engineered cartilage for the rigors of the inflammatory environment *in vivo*. In doing so, we developed a drug delivery system for the anti-inflammatory glucocorticoid (GC) dexamethasone (Chapter 3) and demonstrated its ability to promote cartilage growth and provide protection from pro-inflammatory cytokines *in vitro* (Chapter 4). A biodegradable polymer, poly(lactic-*co*-glycolic acid) (PLGA) was used to encapsulate dexamethasone and provide for a predictable release of the steroid. Unlike intra-articular (IA) injections often used in the clinic, these microspheres released dexamethasone at a concentration nearly 200,000x lower than bolus IA injections used clinically (Goodman, 1996; Sherman *et al.* , 2015b;

Sherman *et al.* , 2015a), minimizing the negative effects typically associated with GCs (Habib, 2009; Habib *et al.* , 2010), and comparable to the concentrations used in standard chondrogenic culture mediums (Bian *et al.* , 2010a; Lima *et al.* , 2007; Lima *et al.* , 2008a). Characterization of the release profile of these microspheres indicate a zero order, sustained release of dexamethasone for at least 90 days. In light of recent work indicating that implant maturity plays a significant role in clinical tissue success (Miot *et al.* , 2012), this prolonged release of dexamethasone may serve to provide construct protection against pro-inflammatory cytokines following implantation, in addition to fostering development of functional tissues *in vitro*. To this end, Chapter 4 demonstrates the chondroprotective capacity of dexamethasone-loaded microspheres *in vitro*. Following four weeks of culture, during which internal delivery of dexamethasone promoted the development of near native levels of mechanical and biochemical properties, tissues were challenged with a supraphysiologic level of pro-inflammatory cytokine. Tissues containing dexamethasone-releasing microspheres were able to maintain tissue properties during chemical insult, while the impact on unprotected tissues was detrimental. These results suggest an approach utilizing dexamethasone-releasing microspheres may be successful in protecting tissue-engineered cartilage in a pre-clinical model of OA and improve gross cartilage repair.

7.1.3 Fabrication process for anatomical resurfacing

In Part III of this dissertation, we developed a universal approach for digitizing, modeling, and fabricating biofidelic osteochondral tissue-engineered constructs. While fresh osteochondral allografts are the gold-standard for large defect cartilage repair, limited availability of suitable grafts and technical demands of the procedure have prompted the search for a cell-based alternative. In addressing this need, the work presented in Chapter 5 developed a general strategy for producing tissue-engineered cartilage with biofidelic shape and detailed how this principle might be applied to the fabrication of an osteochondral allograft. This bilayered structure combined high-resolution laser scanning technology, modeling software, injection molding, and 3D printing to create a highly resolved graft with anatomically-accurate curvatures. In restoring congruency of articulating surfaces, this approach aims to recapitulate normal loading stress and patterns, allowing for improved kinematic function of the joint and improving quality of life for patients.

The work presented in this dissertation leads us to accept our Global Hypothesis. In doing so,

this work provides a strategy for the cultivation of biofidelic, tissue-engineered cartilage well-suited to the mechanical and chemical rigors of everyday life *in vivo*.

7.2 Future Directions

This dissertation presents a holistic strategy for functional tissue engineering of articular cartilage. Moving forward, several avenues should be explored to further this work and address other foci currently investigated in the laboratory. A brief overview of these complementary research areas is below.

7.2.1 Cartilage-cartilage integration in an inflammatory model of focal defect repair

The integration of cartilage tissue grafts with their surrounding host cartilage has a profound impact on the stability of tissue repair as well as viability and functionality of the restored joint surface. As such, the impact of pro-inflammatory cytokines on tissue integration can be detrimental to the success of graft implantation procedures. In a meniscal injury model in vitro, IL-1 has been shown to inhibit integrative repair (Wilusz *et al.* , 2008; McNulty *et al.* , 2010; Hennerbichler *et al.* , 2007), and in an established *in vitro* cartilage defect model (Theodoropoulos *et al.* , 2011; Hunter & Levenston, 2004; Gilbert *et al.* , 2009; Djouad *et al.* , 2009; Reindel *et al.* , 1995; Hunter *et al.* , 2004; Hunter & Levenston, 2002), the integration of tissue-engineered, chondrocyte-laden agarose constructs into native articular cartilage was observed to be inhibited by exposure to pro-inflammatory cytokines and the subsequent activation of extracellular regulated kinase 1/2 (Djouad *et al.* , 2009). Further, inhibition of inflammatory pathways has been shown to improve cartilage repair outcomes in vivo (Kimmerling *et al.* , 2015; Olson *et al.* , 2015), with GC injection being shown to improve integration between cartilage surfaces (Englert *et al.* , 2006). These results indicate that suppression of the inflammatory environment in the joint, potentially via GCs (as described in Chapter 4), is vital to successful integration of engineered cartilage *in vivo* (Morisset *et al.* , 2007).

We have done preliminary work in this effort to investigate the impact of tissue maturity and the influence of pro-inflammatory cytokines on integration of tissue-engineered constructs with native cartilage explants. Tissue-engineered constructs (derived from juvenile bovine chondrocytes) containing either (a) no microspheres, (b) dexamethasone-loaded microspheres, or (c) empty microspheres were implanted in cartilage explant rings at three time points and a supraphysiologic dose

of pro-inflammatory cytokine was applied for the following week. Following this week in culture, push-out testing results indicate (Tam *et al.* , 2007; Tan *et al.* , 2009; Dhert *et al.* , 1992; Gilbert *et al.* , 2009; Hunter & Levenston, 2004), as expected, that periods of increased biosynthetic activity in culture lead to improved integration along the construct-explant interface. Moreover, these results indicate that dexamethasone release internally from tissue-engineered constructs significantly improves construct-explant integration in a pro-inflammatory environment (Figure 7.2).

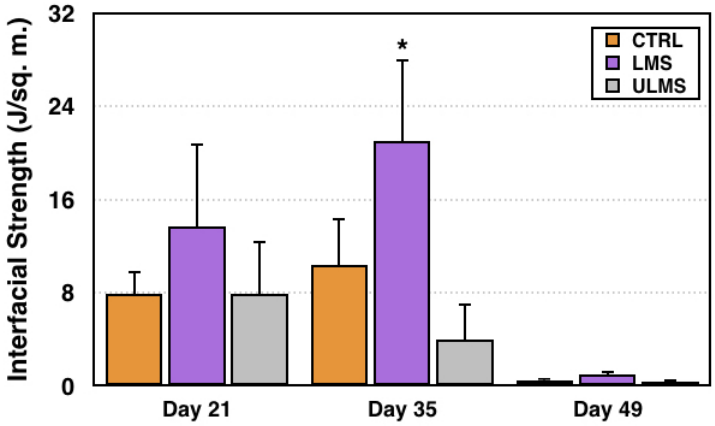

Figure 7.2: LMS tissues, containing dexamethasone-loaded microspheres, demonstrated significantly improved integration when compared with CTRL tissues without microspheres. ULMS tissues, containing empty microspheres, performed similarly to CTRL tissues early in culture, but quickly declined after the cessation of TGF-β3. * indicates a statistically significant difference compared to other tissues.

Additional work is needed to ensure maintenance of tissue properties during cytokine treatment, determine the role of tissue swelling in tissue integration, and explore the likelihood that similar results will be observed in a clinically relevant, adult chondrocyte cell source.

7.2.2 Acellular, microsphere-laden hydrogel for combination therapy with osteochondral autograft transfer system (OATS)

Chapter 4 investigates dexamethasone-loaded PLGA microspheres for applications in cellular-based therapies to protect nascent tissues against the pro-inflammatory environment of the knee joint. As an extension of that work, our laboratory is investigating the use of these microspheres within acellular hydrogels as a pure drug delivery strategy to mitigate the deleterious effect of pro-inflammatory cytokines following surgery. OATS, a common procedure to replace focal defects with cartilage from non-weight bearing areas of the patient's own joint, suffers from exposure to the cytokine rich

synovial environment following surgery. These chemical factors negatively effect graft incorporation and integrity (Amin *et al.* , 2009; Amin *et al.* , 2010; D'Lima *et al.* , 2006; Goldring & Goldring, 2004; Houston *et al.* , 2013; Lotz & Kraus, 2010; Patwari *et al.* , 2003), leading to tissue degradation and failure of the graft to integrate with host tissue (Wilusz *et al.* , 2008; Djouad *et al.* , 2009).

Building from discoveries made during microsphere development in this dissertation (Chapter 3), we propose to backfill the donor site with a dexamethasone-loaded PLGA laden hydrogel plug that serves to 1) prevent donor site morbidity (LaPrade & Botker, 2004) and 2) to deliver a therapeutic level of dexamethasone to the joint space (Lu *et al.* , 2011) to promote tissue repair at the recipient site.

In recognition of osteoarthritis as a disease of the entire knee joint, parallel strategies are being developed to deliver dexamethasone-loaded microspheres via acellular (and cellular) patches affixed to the synovium (Figure 7.3) . In doing so, we intend to treat the articular cartilage as well as the synovial lining of the joint, an often overlooked but integral component to the success of cartilage repair.

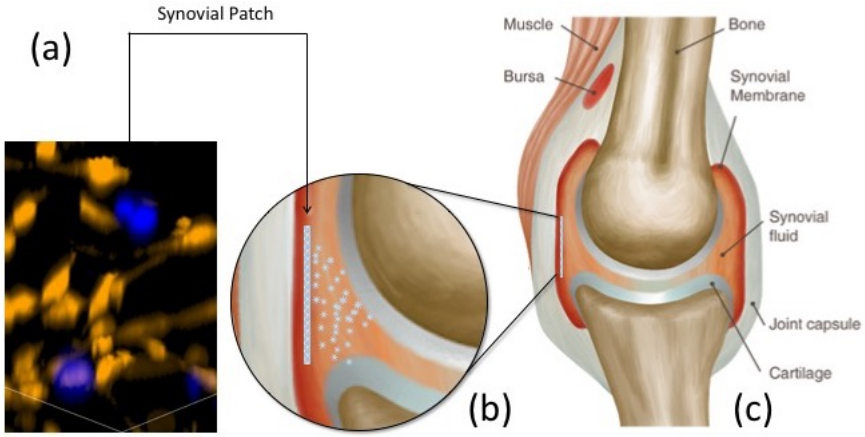

Figure 7.3: Schematic of envisaged synovial patch (a) with dexamethasone releasing microspheres in engineered synovium affixed to inner synovial lining (b) of the knee joint (c). Inset confocal image of canine synovial cells (orange) and fluorescently-labeled dexamethasone microspheres (dexfluorescein, blue).

7.2.3 Dexamethasone fluorescein for single cell analysis

Motivated by Chapter 4 of this dissertation, our laboratory has recently developed an interest in using dexamethasone fluorescein for studies of GC activation and binding in chondrocytes and

fibroblast-like synoviocytes (FLS). The use of dexamethasone, and GCs more generally, as an anti-inflammatory agent in IA injections is well established (Habib, 2009; Habib *et al.* , 2010; Dragoo *et al.* , 2012; Wernecke *et al.* , 2015; Mader *et al.* , 2005). Dexamethasone, a lipid, can enter the cell where it acts directly and indirectly by activating anti-inflammatory proteins in the cytosol (Hafezi-Moghadam *et al.* , 2002; Cato *et al.* , 2002), upregulating pro-anabolic protein production via GC-responsive elements on DNA (Hebbar & Archer, 2003; Nagaich *et al.* , 2004), and by interfering with translocation of other transcriptional factors, namely nuclear factor-kappa B, to the nucleus (McKay & Cidlowski, 1998; McKay & Cidlowski, 1999; De Bosscher *et al.* , 2003). A better understanding of steroid binding kinetics, however, may shed light to the variable responses of patients who receive IA steroid injections. To this end, we have performed preliminary experiments to assess the feasibility of identifying GC-responsive elements in chondrocytes via dexamethasone fluorescein. Early results indicate that binding within the nucleus (Figure 7.4b) and within the cytosol (Figure 7.4c) can be captured.

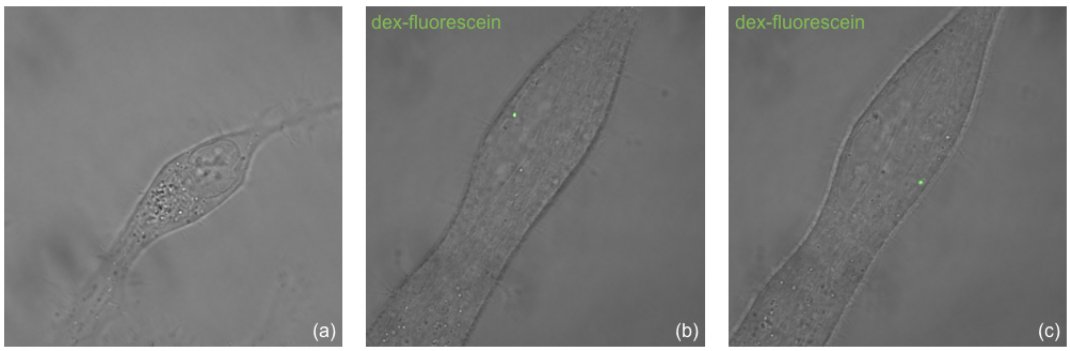

Figure 7.4: Application of dexamethasone fluorescein for single cell analysis of glucocorticoid receptor binding. (a) 0 µM DEX. (b), (c) 1 µM images from different levels within z-stack. Green indicates dexamethasone fluorescein binding the GC-receptor. (b) is nuclear translocation of the GC-complex while (c) is binding in the cytosol. Images acquired with 100x objective.

Using this technique, future investigations should explore the following questions: Is there a delay to onset of benefits from glucocorticoid binding? What is the stability of dexamethasone following binding and activation of the GC-complex? What is the impact of GC receptor antagonist on the anti-inflammatory capacity of dexamethasone?

Moreover, for 3D applications, we have successfully encapsulated dexamethasone fluorescein with PLGA microspheres and embedded them within agarose hydrogels. In this way, mechanistic investigations of chondrocyte response to GCs may more accurately reflect how chondrocytes will

respond *in vivo*.

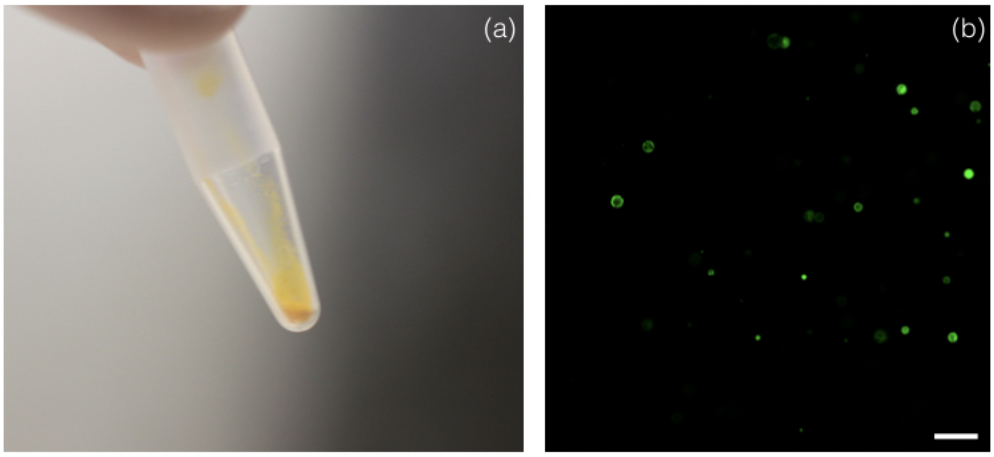

Figure 7.5: (a) Dexamethasone fluorescein-loaded PLGA microspheres (b) embedded within agarose hydrogels. Scale bar = 200 µm.

Part V

References and Appendices

References

Adam, C, Eckstein, F, Milz, S, Schulte, E, Becker, C, & Putz, R. 1998. The distribution of cartilage thickness in the knee-joints of old-aged individuals—measurement by A-mode ultrasound. *Clinical Biomechanics*, **13**(1), 1–10.

Adkisson, H Davis, Martin, James A, Amendola, Richard L, Milliman, Curt, Mauch, Kelsey A, Katwal, Arbindra B, Seyedin, Mitchell, Amendola, Annuziato, Streeter, Philip R, & Buckwalter, Joseph A. 2010. The potential of human allogeneic juvenile chondrocytes for restoration of articular cartilage. *American Journal of Sports Medicine*, **38**(7), 1324–1333.

Ahmad, Christopher S, Cohen, Zohara A, Levine, William N, Ateshian, Gerard A, & Mow, Van C. 2001. Biomechanical and topographic considerations for autologous osteochondral grafting in the knee. *The American journal of sports medicine*, **29**(2), 201–206.

Albro, Michael B, Nims, Robert J, Durney, Krista M, Cigan, Alexander D, Shim, Jay J, Vunjak-Novakovic, Gordana, Hung, Clark T., & Ateshian, Gerard A. 2016. Heterogeneous engineered cartilage growth results from gradients of media-supplemented active TGF-beta and is ameliorated by the alternative supplementation of latent TGF-beta. *Biomaterials*, **77**, 173–185.

Alimohammadi, Younes Hanifehpour, & Joo, Sang Woo. 2014. PLGA-based nanoparticles as cancer drug delivery systems. *Asian Pac J Cancer Prev*, **15**, 517–535.

Amici, E, Clark, A H, Normand, V, & Johnson, N B. 2000. Interpenetrating Network Formation in Gellan−Agarose Gel Composites. *Biomacromolecules*, **1**(4), 721–729.

Amin, Anish K, Huntley, James S, Bush, Peter G, Simpson, A Hamish R W, & Hall, Andrew C. 2009. Chondrocyte death in mechanically injured articular cartilage–the influence of extracellular calcium. *Journal of orthopaedic research : official publication of the Orthopaedic Research Society*, **27**(6), 778–784.

Amin, Anish K, Huntley, James S, Simpson, A Hamish R W, & Hall, Andrew C. 2010. Increasing the osmolarity of joint irrigation solutions may avoid injury to cartilage: a pilot study. *Clinical Orthopaedics and Related Research*, **468**(3), 875–884.

Ateshian, GA, Soslowsky, LJ, & Mow, VC. 1991. Quantitation of articular surface topography and cartilage thickness in knee joints using stereophotogrammetry. *Journal of biomechanics*, **24**(8), 761–776.

Ateshian, GA, Rosenwasser, MP, & Mow, VC. 1992. Curvature characteristics and congruence of the thumb carpometacarpal joint: differences between female and male joints. *Journal of biomechanics*, **25**(6), 591–607.

Ateshian, Gerard A., & Hung, Clark T. 2005. Patellofemoral joint biomechanics and tissue engineering. *Clinical Orthopaedics and Related Research®*, July, 81–90.

Ateshian, Gerard A., Ark, J W, Rosenwasser, M P, Pawluk, R J, Soslowsky, L J, & Mow, V C. 1995. Contact areas in the thumb carpometacarpal joint. *Journal of Orthopaedic Research*, **13**(3), 450–458.

Ateshian, Gerard A, Soltz, Michael A, Mauck, Robert L, Basalo, Ines M, Hung, Clark T, & Lai, W Michael. 2003. The role of osmotic pressure and tension-compression nonlinearity in the frictional response of articular cartilage. *Transport in porous media*, **50**(1-2), 5–33.

Ateshian, Gerard A, Chahine, Nadeen O, Basalo, Ines M, & Hung, Clark T. 2004. The correspondence between equilibrium biphasic and triphasic material properties in mixture models of articular cartilage. *Journal of biomechanics*, **37**(3), 391–400.

Athens, Aristos A, Makris, Eleftherios A, & Hu, Jerry C. 2013. Induced collagen cross-links enhance cartilage integration. *PloS one*, **8**(4), e60719.

Aufderheide, Adam C, & Athanasiou, Kyriacos A. 2006. A Direct Compression Stimulator for Articular Cartilage and Meniscal Explants. *Annals of Biomedical Engineering*, **34**(9), 1463–1474.

Ayers, DC. 1997. Polyethylene wear and osteolysis following total knee replacement. *Instructional course lectures*, **46**, 205.

Backes, Jeffrey R, Bentley, Jared C, Politi, Joel R, & Chambers, Bryan T. 2013. Dexamethasone reduces length of hospitalization and improves postoperative pain and nausea after total joint arthroplasty: a prospective, randomized controlled trial. *The Journal of Arthroplasty*, **28**(8 Suppl), 11–17.

Bae, Soon Eon, Choi, Dong Hoon, Han, Dong Keun, & Park, Kwideok. 2010. Effect of temporally controlled release of dexamethasone on in vivo chondrogenic differentiation of mesenchymal stromal cells. *Journal of controlled release : official journal of the Controlled Release Society*, **143**(1), 23–30.

Ballyns, Jeffery J, Gleghorn, Jason P, Niebrzydowski, Vicki, Rawlinson, Jeremy J, Potter, Hollis G, Maher, Suzanne A, Wright, Timothy M, & Bonassar, Lawrence J. 2008. Image-guided tissue engineering of anatomically shaped implants via MRI and micro-CT using injection molding. *Tissue Engineering. Part A*, **14**(7), 1195–1202.

Ballyns, Jeffrey J, & Bonassar, Lawrence J. 2011. Dynamic compressive loading of image-guided tissue engineered meniscal constructs. *Journal of Biomechanics*, **44**(3), 509–516.

Bank, Ruud A, Soudry, Michael, Maroudas, Alice, Mizrahi, Joseph, & TeKoppele, Johan M. 2000. The increased swelling and instantaneous deformation of osteoarthritic cartilage is highly correlated with collagen degradation. *Arthritis & Rheumatism*, **43**(10), 2202–2210.

Barbero, Andrea, Ploegert, Sabine, Heberer, Michael, & Martin, Ivan. 2003. Plasticity of clonal populations of dedifferentiated adult human articular chondrocytes. *Arthritis & Rheumatism*, **48**(5), 1315–1325.

Barbero, Andrea, Grogan, Shawn, Schäfer, Dirk, Heberer, Michael, Mainil-Varlet, Pierre, & Martin, Ivan. 2004. Age related changes in human articular chondrocyte yield, proliferation and post-expansion chondrogenic capacity. *Osteoarthritis and Cartilage*, **12**(6), 476–484.

Basser, P J, Schneiderman, R, Bank, R A, Wachtel, E, & Maroudas, Alice. 1998. Mechanical properties of the collagen network in human articular cartilage as measured by osmotic stress technique. *Archives of Biochemistry and Biophysics*, **351**(2), 207–219.

Bastiaansen-Jenniskens, Y M, Koevoet, W, de Bart, A C W, van der Linden, J C, Zuurmond, A-M, Weinans, H, Verhaar, J A N, van Osch, G.J.V.M., & DeGroot, J. 2008. Contribution of collagen network features to functional properties of engineered cartilage. *Osteoarthritis and cartilage / OARS, Osteoarthritis Research Society*, **16**(3), 359–366.

Baudis, Stefan, Nehl, Franziska, Ligon, S Clark, Nigisch, Anneliese, Bergmeister, Helga, Bernhard, David, Stampfl, Jürgen, & Liska, Robert. 2011. Elastomeric degradable biomaterials by photopolymerization-based CAD-CAM for vascular tissue engineering. *Biomedical materials (Bristol, England)*, **6**(5), 055003.

Beekhuizen, Michiel, van Osch, Gerjo J V M, Bot, Arjan G J, Hoekstra, Myrthe C L, Saris, Daniel B F, Dhert, Wouter J A, & Creemers, Laura B. 2013. Inhibition of oncostatin M in osteoarthritic synovial fluid enhances GAG production in osteoarthritic cartilage repair. *European cells & materials*, **26**, 80–90– discussion 90.

Benya, P. 1982. Dedifferentiated chondrocytes reexpress the differentiated collagen phenotype when cultured in agarose gels. *Cell*, **30**(1), 215–224.

Bhumiratana, Sarindr, Eton, Ryan E, Oungoulian, Sevan R, Wan, Leo Q, Ateshian, Gerard A, & Vunjak-Novakovic, Gordana. 2014. Large, stratified, and mechanically functional human cartilage grown in vitro by mesenchymal condensation. *Proceedings of the National Academy of Sciences*, **111**(19), 6940–6945.

Bian, Liming, Angione, S. L., Ng, K. W., Lima, E G, Williams, D. Y., Mao, D. Q., Ateshian, Gerard A., & Hung, Clark T. 2009a. Influence of decreasing nutrient path length on the development of engineered cartilage. *Osteoarthritis and cartilage / OARS, Osteoarthritis Research Society*, **17**(5), 677–685.

Bian, Liming, Crivello, Keith M, Ng, Kenneth W, Xu, Duo, Williams, David Y, Ateshian, Gerard A., & Hung, Clark T. 2009b. Influence of temporary chondroitinase ABC-induced glycosaminoglycan suppression on maturation of tissue-engineered cartilage. *Tissue Engineering. Part A*, **15**(8), 2065–2072.

Bian, Liming, Fong, Jason V, Lima, E G, Stoker, Aaron M, Ateshian, Gerard A., Cook, James L, & Hung, Clark T. 2010a. Dynamic mechanical loading enhances functional properties of tissue-engineered cartilage using mature canine chondrocytes. *Tissue Engineering. Part A*, **16**(5), 1781–1790.

Bian, Liming, Stoker, Aaron M, Marberry, Kevin M, Ateshian, Gerard A., Cook, James L, & Hung, Clark T. 2010b. Effects of dexamethasone on the functional properties of cartilage explants during long-term culture. *American Journal of Sports Medicine*, **38**(1), 78–85.

Bonaventure, J, Kadhom, N, Cohen-Solal, L, Ng, KH, Bourguignon, J, Lasselin, C, & Freisinger, P. 1994. Reexpression of cartilage-specific genes by dedifferentiated human articular chondrocytes cultured in alginate beads. *Experimental cell research*, **212**(1), 97–104.

Bouissou, C, Rouse, J J, Price, R, & van der Walle, C F. 2006. The influence of surfactant on PLGA microsphere glass transition and water sorption: remodeling the surface morphology to attenuate the burst release. *Pharmaceutical Research*, **23**(6), 1295–1305.

Bradley, Gary W, Freeman, Michael AR, Tuke, Michael A, & McKellop, Harry A. 1993. Evaluation of wear in an all-polymer total knee replacement. Part 2: clinical evaluation of wear in a polyethylene on polyacetal total knee. *Clinical materials*, **14**(2), 127–132.

Breuner, C W, & Orchinik, M. 2002. Plasma binding proteins as mediators of corticosteroid action in vertebrates. *The Journal of endocrinology*, **175**(1), 99–112.

Brittberg, M, Lindahl, A, Nilsson, A, Ohlsson, C, Isaksson, O, & Peterson, L. 1994. Treatment of deep cartilage defects in the knee with autologous chondrocyte transplantation. *The New England journal of medicine*, **331**(14), 889–895.

Brown, Bryan N, Siebenlist, Nicholas J, Cheetham, Jonathan, Ducharme, Norm G, Rawlinson, Jeremy J, & Bonassar, Lawrence J. 2013. Computed tomography-guided tissue engineering of upper airway cartilage. *Tissue Engineering Part C: Methods*, **20**(6), 506–513.

Buckley, C. T., Meyer, E. G., & Kelly, Daniel J. 2012. The influence of construct scale on the composition and functional properties of cartilaginous tissues engineered using bone marrow-derived mesenchymal stem cells. *Tissue Engineering. Part A*, **18**(3-4), 382–396.

Buckwalter, Joseph. 2004a. *Articular Cartilage Part I: Tissue Design and Chondrocyte-Matrix Interactions*. Informa Healthcare.

Buckwalter, Joseph. 2004b. *Articular Cartilage Part II: Degeneration and Osteoarthrosis, Repair, Regeneration, and Transplantation*. Informa Healthcare.

Buckwalter, Joseph A, & Brown, Thomas D. 2004. Joint Injury, Repair, and Remodeling. *Clinical Orthopaedics and Related Research*, **423**, 7–16.

Bugbee, William D. 2002. Fresh osteochondral allografts. *The journal of knee surgery*, **15**(3), 191–195.

Burdick, Jason A, & Prestwich, Glenn D. 2011. Hyaluronic acid hydrogels for biomedical applications. *Advanced materials*, **23**(12).

Buschmann, Michael D, Gluzband, Yehezkiel A, Grodzinsky, Alan J, & Hunziker, Ernst B. 1995. Mechanical compression modulates matrix biosynthesis in chondrocyte/agarose culture. *Journal of cell science*, **108**(4), 1497–1508.

Buschmann, Michael D, Kim, Young-Jo, Wong, Marcy, Frank, Eliot, Hunziker, Ernst B, & Grodzinsky, Alan J. 1999. Stimulation of Aggrecan Synthesis in Cartilage Explants by Cyclic Loading Is Localized to Regions of High Interstitial Fluid Flow1. *Archives of Biochemistry and Biophysics*, **366**(1), 1–7.

Butler, David L, Goldstein, Steven A, & Guilak, Farshid. 2000. Functional tissue engineering: the role of biomechanics. *Journal of biomechanical engineering*, **122**(6), 570–575.

Butler, David L, Hunter, Shawn A, Chokalingam, Kumar, Cordray, Michael J, Shearn, Jason, Juncosa-Melvin, Natalia, Nirmalanandhan, Sanjit, & Jain, Abhishek. 2009. Using functional tissue engineering and bioreactors to mechanically stimulate tissue-engineered constructs. *Tissue engineering. Part A*, **15**(4), 741–749.

Byers, Benjamin A. 2006. Temporal exposure of TGF-beta3 under serum-free conditions enhance biomechanical and biochemical maturation of tissue-engineered cartilage. *Transactions of the Orthopaedic Research Society*, 31–43.

Byers, Benjamin A, Mauck, Robert L, Chiang, Ian E, & Tuan, Rocky S. 2008. Transient exposure to transforming growth factor beta 3 under serum-free conditions enhances the biomechanical and biochemical maturation of tissue-engineered cartilage. *Tissue Engineering Part A*, **14**(11), 1821–1834.

Campos, Daniela F Duarte, Blaeser, Andreas, Weber, Michael, Jäkel, Jörg, Neuss, Sabine, Jahnen-Dechent, Wilhelm, & Fischer, Horst. 2012. Three-dimensional printing of stem cell-laden hydrogels submerged in a hydrophobic high-density fluid. *Biofabrication*, **5**(1), 015003.

Cao, Y, Vacanti, J P, Paige, K T, Upton, J, & Vacanti, C A. 1997. Transplantation of chondrocytes utilizing a polymer-cell construct to produce tissue-engineered cartilage in the shape of a human ear. *Plastic and reconstructive surgery*, **100**(2), 297–302– discussion 303–4.

Caplan, Arnold I. 2007. Adult mesenchymal stem cells for tissue engineering versus regenerative medicine. *Journal of cellular physiology*, **213**(2), 341–347.

Cassino, Theresa R, Anderson, Roger, Love, Brian J, Huckle, William R, Seamans, Diane K, & Forsten Williams, Kimberly. 2007. Design and application of an oscillatory compression device for cell constructs. *Biotechnology and Bioengineering*, **98**(1), 211–220.

Cato, Andrew C B, Nestl, Andrea, & Mink, Sigrun. 2002. Rapid actions of steroid receptors in cellular signaling pathways. *Science's STKE : signal transduction knowledge environment*, **2002**(138), re9–re9.

Chahine, Nadeen O, Wang, Christopher CB, Hung, Clark T, & Ateshian, Gerard A. 2004. Anisotropic strain-dependent material properties of bovine articular cartilage in the transitional range from tension to compression. *Journal of biomechanics*, **37**(8), 1251–1261.

Chahine, Nadeen O, Chen, Faye H, Hung, Clark T, & Ateshian, Gerard A. 2005. Direct measurement of osmotic pressure of glycosaminoglycan solutions by membrane osmometry at room temperature. *Biophysical journal*, **89**(3), 1543–1550.

Cigan, Alexander D, Nims, Robert J, Albro, Michael B, Esau, John D, Dreyer, Marissa P, Vunjak-Novakovic, Gordana, Hung, Clark T, & Ateshian, Gerard A. 2013. Insulin, ascorbate, and glucose have a much greater influence than transferrin and selenous acid on the in vitro growth of engineered cartilage in chondrogenic media. *Tissue Engineering Part A*, **19**(17-18), 1941–1948.

Cigan, Alexander D, Roach, Brendan L, Nims, Robert J, Tan, Andrea R, Albro, Michael B, Stoker, Aaron M, Cook, James L, Vunjak-Novakovic, Gordana, Hung, Clark T, & Ateshian, Gerard A. 2016. High seeding density of human chondrocytes in agarose produces tissue-engineered cartilage approaching native mechanical and biochemical properties. *Journal of biomechanics*, **49**(9), 1909–1917.

Cleaver, C S. 2001. Interleukin 13 blocks the release of collagen from bovine nasal cartilage treated with proinflammatory cytokines. *Annals of the rheumatic diseases*, **60**(2), 150–157.

Cohen, B, Lai, W. M., & Mow, V C. 1998. A Transversely Isotropic Biphasic Model for Unconfined Compression of Growth Plate and Chondroepiphysis. *Journal of Biomechanical Engineering*, **120**(4), 491.

Cohen, Z A, McCarthy, D M, Kwak, S D, Legrand, P, Fogarasi, F, Ciaccio, E J, & Ateshian, Gerard A. 1999. Knee cartilage topography, thickness, and contact areas from MRI: in-vitro calibration and in-vivo measurements. *Osteoarthritis and Cartilage*, **7**(1), 95–109.

Cooney, W P, & Chao, E Y. 1977. Biomechanical analysis of static forces in the thumb during hand function. *The Journal of Bone and Joint Surgery*, **59**(1), 27–36.

Dang, Tram T, Bratlie, Kaitlin M, Bogatyrev, Said R, Chen, Xiao Y, Langer, Robert, & Anderson, Daniel G. 2011. Spatiotemporal effects of a controlled-release anti-inflammatory drug on the cellular dynamics of host response. *Biomaterials*, **32**(19), 4464–4470.

Davisson, Twana, Kunig, Sabine, Chen, Albert, Sah, Robert, & Ratcliffe, Anthony. 2002. Static and dynamic compression modulate matrix metabolism in tissue engineered cartilage. *Journal of Orthopaedic Research*, **20**(4), 842–848.

Dawes, G J S, Fratila-Apachitei, L E, Necula, B S, Apachitei, I, Witkamp, G J, & Duszczyk, J. 2010. Release of PLGA-encapsulated dexamethasone from microsphere loaded porous surfaces. *Journal of materials science. Materials in medicine*, **21**(1), 215–221.

De Bosscher, Karolien, Vanden Berghe, Wim, & Haegeman, Guy. 2003. The interplay between the glucocorticoid receptor and nuclear factor-kappaB or activator protein-1: molecular mechanisms for gene repression. *Endocrine reviews*, **24**(4), 488–522.

Defail, A. J., Edington, H. D., Edington, H. D., Matthews, S., Matthews, S., Lee, W. C., Lee, W. C., & Marra, K. G. 2006. Controlled release of bioactive doxorubicin from microspheres embedded within gelatin scaffolds. *J. Biomed. Mater. Res. A*, **79**(4), 954–962.

DeRijk, R, Michelson, D, Karp, B, Petrides, J, Galliven, E, Deuster, P, Paciotti, G, Gold, P W, & Sternberg, E M. 1997. Exercise and circadian rhythm-induced variations in plasma cortisol differentially regulate interleukin-1 beta (IL-1 beta), IL-6, and tumor necrosis factor-alpha (TNF alpha) production in humans: high sensitivity of TNF alpha and resistance of IL-6. *The Journal of clinical endocrinology and metabolism*, **82**(7), 2182–2191.

Dhert, Wouter J A, Verheyen, C C P M, Braak, L H, de Wijn, J R, Klein, C P A T, de Groot, K, & Rozing, P M. 1992. A Finite-Element Analysis of the Push-Out Test - Influence of Test Conditions. *Journal of biomedical materials research*, **26**(1), 119–130.

Diekman, Brian O, Rowland, Christopher R, Lennon, Donald P, Caplan, Arnold I, & Guilak, Farshid. 2010. Chondrogenesis of Adult Stem Cells from Adipose Tissue and Bone Marrow: Induction by Growth Factors and Cartilage-Derived Matrix. *Tissue Engineering. Part A*, **16**(2), 523–533.

Djouad, Farida, Rackwitz, Lars, Song, Yingjie, Janjanin, Sasa, & Tuan, Rocky S. 2009. ERK1/2 activation induced by inflammatory cytokines compromises effective host tissue integration of engineered cartilage. *Tissue Engineering. Part A*, **15**(10), 2825–2835.

D'Lima, Darryl D., Hermida, Juan, Hashimoto, Sanshiro, Colwell, Clifford, & Lotz, Martin. 2006. Caspase inhibitors reduce severity of cartilage lesions in experimental osteoarthritis. *Arthritis & Rheumatism*, **54**(6), 1814–1821.

Dragoo, Jason L, Danial, Christina M, Braun, Hillary J, Pouliot, Michael A, & Kim, Hyeon-Joo. 2012. The chondrotoxicity of single-dose corticosteroids. *Knee surgery, sports traumatology, arthroscopy : official journal of the ESSKA*, **20**(9), 1809–1814.

Dvorak, Laura D, Cook, James L, Kreeger, John M, Kuroki, Keiichi, & Tomlinson, James L. 2002. Effects of carprofen and dexamethasone on canine chondrocytes in a three-dimensional culture model of osteoarthritis. *American journal of veterinary research*, **63**(10), 1363–1369.

Eberhardt, A W, Keer, L M, Lewis, J L, & Vithoontien, V. 1990. An Analytical Model of Joint Contact. *Journal of Biomechanical Engineering*, **112**(4), 407.

Eckstein, Felix, Sittek, H, Milz, S, Putz, R, & Reiser, M. 1994. The morphology of articular cartilage assessed by magnetic resonance imaging (MRI). *Surgical and Radiologic Anatomy*, **16**(4), 429–438.

Eckstein, Felix, Buck, Robert J, Wyman, Bradley T, Kotyk, John J, Graverand, Le, Hellio, Marie-Pierre, Remmers, Ann E, Evelhoch, Jeffrey L, Hudelmaier, Martin, & Charles, H Cecil. 2007. Quantitative imaging of cartilage morphology at 3.0 Tesla in the presence of gadopentate dimeglumine (Gd-DTPA). *Magnetic resonance in medicine*, **58**(2), 402–406.

Ehrlich, S, Wolff, N, Schneiderman, R, Maroudas, A, Parker, KH, & Winlove, CP. 1998. The osmotic pressure of chondroitin sulphate solutions: experimental measurements and theoretical analysis. *Biorheology*, **35**(6), 383–397.

Elder, Benjamin D, Mohan, Arvind, & Athanasiou, Kyriacos A. 2011. Beneficial effects of exogenous crosslinking agents on self-assembled tissue engineered cartilage construct biomechanical properties. *Journal of Mechanics in Medicine and Biology*, **11**(02), 433–443.

Eleswarapu, Sriram V, & Athanasiou, Kyriacos A. 2013. TRPV4 channel activation improves the tensile properties of self-assembled articular cartilage constructs. *Acta biomaterialia*, **9**(3), 5554–5561.

Eleswarapu, Sriram V, Chen, Justin A, & Athanasiou, Kyriacos A. 2011. Temporal assessment of ribose treatment on self-assembled articular cartilage constructs. *Biochemical and biophysical research communications*, **414**(2), 431–436.

Elsaid, K A, Zhang, L, Shaman, Z, Patel, C, Schmidt, T A, & Jay, G D. 2015. The impact of early intra-articular administration of interleukin-1 receptor antagonist on lubricin metabolism and cartilage degeneration in an anterior cruciate ligament transection model. *Osteoarthritis and cartilage / OARS, Osteoarthritis Research Society*, **23**(1), 114–121.

Elsaid, Khaled A, Ubhe, Anand, Shaman, Ziyad, & D'Souza, Gerard. 2016. Intra-articular interleukin-1 receptor antagonist (IL1-ra) microspheres for posttraumatic osteoarthritis: in vitro biological activity and in vivo disease modifying effect. *Journal of experimental orthopaedics*, **3**(1), 18.

Englert, Carsten, Blunk, Torsten, Fierlbeck, Johann, Kaiser, Julia, Stosiek, Wolfgang, Angele, Peter, Hammer, Joachim, & Straub, Rainer H. 2006. Steroid hormones strongly support bovine articular cartilage integration in the absence of interleukin-1beta. *Arthritis & Rheumatism*, **54**(12), 3890–3897.

Englund, M, Roos, E M, & Lohmander, L Stefan. 2003. Impact of type of meniscal tear on radiographic and symptomatic knee osteoarthritis: A sixteen-year followup of meniscectomy with matched controls. *Arthritis & Rheumatism*, **48**(8), 2178–2187.

Estes, Bradley T, Wu, Arthur W, Wu, Arthur W, Storms, Robert W, Storms, Robert W, & Guilak, Farshid. 2006a. Extended passaging, but not aldehyde dehydrogenase activity, increases the chondrogenic potential of human adipose-derived adult stem cells. *Journal of cellular physiology*, **209**(3), 987–995.

Estes, Bradley T, Wu, Arthur W, & Guilak, Farshid. 2006b. Potent induction of chondrocytic differentiation of human adipose-derived adult stem cells by bone morphogenetic protein 6. *Arthritis & Rheumatism*, **54**(4), 1222–1232.

Estes, Bradley T, Diekman, Brian O, & Guilak, Farshid. 2008. Monolayer cell expansion conditions affect the chondrogenic potential of adipose-derived stem cells. *Biotechnology and Bioengineering*, **99**(4), 986–995.

Eyre, David R, & Wu, Jiann-Jiu. 2005. Collagen cross-links. *Pages 207–229 of: Collagen*. Springer.

Fargnoli, Anthony S, Mu, Anbin, Katz, Michael G, Williams, Richard D, Margulies, Kenneth B, Weiner, David B, Yang, Shu, & Bridges, Charles R. 2014. Anti-inflammatory loaded poly-lactic glycolic acid nanoparticle formulations to enhance myocardial gene transfer: an in-vitro assessment of a drug/gene combination therapeutic approach for direct injection. *Journal of translational medicine*, **12**(1), 1.

Farndale, Richard W, Buttle, David J, & Barrett, Alan J. 1986. Improved quantitation and discrimination of sulphated glycosaminoglycans by use of dimethylmethylene blue. *Biochimica et Biophysica Acta (BBA)-General Subjects*, **883**(2), 173–177.

Farquhar, T, Xia, Y, Mann, K, Bertram, J, Burton-Wurster, N, Jelinski, L, & Lust, G. 1996. Swelling and fibronectin accumulation in articular cartilage explants after cyclical impact. *Journal of Orthopaedic Research*, **14**(3), 417–423.

Feinberg, Stephen E, Hollister, Scott J, Halloran, John W, Chu, TM Gabe, & Krebsbach, Paul H. 2001. Image-based biomimetic approach to reconstruction of the temporomandibular joint. *Cells Tissues Organs*, **169**(3), 309–321.

Filardo, Giuseppe, Vannini, Francesca, Marcacci, Maurilio, Andriolo, Luca, Ferruzzi, Alberto, Giannini, Sandro, & Kon, Elizaveta. 2013. Matrix-assisted autologous chondrocyte transplantation for cartilage regeneration in osteoarthritic knees: results and failures at midterm follow-up. *American Journal of Sports Medicine*, **41**(1), 95–100.

Florine, E M, Miller, R E, Porter, R M, Evans, C H, Kurz, B., & Grodzinsky, Alan J. 2012. Effects of Dexamethasone on Mesenchymal Stromal Cell Chondrogenesis and Aggrecanase Activity: Comparison of Agarose and Self-Assembling Peptide Scaffolds. *Cartilage*, **4**(1), 63–74.

Francioli, Silvia, Cavallo, Carola, Grigolo, Brunella, Martin, Ivan, & Barbero, Andrea. 2011. Engineered cartilage maturation regulates cytokine production and interleukin-1beta response. *Clinical Orthopaedics and Related Research*, **469**(10), 2773–2784.

Francioli, Silvia-Elena, Martin, Ivan, Sie, Christina-Priska, Hagg, Rupert, Tommasini, Roberto, Candrian, Christian, Heberer, Michael, & Barbero, Andrea. 2007. Growth factors for clinical-scale expansion of human articular chondrocytes: relevance for automated bioreactor systems. *Tissue Engineering*, **13**(6), 1227–1234.

Freed, LE, Vunjak-Novakovic, G., & Langer, R. 1993. Cultivation of cell-polymer cartilage implants in bioreactors. *Journal of Cellular Biochemistry*, **51**(257), 8.

Freed, Lisa E, Langer, Robert, Martin, Ivan, Pellis, Neal R, & Vunjak-Novakovic, Gordana. 1997. Tissue engineering of cartilage in space. *Proceedings of the National Academy of Sciences*, **94**(25), 13885–13890.

Galeska, Isabela, Kim, Tae-Kyoung, Patil, Siddhesh D, Bhardwaj, Upkar, Chatttopadhyay, Debjit, Papadimitrakopoulos, Fotios, & Burgess, Diane J. 2005. Controlled release of dexamethasone from PLGA microspheres embedded within polyacid-containing PVA hydrogels. *The AAPS journal*, **7**(1), E231–40.

Gaspar, A, Moldovan, L, Constantin, D, Stanciuc, A M, Sarbu Boeti, P M, & Efrimescu, I C. 2011. Collagen–based scaffolds for skin tissue engineering . *Journal of Medicine and Life*, **4**(2), 172.

Gasparini, G, Kosvintsev, S R, Stillwell, M T, & Holdich, R G. 2008. Preparation and characterization of PLGA particles for subcutaneous controlled drug release by membrane emulsification. *Colloids and surfaces. B, Biointerfaces*, **61**(2), 199–207.

Gelber, Allan C, Hochberg, Marc C., Mead, Lucy A, Wang, Nae-Yuh, Wigley, Fredrick M, & Klag, Michael J. 2000. Joint Injury in Young Adults and Risk for Subsequent Knee and Hip Osteoarthritis. *Annals of internal medicine*, **133**(5), 321–328.

Gemmiti, Christopher V, & Guldberg, Robert E. 2006. Fluid flow increases type II collagen deposition and tensile mechanical properties in bioreactor-grown tissue-engineered cartilage. *Tissue engineering*, **12**(3), 469–479.

Gemmiti, Christopher V, & Guldberg, Robert E. 2009. Shear stress magnitude and duration modulates matrix composition and tensile mechanical properties in engineered cartilaginous tissue. *Biotechnology and bioengineering*, **104**(4), 809–820.

Gerwin, Nicole, Hops, Caroline, & Lucke, Andrea. 2006. Intraarticular drug delivery in osteoarthritis. *Advanced Drug Delivery Reviews*, **58**(2), 226–242.

Ghosh, Sanjib K. 1983. A close-range photogrammetric system for 3-D measurements and perspective diagramming in biomechanics. *Journal of biomechanics*, **16**(8), 667–674.

Gilbert, Sophie J, Singhrao, Sim K, Khan, Ilyas M, Gonzalez, Lee G, Thomson, Brian M, Burdon, Drew, Duance, Victor C, & Archer, Charles W. 2009. Enhanced tissue integration during cartilage repair in vitro can be achieved by inhibiting chondrocyte death at the wound edge. *Tissue Engineering. Part A*, **15**(7), 1739–1749.

Glaser, Ronald, & Kiecolt-Glaser, Janice K. 2005. Stress-induced immune dysfunction: implications for health. *Nature reviews. Immunology*, **5**(3), 243–251.

Goldring, Steven R, & Goldring, Mary B. 2004. The role of cytokines in cartilage matrix degeneration in osteoarthritis. *Clinical Orthopaedics and Related Research®*, Oct., S27–36.

Gooch, Keith J, Blunk, Torsten, Courter, DL, Sieminski, AL, Bursac, Predrag M, Vunjak-Novakovic, Gordana, & Freed, Lisa E. 2001. IGF-I and mechanical environment interact to modulate engineered cartilage development. *Biochemical and biophysical research communications*, **286**(5), 909–915.

Goodman, L S. 1996. *Goodman and Gilman's the pharmacological basis of therapeutics.*

Gray, Martha L, Pizzanelli, Angelina M, Grodzinsky, Alan J, & Lee, Raphael C. 1988. Mechanical and physicochemical determinants of the chondrocyte biosynthetic response. *Journal of orthopaedic research : official publication of the Orthopaedic Research Society*, **6**(6), 777–792.

Grayson, Warren L, Fröhlich, Mirjam, Yeager, Keith, Bhumiratana, Sarindr, Chan, M Ete, Cannizzaro, Christopher, Wan, Leo Q, Liu, X Sherry, Guo, X Edward, & Vunjak-Novakovic, Gordana. 2010. Engineering anatomically shaped human bone grafts. *Proceedings of the National Academy of Sciences*, **107**(8), 3299–3304.

Grodzinsky, Alan J. 1982. Electromechanical and physicochemical properties of connective tissue. *Critical reviews in biomedical engineering*, **9**(2), 133–199.

Gu, Bing, & Burgess, Diane J. 2015. Prediction of dexamethasone release from PLGA microspheres prepared with polymer blends using a design of experiment approach. *International Journal of Pharmaceutics*, **495**(1), 393–403.

Gu, Bing, Wang, Yan, & Burgess, Diane J. 2015. In vitro and in vivo performance of dexamethasone loaded PLGA microspheres prepared using polymer blends. *International Journal of Pharmaceutics*, **496**(2), 534–540.

Guilak, F., Meyer, B C, Ratcliffe, A., & Mow, V C. 1994. The effects of matrix compression on proteoglycan metabolism in articular cartilage explants. *Osteoarthritis and Cartilage*, **2**(2), 91–101.

Guilak, F., Ratcliffe, A., & Mow, V C. 1995. Chondrocyte deformation and local tissue strain in articular cartilage: a confocal microscopy study. *Journal of Orthopaedic Research*, **13**(3), 410–421.

Guilak, Farshid, Awad, Hani A, Fermor, Beverley, Leddy, Holly A, & Gimble, Jeffrey M. 2004. Adipose-derived adult stem cells for cartilage tissue engineering. *Biorheology*, **41**(3-4), 389–399.

Habib, George S. 2009. Systemic effects of intra-articular corticosteroids. *Clinical rheumatology*, **28**(7), 749–756.

Habib, George S, Saliba, Walid, & Nashashibi, Munir. 2010. Local effects of intra-articular corticosteroids. *Clinical rheumatology*, **29**(4), 347–356.

Hafezi-Moghadam, Ali, Simoncini, Tommaso, Yang, Zequan, Limbourg, Florian P, Plumier, Jean-Christophe, Rebsamen, Michael C, Hsieh, Chung-Ming, Chui, Dao-Shan, Thomas, Kennard L, Prorock, Alyson J, Laubach, Victor E, Moskowitz, Michael A, French, Brent A, Ley, Klaus, & Liao, James K. 2002. Acute cardiovascular protective effects of corticosteroids are mediated by non-transcriptional activation of endothelial nitric oxide synthase. *Nature medicine*, **8**(5), 473–479.

Hainque, B, Dominice, J, Jaffray, P, Ronot, X, & Adolphe, M. 1987. Effects of Dexamethasone on the Growth of Cultured Rabbit Articular Chondrocytes - Relation with the Nuclear Glucocorticoid-Receptor Complex. *Annals of the rheumatic diseases*, **46**(2), 146–152.

Hammarlund, E Roy, & Rising, L. 1953. The electrophoretic analysis and antibacterial determination of madronin in agar gel. *Journal of the American Pharmaceutical Association*, **42**(7), 431–433.

Hangody, László, & Füles, Péter. 2003. Autologous osteochondral mosaicplasty for the treatment of full-thickness defects of weight-bearing joints: ten years of experimental and clinical experience. *The Journal of Bone and Joint Surgery*, **85-A Suppl 2**, 25–32.

Hangody, Laszlo, Kish, G, Karpati, Z, Szerb, I, & Udvarhelyi, I. 1997. Arthroscopic autogenous osteochondral mosaicplasty for the treatment of femoral condylar articular defects A preliminary report. *Knee Surgery, Sports Traumatology, Arthroscopy*, **5**(4), 262–267.

He, Fan, Chen, Xiaodong, & Pei, Ming. 2009. Reconstruction of an in vitro tissue-specific microenvironment to rejuvenate synovium-derived stem cells for cartilage tissue engineering. *Tissue Engineering Part A*, **15**(12), 3809–3821.

Hebbar, Pratibha B, & Archer, Trevor K. 2003. Chromatin remodeling by nuclear receptors. *Chromosoma*, **111**(8), 495–504.

Henderson, J H, Welter, J F, Welter, J F, Mansour, J M, Niyibizi, C, Caplan, A I, & Dennis, J E. 2007. Cartilage tissue engineering for laryngotracheal reconstruction: comparison of chondrocytes from three anatomic locations in the rabbit. *Tissue Engineering*, **13**(4), 843–853.

Hennerbichler, A, Moutos, F T, Hennerbichler, D, Weinberg, J. B., & Guilak, F. 2007. Interleukin-1 and tumor necrosis factor alpha inhibit repair of the porcine meniscus in vitro. *Osteoarthritis and Cartilage*, **15**(9), 1053–1060.

Hickey, T, Kreutzer, D, Burgess, D J, & Moussy, F. 2002a. Dexamethasone/PLGA microspheres for continuous delivery of an anti-inflammatory drug for implantable medical devices. *Biomaterials*, **23**(7), 1649–1656.

Hickey, T, Kreutzer, D, Burgess, D J, & Moussy, F. 2002b. In vivo evaluation of a dexamethasone/PLGA microsphere system designed to suppress the inflammatory tissue response to implantable medical devices. *Journal of biomedical materials research*, **61**(2), 180–187.

Higaki, M, Ishihara, T, Izumo, N, Takatsu, M, & Mizushima, Y. 2005. Treatment of experimental arthritis with poly(D, L-lactic/glycolic acid) nanoparticles encapsulating betamethasone sodium phosphate. *Annals of the rheumatic diseases*, **64**(8), 1132–1136.

Hines, Daniel J, & Kaplan, David L. 2013. Poly (lactic-co-glycolic) acid- controlled-release systems: experimental and modeling insights. *Critical Reviews™ in Therapeutic Drug Carrier Systems*, **30**(3).

Hootman, Jennifer M, & Helmick, Charles G. 2006. Projections of US prevalence of arthritis and associated activity limitations. *Arthritis & Rheumatism*, **54**(1), 226–229.

Houston, D A, Amin, A K, White, T O, Smith, I D M, & Hall, A. C. 2013. Chondrocyte death after drilling and articular screw insertion in a bovine model. *Osteoarthritis and cartilage / OARS, Osteoarthritis Research Society*, **21**(5), 721–729.

Huang, A. H., Yeger-McKeever, M, Stein, A, & Mauck, Robert L. 2008. Tensile properties of engineered cartilage formed from chondrocyte- and MSC-laden hydrogels. *Osteoarthritis and cartilage / OARS, Osteoarthritis Research Society*, **16**(9), 1074–1082.

Huang, Alice H, Stein, Ashley, Tuan, Rocky S, & Mauck, Robert L. 2009. Transient exposure to transforming growth factor beta 3 improves the mechanical properties of mesenchymal stem cell-laden cartilage constructs in a density-dependent manner. *Tissue Engineering. Part A*, **15**(11), 3461–3472.

Huang, Alice H, Farrell, Megan J, Kim, Minwook, & Mauck, Robert L. 2010. Long-term dynamic loading improves the mechanical properties of chondrogenic mesenchymal stem cell-laden hydrogel. *European cells & materials*, **19**, 72–85.

Huang, Alice H, Baker, Brendon M, Ateshian, Gerard A, & Mauck, Robert L. 2012. Sliding contact loading enhances the tensile properties of mesenchymal stem cell-seeded hydrogels. *Eur Cell Mater*, **24**, 29–45.

Huang, Brian J, Hu, Jerry C, & Athanasiou, Kyriacos A. 2016a. Effects of passage number and post-expansion aggregate culture on tissue engineered, self-assembled neocartilage. *Acta Biomaterialia*, **43**(Oct.), 150–159.

Huang, Brian J, Huey, Daniel J, Hu, Jerry C, & Athanasiou, Kyriacos A. 2016b. Engineering biomechanically functional neocartilage derived from expanded articular chondrocytes through the manipulation of cell-seeding density and dexamethasone concentration. *Journal of tissue engineering and regenerative medicine*.

Huang, Chun-Yuh, & Gu, Wei Yong. 2006. Effects of Tension-Compression Nonlinearity on Solute Transport in Charged Hydrated Fibrous Tissues Under Dynamic Unconfined Compression. *Journal of Biomechanical Engineering*, **129**(3), 423.

Huang, Chun-Yuh, Mow, Van C, & Ateshian, Gerard A. 2001. The Role of Flow-Independent Viscoelasticity in the Biphasic Tensile and Compressive Responses of Articular Cartilage. *Journal of Biomechanical Engineering*, **123**(5), 410.

Huang, Chun-Yuh, Soltz, Michael A, Kopacz, Monika, Mow, Van C, & Ateshian, Gerard A. 2003. Experimental Verification of the Roles of Intrinsic Matrix Viscoelasticity and Tension-Compression Nonlinearity in the Biphasic Response of Cartilage. *Journal of Biomechanical Engineering*, **125**(1), 84.

Huang, Chun-Yuh, Stankiewicz, Anna, Ateshian, Gerard A., & Mow, Van C. 2005. Anisotropy, inhomogeneity, and tension–compression nonlinearity of human glenohumeral cartilage in finite deformation. *Journal of Biomechanics*, **38**(4), 799–809.

Huberti, H H, & Hayes, W C. 1984. Patellofemoral contact pressures. The influence of q-angle and tendofemoral contact. *The Journal of Bone and Joint Surgery*, **66**(5), 715–724.

Huebner, Kyla D, Shrive, Nigel G, & Frank, Cyril B. 2013. New surgical model of post-traumatic osteoarthritis: isolated intra-articular bone injury in the rabbit. *Journal of orthopaedic research : official publication of the Orthopaedic Research Society*, **31**(6), 914–920.

Huebner, Kyla D, Shrive, Nigel G, & Frank, Cyril B. 2014. Dexamethasone inhibits inflammation and cartilage damage in a new model of post-traumatic osteoarthritis. *Journal of orthopaedic research : official publication of the Orthopaedic Research Society*, **32**(4), 566–572.

Huiskes, R, Kremers, J, De Lange, A, Woltring, HJ, Selvik, G, & Van Rens, Th JG. 1985. Analytical stereophotogrammetric determination of three-dimensional knee-joint geometry. *Journal of biomechanics*, **18**(8), 559–570.

Hung, Clark T, Lima, Eric G, Mauck, Robert L, Taki, Erica, LeRoux, Michelle A, Lu, Helen H, Stark, Robert G, Guo, X Edward, & Ateshian, Gerard A. 2003. Anatomically shaped osteochondral constructs for articular cartilage repair. *Journal of biomechanics*, **36**(12), 1853–1864.

Hung, Clark T, Mauck, Robert L, Wang, Christopher C-B, Lima, Eric G, & Ateshian, Gerard A. 2004. A paradigm for functional tissue engineering of articular cartilage via applied physiologic deformational loading. *Annals of biomedical engineering*, **32**(1), 35–49.

Hunter, Christopher J, & Levenston, Marc E. 2002. The influence of repair tissue maturation on the response to oscillatory compression in a cartilage defect repair model. *Biorheology*, **39**(1-2), 79–88.

Hunter, Christopher J, & Levenston, Marc E. 2004. Maturation and integration of tissue-engineered cartilages within an in vitro defect repair model. *Tissue Engineering*, **10**(5-6), 736–746.

Hunter, Christopher J, Mouw, Janna K, & Levenston, Marc E. 2004. Dynamic compression of chondrocyte-seeded fibrin gels: effects on matrix accumulation and mechanical stiffness. *Osteoarthritis and Cartilage*, **12**(2), 117–130.

Hwang, Yongsung, Sangaj, Nivedita, & Varghese, Shyni. 2010. Interconnected macroporous poly (ethylene glycol) cryogels as a cell scaffold for cartilage tissue engineering. *Tissue Engineering Part A*, **16**(10), 3033–3041.

Ikeuchi, Masahiko, Kamimoto, Yuko, Izumi, Masashi, Fukunaga, Kayo, Aso, Koji, Sugimura, Natsuki, Yokoyama, Masataka, & Tani, Toshikazu. 2013. Effects of dexamethasone on local infiltration analgesia in total knee arthroplasty: a randomized controlled trial. *Knee Surgery, Sports Traumatology, Arthroscopy*, **22**(7), 1638–1643.

Irie, Kazunori, Uchiyama, Eiji, & Iwaso, Hiroshi. 2003. Intraarticular inflammatory cytokines in acute anterior cruciate ligament injured knee. *The Knee*, **10**(1), 93–96.

Ito, Fuminori, Fujimori, Hiroyuki, & Makino, Kimiko. 2007. Incorporation of water-soluble drugs in PLGA microspheres. *Colloids and surfaces. B, Biointerfaces*, **54**(2), 173–178.

Jain, R A. 2000. The manufacturing techniques of various drug loaded biodegradable poly(lactide-co-glycolide) (PLGA) devices. *Biomaterials*, **21**(23), 2475–2490.

Johnstone, B, Hering, T M, Caplan, A I, Goldberg, V M, & Yoo, J U. 1998. Chondrogenesis of Bone Marrow-Derived Mesenchymal Progenitor Cells. *Experimental Cell Research*, Jan., 265–272.

Joosten, LAB, Lubberts, E, & Durez, P. 1997. Role of interleukin-4 and interleukin-10 in murine collagen-induced arthritis. Protective effect of interleukin-4 and interleukin-10 treatment on cartilage destruction. *Arthritis & ...*, **40**(2), 249–260.

Joosten, Leo AB, Lubberts, Erik, Helsen, Monique MA, Saxne, Tore, Roo, Christina JJ Coenen-de, Heinegård, Dick, & van den Berg, Wim B. 1999. Protection against cartilage and bone destruction by systemic interleukin-4 treatment in established murine type II collagen-induced arthritis. *Arthritis Research*, **1**(1), 81–91.

Kawai, T, & Akira, S. 2006. TLR signaling. *Cell death and differentiation*, **13**(5), 816–825.

Kaysen, JH, Campbell, WC, Majewski, RR, Goda, FO, Navar, GL, Lewis, FC, Goodwin, TJ, & Hammond, TG. 1999. Select de novo gene and protein expression during renal epithelial cell culture in rotating wall vessels is shear stress dependent. *The Journal of membrane biology*, **168**(1), 77–89.

Kelly, Terri-Ann N, Wang, Christopher C. B., Mauck, Robert L., Ateshian, Gerard A., & Hung, Clark T. 2004. Role of cell-associated matrix in the development of free-swelling and dynamically loaded chondrocyte-seeded agarose gels. *Biorheology*, **41**(3-4), 223–237.

Kelly, Terri-Ann N, Ng, Kenneth W, Wang, Christopher C-B, Ateshian, Gerard A, & Hung, Clark T. 2006. Spatial and temporal development of chondrocyte-seeded agarose constructs in free-swelling and dynamically loaded cultures. *Journal of biomechanics*, **39**(8), 1489–1497.

Kelly, Terri-Ann N, Ng, K. W., Ateshian, Gerard A., & Hung, Clark T. 2009. Analysis of radial variations in material properties and matrix composition of chondrocyte-seeded agarose hydrogel constructs. *Osteoarthritis and cartilage / OARS, Osteoarthritis Research Society*, **17**(1), 73–82.

Kelly, Terri-Ann N, Roach, Brendan L, Weidner, Zachary D, Mackenzie-Smith, Charles R, O'Connell, Grace D, Lima, E G, Stoker, Aaron M, Cook, James L, Ateshian, Gerard A., & Hung, Clark T. 2013. Tissue-engineered articular cartilage exhibits tension-compression nonlinearity reminiscent of the native cartilage. *Journal of Biomechanics*, **46**(11), 1784–1791.

Kelmendi-Doko, Arta, Marra, Kacey G, Vidic, Natasa, Tan, Huaping, & Rubin, J Peter. 2014. Adipogenic factor-loaded microspheres increase retention of transplanted adipose tissue. *Tissue Engineering. Part A*, **20**(17-18), 2283–2290.

Kempson, GE, Freeman, MAR, & Swanson, SAV. 1968. Tensile properties of articular cartilage. *Nature*.

Khaing, Zin Z, & Schmidt, Christine E. 2012. Advances in natural biomaterials for nerve tissue repair. *Neuroscience letters*, **519**(2), 103–114.

Kim, Dong-Hwan, & Martin, David C. 2006. Sustained release of dexamethasone from hydrophilic matrices using PLGA nanoparticles for neural drug delivery. *Biomaterials*, **27**(15), 3031–3037.

Kimmerling, K A, Furman, B. D., Mangiapani, D S, Moverman, M A, Sinclair, S M, Huebner, J L, Chilkoti, A, Kraus, V B, Setton, L A, Guilak, F., & Olson, S A. 2015. Sustained intra-articular delivery of IL-1RA from a thermally-responsive elastin-like polypeptide as a therapy for post-traumatic arthritis. *European cells & materials*, **29**, 124–39– discussion 139–40.

Kisiday, John D, Jin, Moonsoo, DiMicco, Michael A, Kurz, Bodo, & Grodzinsky, Alan J. 2004. Effects of dynamic compressive loading on chondrocyte biosynthesis in self-assembling peptide scaffolds. *Journal of Biomechanics*, **37**(5), 595–604.

Kisiday, John D, Lee, Jennifer H, Siparsky, Patrick N, Frisbie, David D, Flannery, Carl R, Sandy, John D, & Grodzinsky, Alan J. 2009. Catabolic Responses of Chondrocyte-Seeded Peptide Hydrogel to Dynamic Compression. *Annals of Biomedical Engineering*, **37**(7), 1368–1375.

Kiviranta, P, Lammentausta, E, Toyras, J, Kiviranta, I, & Jurvelin, J S. 2008. Indentation diagnostics of cartilage degeneration. *Osteoarthritis and Cartilage*, **16**(7), 796–804.

Knight, M M, Lee, D. A., & Bader, D. L. 1998. The influence of elaborated pericellular matrix on the deformation of isolated articular chondrocytes cultured in agarose. *Biochimica et Biophysica Acta (BBA)-Molecular Cell Research*, **1405**(1), 67–77.

Knutsen, Gunnar, Engebretsen, Lars, Ludvigsen, Tom C, Drogset, Jon Olav, Grøntvedt, Torbjørn, Solheim, Eirik, Strand, Torbjørn, Roberts, Sally, Isaksen, Vidar, & Johansen, Oddmund. 2004. Autologous chondrocyte implantation compared with microfracture in the knee. *J Bone Joint Surg Am*, **86**(3), 455–464.

Koo, Seungbum, Giori, Nicholas J, Gold, Garry E, Dyrby, Chris O, & Andriacchi, Thomas P. 2009. Accuracy of 3D cartilage models generated from MR images is dependent on cartilage thickness: laser scanner based validation of in vivo cartilage. *Journal of biomechanical engineering*, **131**(12), 121004.

Koo, Seungbum, Hargreaves, Brian A, Gold, Garry E, & Dragoo, Jason L. 2010. Fabrication of custom-shaped grafts for cartilage regeneration. *The International journal of artificial organs*, **33**(10), 731–737.

Krishnan, R., Caligaris, M., Mauck, Robert L., Hung, Clark T., Costa, K. D., & Ateshian, Gerard A. 2004. Removal of the superficial zone of bovine articular cartilage does not increase its frictional coefficient. *Osteoarthritis and Cartilage*, **12**(12), 947–955.

Kumar, A, Bendele, A M, Blanks, R C, & Bodick, N. 2015. Sustained efficacy of a single intra-articular dose of FX006 in a rat model of repeated localized knee arthritis. *Osteoarthritis and cartilage / OARS, Osteoarthritis Research Society*, **23**(1), 151–160.

Kumar, Deepak, Manal, Kurt T, & Rudolph, Katherine S. 2013. Knee joint loading during gait in healthy controls and individuals with knee osteoarthritis. *Osteoarthritis and Cartilage*, **21**(2), 298–305.

Kuroki, Keiichi, Stoker, Aaron M, & Cook, James L. 2005. Effects of proinflammatory cytokines on canine articular chondrocytes in a three-dimensional culture. *American journal of veterinary research*, **66**(7), 1187–1196.

Lai, W Michael, Hou, JS, & Mow, Van C. 1991. A triphasic theory for the swelling and deformation behaviors of articular cartilage. *Journal of biomechanical engineering*, **113**(3), 245–258.

Lamiable, P D, Vistelle, R, Millart, H, Sulmont, P V, Fay, R, Caron, J, & Choisy, H. 1986. High-performance liquid chromatographic determination of dexamethasone in human plasma. *Journal of Chromatography B: Biomedical Sciences and Applications*, **378**(Jan.), 486–491.

Lanir, Y. 1986. Biorheology and fluid flux in swelling tissues, II. Analysis of unconfined compressive response of transversely isotropic cartilage disc. *Biorheology*, **24**(2), 189–205.

LaPrade, Robert F, & Botker, Jesse C. 2004. Donor-site morbidity after osteochondral autograft transfer procedures. *Arthroscopy: The Journal of Arthroscopic & Related Surgery*, **20**(7), e69–e73.

Lee, C R, Grodzinsky, Alan J, & Spector, M. 2003. Biosynthetic response of passaged chondrocytes in a type II collagen scaffold to mechanical compression. *J. Biomed. Mater. Res. A*, **64**(3), 560–569.

Lee, Chang H, Cook, James L, Mendelson, Avital, Moioli, Eduardo K, Yao, Hai, & Mao, Jeremy J. 2010. Regeneration of the articular surface of the rabbit synovial joint by cell homing: a proof of concept study. *Lancet*, **376**(9739), 440–448.

Lee, CR, Grodzinsky, AJ, Hsu, H-P, Martin, SD, & Spector, M. 2000a. Effects of harvest and selected cartilage repair procedures on the physical and biochemical properties of articular cartilage in the canine knee. *Journal of Orthopaedic Research*, **18**(5), 790–799.

Lee, D. A., Noguchi, T, Frean, S P, Lees, P, & Bader, D. L. 2000b. The influence of mechanical loading on isolated chondrocytes seeded in agarose constructs. *Biorheology*, **37**(1-2), 149–161.

Lee, David A, & Bader, Dan L. 1997. Compressive strains at physiological frequencies influence the metabolism of chondrocytes seeded in agarose. *Journal of Orthopaedic Research*, **15**(2), 181–188.

Lee, David A, & Bader, Daniel L. 1995. The development and characterization of an in vitro system to study strain-induced cell deformation in isolated chondrocytes. *In Vitro Cell. Dev. Biol. - Animal*, **31**(11), 828–835.

Lee, David A, Noguchi, Takashi, Knight, Martin M, O'donnell, Liam, Bentley, George, & Bader, Dan L. 1998. Response of chondrocyte subpopulations cultured within unloaded and loaded agarose. *Journal of orthopaedic research*, **16**(6), 726–733.

Lee, David A, Knight, Martin M, F Bolton, John, Idowu, Bernadine D, Kayser, Michael V, & Bader, Dan L. 2000c. Chondrocyte deformation within compressed agarose constructs at the cellular and sub-cellular levels. *Journal of Biomechanics*, **33**(1), 81–95.

Leigh, J P, Seavey, W, & Leistikow, B. 2001. Estimating the costs of job related arthritis. *The Journal of Rheumatology*, **28**(7), 1647–1654.

Li, J., Li, J., Pei, M., & Pei, M. 2011. Optimization of an in vitro three-dimensional microenvironment to reprogram synovium-derived stem cells for cartilage tissue engineering. *Tissue Engineering. Part A*, **17**(5-6), 703–712.

Lima, E G, Mauck, Robert L., Han, Shelley H, Park, Seonghun, Ng, Kenneth W, Ateshian, Gerard A., & Hung, Clark T. 2004. Functional tissue engineering of chondral and osteochondral constructs. *Biorheology*, **41**(3-4), 577–590.

Lima, E G, Bian, Liming, Ng, K. W., Mauck, Robert L., Byers, B A, Tuan, R S, Ateshian, Gerard A., & Hung, Clark T. 2007. The beneficial effect of delayed compressive loading on tissue-engineered cartilage constructs cultured with TGF-beta3. *Osteoarthritis and Cartilage*, **15**(9), 1025–1033.

Lima, E G, Tan, Andrea R, Tai, Timon, Bian, Liming, Stoker, Aaron M, Ateshian, Gerard A., Cook, James L, & Hung, Clark T. 2008a. Differences in interleukin-1 response between engineered and native cartilage. *Tissue engineering. Part A*, **14**(10), 1721–1730.

Lima, E G, Tan, Andrea R, Tai, Timon, Bian, Liming, Ateshian, Gerard A., Cook, James L, & Hung, Clark T. 2008b. Physiologic deformational loading does not counteract the catabolic effects of interleukin-1 in long-term culture of chondrocyte-seeded agarose constructs. *Journal of Biomechanics*, **41**(15), 3253–3259.

Lo, Sansan S, Hung, Clark T., Seyhan, Sara L, Palmer, Glyn D, Mauck, Robert L., & Mow, Van C. 2001. Mechanical loading modulates gene expression in chondrocyte-seeded agarose hydrogels. *American Society of Mechanical Engineers, Bioengineering Division Publication BED*, **51**(Jan.), 291–292.

Lohmander, L Stefan, Atley, Lynne M, Pietka, Terri A, & Eyre, David R. 2003. The release of crosslinked peptides from type II collagen into human synovial fluid is increased soon after joint injury and in osteoarthritis. *Arthritis & Rheumatism*, **48**(11), 3130–3139.

Lohmander, L Stefan, Englund, P Martin, Dahl, Ludvig L, & Roos, Ewa M. 2007. The long-term consequence of anterior cruciate ligament and meniscus injuries: osteoarthritis. *American Journal of Sports Medicine*, **35**(10), 1756–1769.

Lotz, Martin K, & Kraus, Virginia B. 2010. New developments in osteoarthritis. Posttraumatic osteoarthritis: pathogenesis and pharmacological treatment options. *Arthritis research & therapy*, **12**(3), 211.

Lu, Yihong C S, Lu, Yihong C S, Evans, Christopher H, Evans, Christopher H, & Grodzinsky, Alan J. 2011. Effects of short-term glucocorticoid treatment on changes in cartilage matrix degradation and chondrocyte gene expression induced by mechanical injury and inflammatory cytokines. *Arthritis research & therapy*, **13**(5), R142.

Lujan, Trevor J, Wirtz, Kyle M, Bahney, Chelsea S, Madey, Steven M, Johnstone, Brian, & Bottlang, Michael. 2011. A Novel Bioreactor for the Dynamic Stimulation and Mechanical Evaluation of Multiple Tissue-Engineered Constructs. *Tissue engineering. Part C, Methods*, **17**(3), 367–374.

Mackay, A M, Beck, S C, Murphy, J M, Barry, F P, Chichester, C O, & Pittenger, M F. 1998. Chondrogenic differentiation of cultured human mesenchymal stem cells from marrow. **4**(4), 415–428.

MacMahon, Peter J, Eustace, Stephen J, & Kavanagh, Eoin C. 2009. Injectable corticosteroid and local anesthetic preparations: a review for radiologists. *Radiology*, **252**(3), 647–661.

Mader, Reuven, Lavi, Idit, & Luboshitzky, Rafael. 2005. Evaluation of the pituitary-adrenal axis function following single intraarticular injection of methylprednisolone. *Arthritis & Rheumatism*, **52**(3), 924–928.

Malfait, Anne Marie, D Tortorella, Micky, Thompson, J, Hills, R, Meyer, D M, Jaffee, B D, Chinn, K, Ghoreishi-Haack, N, Markosyan, S, & Arner, E C. 2009. Intra-articular injection of tumor necrosis factor-alpha in the rat: an acute and reversible in vivo model of cartilage proteoglycan degradation. *Osteoarthritis and Cartilage*, **17**(5), 627–635.

Mankin, Henry J. 1974. The reaction of articular cartilage to injury and osteoarthritis. *New England Journal of Medicine*, **291**(24), 1285–1292.

Mankin, Henry J, & LIPPIELLO, LOUIS. 1970. Biochemical and metabolic abnormalities in articular cartilage from osteo-arthritic human hips. *J Bone Joint Surg Am*, **52**(3), 424–434.

Mankin, HENRY J, Johnson, ME, & Lippiello, L. 1981. Biochemical and metabolic abnormalities in articular cartilage from osteoarthritic human hips. III. Distribution and metabolism of amino sugar-containing macromolecules. *J Bone Joint Surg Am*, **63**(1), 131–139.

Mao, Shirui, Xu, Jing, Cai, Cuifang, Germershaus, Oliver, Schaper, Andreas, & Kissel, Thomas. 2007. Effect of WOW process parameters on morphology and burst release of FITC-dextran loaded PLGA microspheres. *International Journal of Pharmaceutics*, **334**(1-2), 137–148.

Maroudas, Alice. 1976. Balance between swelling pressure and collagen tension in normal and degenerate cartilage. *Nature*, **260**(5554), 808–809.

Martin, JA, & Buckwalter, JA. 2000. The role of chondrocyte–matrix interactions in maintaining and repairing articular cartilage. *Biorheology*, **37**(1, 2), 129–140.

Martin, JA, Miller, BA, Scherb, MB, Lembke, LA, & Buckwalter, JA. 2002. Co-localization of insulin-like growth factor binding protein 3 and fibronectin in human articular cartilage. *Osteoarthritis and cartilage*, **10**(7), 556–563.

Mauck, Robert L. 2003. Growth factor supplementation and dynamic hydrostatic pressurization for articular cartilage tissue engineering. *Advances in Bioengineering*.

Mauck, Robert L., Soltz, Michael A, Wang, Christopher C. B., Wong, Dennis D, Grace Chao, Pen-hsiu, Valhmu, Wilmot B, Hung, Clark T., & Ateshian, Gerard A. 2000a. Functional Tissue Engineering of Articular Cartilage Through Dynamic Loading of Chondrocyte-Seeded Agarose Gels. *Journal of Biomechanical Engineering*, **122**(3), 252.

Mauck, Robert L, Soltz, Michael A, Wang, Christopher CB, Wong, Dennis D, Chao, Pen-Hsiu Grace, Valhmu, Wilmot B, Hung, Clark T, & Ateshian, Gerard A. 2000b. Functional tissue engineering of articular cartilage through dynamic loading of chondrocyte-seeded agarose gels. *Journal of biomechanical engineering*, **122**(3), 252–260.

Mauck, Robert L, Seyhan, Sara L, Ateshian, Gerard A, & Hung, Clark T. 2002. Influence of seeding density and dynamic deformational loading on the developing structure/function relationships of chondrocyte-seeded agarose hydrogels. *Annals of biomedical engineering*, **30**(8), 1046–1056.

Mauck, Robert L, Nicoll, Steven B, Seyhan, Sara L, Ateshian, Gerard A, & Hung, Clark T. 2003. Synergistic action of growth factors and dynamic loading for articular cartilage tissue engineering. *Tissue engineering*, **9**(4), 597–611.

McGowan, KB, Kurtis, MS, Lottman, LM, Watson, D, & Sah, RL. 2002. Biochemical quantification of DNA in human articular and septal cartilage using PicoGreen® and Hoechst 33258. *Osteoarthritis and Cartilage*, **10**(7), 580–587.

McKay, L I, & Cidlowski, J A. 1998. Cross-talk between nuclear factor-kappa B and the steroid hormone receptors: mechanisms of mutual antagonism. *Molecular endocrinology (Baltimore, Md.)*, **12**(1), 45–56.

McKay, L I, & Cidlowski, J A. 1999. Molecular control of immune/inflammatory responses: interactions between nuclear factor-kappa B and steroid receptor-signaling pathways. *Endocrine reviews*, **20**(4), 435–459.

McNulty, A L, Estes, B. T., Wilusz, R E, Weinberg, J. B., & Guilak, F. 2010. Dynamic loading enhances integrative meniscal repair in the presence of interleukin-1. *Osteoarthritis and cartilage / OARS, Osteoarthritis Research Society*, **18**(6), 830–838.

McNulty, Amy L, Moutos, Franklin T, Weinberg, J Brice, & Guilak, Farshid. 2007. Enhanced integrative repair of the porcine meniscus in vitro by inhibition of interleukin-1 or tumor necrosis factor α. *Arthritis & Rheumatism*, **56**(9), 3033–3043.

McNulty, Amy L, Rothfusz, Nicole E, Rothfusz, Nicole E, Leddy, Holly A, Leddy, Holly A, Guilak, Farshid, & Guilak, Farshid. 2013. Synovial fluid concentrations and relative potency of interleukin-1 alpha and beta in cartilage and meniscus degradation. *Journal of orthopaedic research : official publication of the Orthopaedic Research Society*, **31**(7), 1039–1045.

Miot, Sylvie, Brehm, W, Dickinson, S, Sims, T, Wixmerten, A, Longinotti, C, Hollander, A P, Mainil-Varlet, P, & Martin, I. 2012. Influence of in vitro maturation of engineered cartilage on the outcome of osteochondral repair in a goat model. *European cells & materials*, **23**, 222–236.

Mironov, Vladimir, Boland, Thomas, Trusk, Thomas, Forgacs, Gabor, & Markwald, Roger R. 2003. Organ printing: computer-aided jet-based 3D tissue engineering. *Trends in biotechnology*, **21**(4), 157–161.

Morisset, Sophie, Frisbie, David D, Robbins, Paul D, Nixon, Alan J, & McIlwraith, C Wayne. 2007. IL-1ra/IGF-1 gene therapy modulates repair of microfractured chondral defects. *Clinical Orthopaedics and Related Research*, **462**(Sept.), 221–228.

Moseley, J Bruce, Anderson, Allen F, Browne, Jon E, Mandelbaum, Bert R, Micheli, Lyle J, Fu, Freddie, & Erggelet, Christoph. 2010. Long-term durability of autologous chondrocyte implantation: a multicenter, observational study in US patients. *American Journal of Sports Medicine*, **38**(2), 238–246.

Moutos, Franklin T, & Guilak, Farshid. 2009. Functional properties of cell-seeded three-dimensionally woven poly (epsilon-caprolactone) scaffolds for cartilage tissue engineering. *Tissue Engineering Part A*, **16**(4), 1291–1301.

Mow, Van C, Holmes, Mark H, & Lai, W Michael. 1984. Fluid transport and mechanical properties of articular cartilage: a review. *Journal of biomechanics*, **17**(5), 377–394.

Mow, VC, & Lai, M. 1990. Biorheology of swelling tissue. *Biorheology*, **27**(1), 110.

Mow, VC, Ateshian, GA, Lai, WM, & Gu, WY. 1998. Effects of fixed charges on the stress–relaxation behavior of hydrated soft tissues in a confined compression problem. *International Journal of Solids and Structures*, **35**(34), 4945–4962.

Mowery, Carol, Botte, Michael, & Bradley, Gary. 1987. Fracture of polyethylene tibial component in a total knee replacement: a case report. *Orthopedics*, **10**(2), 309–313.

Mueller, Michael B, & Tuan, Rocky S. 2011. Anabolic/catabolic balance in pathogenesis of osteoarthritis: identifying molecular targets. *PM&R*, **3**(6), S3–S11.

Nagaich, Akhilesh K, Rayasam, Geetha V, Martinez, Elisabeth D, Becker, Matthias, Qiu, Yi, Johnson, Thomas A, Elbi, Cem, Fletcher, Terace M, John, Sam, & Hager, Gordon L. 2004. Subnuclear trafficking and gene targeting by steroid receptors. *Annals of the New York Academy of Sciences*, **1024**(1), 213–220.

Natoli, Roman M, Revell, Christopher M, & Athanasiou, Kyriacos A. 2009a. Chondroitinase ABC treatment results in greater tensile properties of self-assembled tissue-engineered articular cartilage. *Tissue Engineering Part A*, **15**(10), 3119–3128.

Natoli, Roman M, Responte, Donald J, Lu, Benjamin Y, & Athanasiou, Kyriacos A. 2009b. Effects of multiple chondroitinase ABC applications on tissue engineered articular cartilage. *Journal of orthopaedic research : official publication of the Orthopaedic Research Society*, **27**(7), 949–956.

Natoli, Roman M, Skaalure, Stacey, Bijlani, Shweta, Chen, Ke X, Hu, Jerry, & Athanasiou, Kyriacos A. 2010. Intracellular Na+ and Ca2+ modulation increases the tensile properties of developing engineered articular cartilage. *Arthritis & Rheumatism*, **62**(4), 1097–1107.

Neidert, Michael R, & Tranquillo, Robert T. 2006. Tissue-Engineered Valves with Commissural Alignment. *Tissue Engineering*, **12**(4), 891–903.

Neustadt, David H. 2006. Intra-articular injections for osteoarthritis of the knee. *Cleveland Clinic journal of medicine*, **73**(10), 897–8– 901–4– 906–11.

Ng, Kenneth W, Wang, Christopher C. B., Mauck, Robert L., Kelly, Terri-Ann N, Chahine, Nadeen O, Costa, Kevin D, Ateshian, Gerard A., & Hung, Clark T. 2005. A layered agarose approach to fabricate depth-dependent inhomogeneity in chondrocyte-seeded constructs. *Journal of Orthopaedic Research*, **23**(1), 134–141.

Ng, Kenneth W, Mauck, Robert L., Statman, Lauren Y, Lin, Evan Y, Ateshian, Gerard A., & Hung, Clark T. 2006. Dynamic deformational loading results in selective application of mechanical stimulation in a layered, tissue-engineered cartilage construct. *Biorheology*, **43**(3-4), 497–507.

Ng, Kenneth W, Mauck, Robert L., Wang, Christopher C. B., Kelly, Terri-Ann N, Ho, Mandy M Y, Chen, Faye Hui, Ateshian, Gerard A., & Hung, Clark T. 2009. Duty Cycle of Deformational Loading Influences the Growth of Engineered Articular Cartilage. *Cellular and molecular bioengineering*, **2**(3), 386–394.

Ng, Kenneth W, Lima, E G, Bian, Liming, O'Conor, Christopher J, Jayabalan, Prakash S, Stoker, Aaron M, Kuroki, Keiichi, Cook, Cristi R, Ateshian, Gerard A., Cook, James L, & Hung, Clark T. 2010. Passaged adult chondrocytes can form engineered cartilage with functional mechanical properties: a canine model. *Tissue Engineering. Part A*, **16**(3), 1041–1051.

Nims, Robert J, Cigan, Alexander D, Albro, Michael B, Hung, Clark T, & Ateshian, Gerard A. 2014. Synthesis rates and binding kinetics of matrix products in engineered cartilage constructs using chondrocyte-seeded agarose gels. *Journal of biomechanics*, **47**(9), 2165–2172.

Nims, Robert J, Cigan, Alexander D, Albro, Michael B, Vunjak-Novakovic, Gordana, Hung, Clark T., & Ateshian, Gerard A. 2015. Matrix Production in Large Engineered Cartilage Constructs Is Enhanced by Nutrient Channels and Excess Media Supply. *Tissue engineering. Part C, Methods*, **21**(7), 747–757.

Normand, Valéry, Lootens, Didier L, Amici, Eleonora, Plucknett, Kevin P, & Aymard, Pierre. 2000. New Insight into Agarose Gel Mechanical Properties. *Biomacromolecules*, **1**(4), 730–738.

Nover, Adam B, Lee, Stephanie L, Georgescu, Maria S, Howard, Daniel R, Saunders, Reuben A, Yu, William T, Klein, Robert W, Napolitano, Anthony P, Ateshian, Gerard A., & Hung, Clark T. 2015. Porous titanium bases for osteochondral tissue engineering. *Acta Biomaterialia*, **27**(Nov.), 286–293.

Nover, Adam B, Stefani, Robert M, Lee, Stephanie L, Ateshian, Gerard A., Stoker, Aaron M, Cook, James L, & Hung, Clark T. 2016. Long-term storage and preservation of tissue engineered articular cartilage. *Journal of orthopaedic research : official publication of the Orthopaedic Research Society*, **34**(1), 141–148.

Obradovic, Bojana, Carrier, Rebecca L, Vunjak-Novakovic, Gordana, Freed, Lisa E, *et al.* . 1999. Gas exchange is essential for bioreactor cultivation of tissue engineered cartilage. *Biotechnology and bioengineering*, **63**(2), 197–205.

O'Connell, Grace D, Tan, Andrea R, Cui, Victoria, Bulinski, J Chloë, Cook, James L, Attur, Mukundan, Abramson, Steven B, Ateshian, Gerard A., & Hung, Clark T. 2015. Human chondrocyte migration behaviour to guide the development of engineered cartilage. *Journal of tissue engineering and regenerative medicine*, Jan., n/a–n/a.

O'Driscoll, Shawn WM, Saris, Daniel BF, Ito, Yoichi, & Fitzimmons, James S. 2001. The chondrogenic potential of periosteum decreases with age. *Journal of Orthopaedic Research*, **19**(1), 95–103.

Olson, Steven A, & Guilak, Farshid (eds). 2015. *Post-Traumatic Arthritis*. 1 edn. Pathogenesis, Diagnosis and Management. Boston, MA: Springer US.

Olson, Steven A, Horne, Phillip, Furman, Bridgette, Huebner, Janet, Al-Rashid, Mamun, Kraus, Virginia Byers, & Guilak, Farshid. 2014. The role of cytokines in posttraumatic arthritis. *The Journal of the American Academy of Orthopaedic Surgeons*, **22**(1), 29–37.

Olson, Steven A, Furman, Bridgette D, Kraus, Virginia B, Huebner, Janet L, & Guilak, Farshid. 2015. Therapeutic opportunities to prevent post-traumatic arthritis: Lessons from the natural history of arthritis after articular fracture. *Journal of orthopaedic research : official publication of the Orthopaedic Research Society*, **33**(9), 1266–1277.

Overbeek, J Th. 1956. The Donnan equilibrium. *Progress in biophysics and biophysical chemistry*, **6**, 57.

Ozsoy, Mehmet Hakan, Aydogdu, Semih, Taskiran, Dilek, Sezak, Murat, Hayran, Mutlu, Oztop, Fikri, & Ozsoy, Arzu. 2009. The effects of early or late treatment of osteochondral defects on joint homoeostasis: an experimental study in rabbits. *Knee surgery, sports traumatology, arthroscopy : official journal of the ESSKA*, **17**(6), 578–589.

Pandit, V, Pandit, Vaibhav, Zuidema, J M, Zuidema, Jonathan M, Venuto, Kathryn N, Venuto, K N, Macione, J, Macione, James, Dai, Guohao, Dai, G, Gilbert, Ryan J, Kotha, Shiva P, & Kotha, S P. 2013. Evaluation of Multifunctional Polysaccharide Hydrogels with Varying Stiffness for Bone Tissue Engineering. *Tissue Engineering. Part A*, **19**(21-22), 2452–2463.

Park, Seonghun, & Ateshian, Gerard A. 2006. Dynamic response of immature bovine articular cartilage in tension and compression, and nonlinear viscoelastic modeling of the tensile response. *Journal of biomechanical engineering*, **128**(4), 623–630.

Park, Seonghun, Krishnan, Ramaswamy, Nicoll, Steven B, & Ateshian, Gerard A. 2003. Cartilage interstitial fluid load support in unconfined compression. *Journal of Biomechanics*, **36**(12), 1785–1796.

Park, Seonghun, Hung, Clark T., & Ateshian, Gerard A. 2004. Mechanical response of bovine articular cartilage under dynamic unconfined compression loading at physiological stress levels. *Osteoarthritis and Cartilage*, **12**(1), 65–73.

Parma, H, Gilmore, R S, & Palfrey, A J. 1988. The area of the articular surface of the distal end of the human femur. *Journal of anatomy*, **157**(Apr.), 233–234.

Patwari, P rth, Cook, Michael N, DiMicco, Michael A, Blake, Simon M, James, Ian E, Kumar, Sanjay, Cole, Ada A, Lark, Michael W, & Grodzinsky, Alan J. 2003. Proteoglycan degradation after injurious compression of bovine and human articular cartilage in vitro: Interaction with exogenous cytokines. *Arthritis & Rheumatism*, **48**(5), 1292–1301.

Pazzano, D, Mercier, K A, Moran, J M, Fong, S S, DiBiasio, D D, Rulfs, J X, Kohles, S S, & Bonassar, L. J. 2000. Comparison of chondrogensis in static and perfused bioreactor culture. *Biotechnology Progress*, **16**(5), 893–896.

Pei, Ming, & He, Fan. 2012. Extracellular matrix deposited by synovium-derived stem cells delays replicative senescent chondrocyte dedifferentiation and enhances redifferentiation. *Journal of cellular physiology*, **227**(5), 2163–2174.

Pernodet, Nadine, Maaloum, Mounir, & Tinland, Bernard. 1997. Pore size of agarose gels by atomic force microscopy. *Electrophoresis*, **18**(1), 55–58.

Pittenger, M F, Mackay, A M, Beck, S C, Jaiswal, R K, Douglas, R, Mosca, J D, Moorman, M A, Simonetti, D W, Craig, S, & Marshak, D R. 1999. Multilineage potential of adult human mesenchymal stem cells. *Science (New York, N.Y.)*, **284**(5411), 143–147.

Raynauld, Jean Pierre, Buckland Wright, Chris, Ward, Rupert, Choquette, Denis, Haraoui, Boulos, Martel Pelletier, Johanne, Uthman, Imad, Khy, Visithan, Tremblay, Jean Luc, Bertrand, Carole, & Pelletier, Jean-Pierre. 2003. Safety and efficacy of long-term intraarticular steroid injections in osteoarthritis of the knee: a randomized, double-blind, placebo-controlled trial. *Arthritis & Rheumatism*, **48**(2), 370–377.

Reindel, E S, Ayroso, A M, Chen, A. C., Chun, D M, Schinagl, R M, & Sah, R. L. 1995. Integrative repair of articular cartilage in vitro: adhesive strength of the interface region. *Journal of Orthopaedic Research*, **13**(5), 751–760.

Rhen, Turk, & Cidlowski, John A. 2005. Antiinflammatory Action of Glucocorticoids — New Mechanisms for Old Drugs. *New England Journal of Medicine*, **353**(16), 1711–1723.

Riesle, J, Hollander, AP, Langer, R, Freed, LE, & Vunjak-Novakovic, G. 1998. Collagen in tissue-engineered cartilage: Types, structure, and crosslinks. *Journal of cellular biochemistry*, **71**(3), 313–327.

Roach, Brendan L, Hung, Clark T., Cook, James L, Ateshian, Gerard A., & Tan, Andrea R. 2015. Fabrication of tissue engineered osteochondral grafts for restoring the articular surface of diarthrodial joints. *Methods (San Diego, Calif.)*, **84**(Aug.), 103–108.

Roach, Brendan L, Kelmendi-Doko, Arta, Balutis, Elaine C, Marra, Kacey G, Ateshian, Gerard A., & Hung, Clark T. 2016. Dexamethasone Release from Within Engineered Cartilage as a Chondroprotective Strategy Against Interleukin-1a. *Tissue Engineering. Part A*, **22**(7-8), 621–632.

Rodrigo, J J, Steadman, J R, Syftestad, G, Benton, H, & Silliman, J. 1995. Effects of human knee synovial fluid on chondrogenesis in vitro. *The American journal of knee surgery*, **8**(4), 124–129.

Rodríguez Villanueva, Javier, Bravo-Osuna, Irene, Herrero-Vanrell, Rocío, Molina Martínez, Irene Teresa, & Guzmán Navarro, Manuel. 2016. Optimising the controlled release of dexamethasone from a new generation of PLGA-based microspheres intended for intravitreal administration. *European journal of pharmaceutical sciences : official journal of the European Federation for Pharmaceutical Sciences*, **92**(Sept.), 287–297.

Roos, Ewa M. 2005. Joint injury causes knee osteoarthritis in young adults. *Current Opinion in Rheumatology*, **17**(2), 195–200.

Roos, H, Adalberth, T, Dahlberg, L, & Lohmander, L Stefan. 1995. Osteoarthritis of the knee after injury to the anterior cruciate ligament or meniscus: the influence of time and age. *Osteoarthritis and Cartilage*, **3**(4), 261–267.

Rubin, J Peter, DeFail, A., Rajendran, N., Rajendran, Nithya, Marra, Kacey G, & Marra, K. G. 2009. Encapsulation of adipogenic factors to promote differentiation of adipose-derived stem cells. *Journal of drug targeting*, **17**(3), 207–215.

Ruhe, P Quinten, Hedberg, Elizabeth L, Padron, Nestor Torio, Spauwen, Paul H M, Jansen, John A, & Mikos, Antonios G. 2003. rhBMP-2 release from injectable poly(DL-lactic-co-glycolic acid)/calcium-phosphate cement composites. *The Journal of Bone and Joint Surgery*, **85-A Suppl 3**, 75–81.

Saito, S, Katoh, M, Masumoto, M, Matsumoto, S, & Masuho, Y. 1999. Dexamethasone inhibits collagen degradation induced by the combination of interleukin-1 and plasminogen in cartilage explant culture. *Biological & pharmaceutical bulletin*, **22**(7), 727–730.

Sampat, Sonal R, O'Connell, Grace D, Fong, Jason V, Alegre-Aguarón, Elena, Ateshian, Gerard A., & Hung, Clark T. 2011. Growth factor priming of synovium-derived stem cells for cartilage tissue engineering. *Tissue Engineering. Part A*, **17**(17-18), 2259–2265.

Saris, D B F, Dhert, Wouter J A, & Verbout, A J. 2003. Joint homeostasis. *The Journal of Bone and Joint Surgery*, **85**(7), 1067–1076.

Schek, Rachel M, Taboas, Juan M, Segvich, Sharon J, Hollister, Scott J, & Krebsbach, Paul H. 2004. Engineered osteochondral grafts using biphasic composite solid free-form fabricated scaffolds. *Tissue engineering*, **10**(9-10), 1376–1385.

Sekiya, Ichiro, Vuoristo, Jussi T, Larson, Benjamin L, & Prockop, Darwin J. 2002. In vitro cartilage formation by human adult stem cells from bone marrow stroma defines the sequence of cellular and molecular events during chondrogenesis. *Proceedings of the National Academy of Sciences of the United States of America*, **99**(7), 4397–4402.

Selmi, T A S, Neyret, Ph, Verdonk, P C M, & Barnouin, L. 2007. Autologous Chondrocyte Transplantation in Combination With an Alginate-Agarose Based Hydrogel (Cartipatch). *Techniques in Knee Surgery*, **6**(4), 253–258.

Selmi, T A S, Verdonk, P, Chambat, P, Dubrana, F, Potel, J F, Barnouin, L, & Neyret, P. 2008. Autologous chondrocyte implantation in a novel alginate-agarose hydrogel OUTCOME AT TWO YEARS. *Journal of Bone & Joint Surgery, British Volume*, **90**(5), 597–604.

Setton, LA, Tohyama, H, & Mow, VC. 1998. Swelling and curling behaviors of articular cartilage. *Journal of biomechanical engineering*, **120**(3), 355–361.

Shepherd, DET, & Seedhom, B B. 1999. Thickness of human articular cartilage in joints of the lower limb. *Annals of Rheumatic Disorders*, **58**(27), 8.

Sherman, S L, Khazai, R S, James, C H, Stoker, A. M., Flood, D L, & Cook, J. L. 2015a. In Vitro Toxicity of Local Anesthetics and Corticosteroids on Chondrocyte and Synoviocyte Viability and Metabolism. *Cartilage*, **6**(4), 233–240.

Sherman, S L, James, C, Stoker, A. M., Cook, C R, Khazai, R S, Flood, D L, & Cook, J. L. 2015b. In Vivo Toxicity of Local Anesthetics and Corticosteroids on Chondrocyte and Synoviocyte Viability and Metabolism. *Cartilage*, **6**(2), 106–112.

Sherwood, Jill K, Riley, Susan L, Palazzolo, Robert, Brown, Scott C, Monkhouse, Donald C, Coates, Matt, Griffith, Linda G, Landeen, Lee K, & Ratcliffe, Anthony. 2002. A three-dimensional osteochondral composite scaffold for articular cartilage repair. *Biomaterials*, **23**(24), 4739–4751.

Shinmei, M, Masuda, K, Kikuchi, T, & Shimomura, Y. 1989. The role of cytokines in chondrocyte mediated cartilage degradation. *The Journal of rheumatology. Supplement*, **18**(Aug.), 32–34.

Shinmei, M, Masuda, K, Kikuchi, T, Shimomura, Y, & Okada, Y. 1991. Production of cytokines by chondrocytes and its role in proteoglycan degradation. *The Journal of rheumatology. Supplement*, **27**(Feb.), 89–91.

Siegel, Steven J, Kahn, Jonathan B, Metzger, Kayla, Winey, Karen I, Werner, Kathryn, & Dan, Nily. 2006. Effect of drug type on the degradation rate of PLGA matrices. *European Journal of Pharmaceutics and Biopharmaceutics*, **64**(3), 287–293.

Singh, A, Zelazowska, E B, Petrides, J S, Raybourne, R B, Sternberg, E M, Gold, P W, & Deuster, P A. 1996. Lymphocyte subset responses to exercise and glucocorticoid suppression in healthy men. *Medicine and science in sports and exercise*, **28**(7), 822–828.

Singh, Gurkirpal. 1996. Gastrointestinal Tract Complications of Nonsteroidal Anti-inflammatory Drug Treatment in Rheumatoid Arthritis. *Archives of Internal Medicine*, **156**(14), 1530.

Smeriglio, Piera, Lai, Janice H, Dhulipala, Lakshmi, Behn, Anthony W, Goodman, Stuart B, Smith, Robert L, Maloney, William J, Yang, Fan, & Bhutani, Nidhi. 2015. Comparative potential of juvenile and adult human articular chondrocytes for cartilage tissue formation in three-dimensional biomimetic hydrogels. *Tissue Engineering. Part A*, **21**(1-2), 147–155.

Smetana Jr, K, & Vilím, V. 1991. Biochemical properties of cartilage and multinucleate chondroclast formation. *Functional and developmental morphology*, **2**(3), 163–165.

Soltz, Michael A, & Ateshian, Gerard A. 2000. A Conewise Linear Elasticity Mixture Model for the Analysis of Tension-Compression Nonlinearity in Articular Cartilage. *Journal of Biomechanical Engineering-Transactions of the Asme*, **122**(6), 576–586.

Song, Ruo Hua, Tortorella, Micky D, Malfait, Anne Marie, Alston, James T, Yang, Zhiyong, Arner, Elizabeth C, & Griggs, David W. 2007. Aggrecan degradation in human articular cartilage explants is mediated by both ADAMTS-4 and ADAMTS-5. *Arthritis & Rheumatism*, **56**(2), 575–585.

Song, Yu Wen, Zhang, Tao, & Wang, Wen Bo. 2012. Gluococorticoid could influence extracellular matrix synthesis through Sox9 via p38 MAPK pathway. *Rheumatology international*, **32**(11), 3669–3673.

Sophia Fox, Alice J, Bedi, Asheesh, & Rodeo, Scott A. 2009. The basic science of articular cartilage: structure, composition, and function. *Sports health*, **1**(6), 461–468.

Soprano, Joyce V. 2005. Musculoskeletal Injuries in the Pediatric and Adolescent Athlete. *Current Sports Medicine Reports*, **4**(6), 329–334.

Soulhat, J, Buschmann, M. D., & Shirazi-Adl, A. 1999. A Fibril-Network-Reinforced Biphasic Model of Cartilage in Unconfined Compression. *Journal of Biomechanical Engineering-Transactions of the Asme*, **121**(3), 340–347.

Stäubli, H-U, Dürrenmatt, U, Porcellini, B, & Rauschning, W. 1999. Anatomy and surface geometry of the patellofemoral joint in the axial plane. *Bone & Joint Journal*, **81**(3), 452–458.

Steadman, J R, Steadman, J R, Rodkey, W G, Rodkey, W G, Rodrigo, J J, & Rodrigo, J J. 2001. Microfracture: Surgical Technique and Rehabilitation to Treat Chondral Defects. *Clinical Orthopaedics and Related Research*, Oct., 8.

Stegemann, Hermann, & Stalder, Karlheinz. 1967. Determination of hydroxyproline. *Clinica Chimica Acta*, **18**(2), 267–273.

Stockwell, RA. 1967. The cell density of human articular and costal cartilage. *Journal of anatomy*, **101**(Pt 4), 753.

Tam, Hok Kei, Srivastava, Ajay, Colwell, Clifford W., & D'Lima, Darryl D. 2007. In vitro model of full-thickness cartilage defect healing. *Journal of Orthopaedic Research*, **25**(9), 1136–1144.

Tan, Andrea R, VandenBerg, Curtis D, Attur, Mukundan, Abramson, Steven B, Knight, Martin M, Bulinski, J Chloë, Ateshian, Gerard A., Cook, James L, & Hung, Clark T. 2015. Cytokine preconditioning of engineered cartilage provides protection against interleukin-1 insult. *Arthritis Research & Therapy*, **17**(1), 345.

Tan, H, Wu, J, Wu, J, Lao, L, Lao, L, Gao, C, & Gao, C. 2009. Gelatin/chitosan/hyaluronan scaffold integrated with PLGA microspheres for cartilage tissue engineering. *Acta Biomaterialia*, **5**(1), 328–337.

Tang, GongWen, Yang, YanFang, Sun, AiPing, Song, TianTian, Zhao, YunHui, Yuan, XuBo, Yuan, XiaoYan, Fan, YuBo, & Wang, Min. 2010. Controlled release of dexamethasone from porous PLGA scaffolds under cyclic loading. *Science China Chemistry*, **53**(3), 594–598.

Theodoropoulos, John S, De Croos, J N Amritha, Park, Sam S, Pilliar, Robert, & Kandel, Rita A. 2011. Integration of tissue-engineered cartilage with host cartilage: an in vitro model. *Clinical Orthopaedics and Related Research*, **469**(10), 2785–2795.

Torzilli, Peter A, Grigiene, Rita, Huang, Charles, Friedman, Steven M, Doty, Stephen B, Boskey, Adele L, & Lust, George. 1997. Characterization of cartilage metabolic response to static and dynamic stress using a mechanical explant test system. *Journal of Biomechanics*, **30**(1), 1–9.

Tsuchida, Anika I, Beekhuizen, Michiel, T Hart, Marieke C, Radstake, Timothy R D J, Dhert, Wouter J A, Saris, Daniel B F, van Osch, Gerjo J V M, & Creemers, Laura B. 2014. Cytokine profiles in the joint depend on pathology, but are different between synovial fluid, cartilage tissue and cultured chondrocytes. *Arthritis research & therapy*, **16**(5), 441.

Tuan, Rocky S, Boland, Genevieve, & Tuli, Richard. 2002. Adult mesenchymal stem cells and cell-based tissue engineering. *Arthritis Res Ther*, **5**(1), 1.

Undt, Gerhard, Wild, Klaus, Reuther, Gerd, & Ewers, Rolf. 2000. MRI-based stereolithographic models of the temporomandibular joint: technical innovation. *Journal of Cranio-Maxillofacial Surgery*, **28**(5), 258–263.

Vacanti, C A, Bonassar, L. J., Vacanti, M P, & Shufflebarger, J. 2001. Replacement of an avulsed phalanx with tissue-engineered bone. *The New England journal of medicine*, **344**(20), 1511–1514.

Vanlauwe, J, Vanlauwe, J, Saris, D B, Saris, D B, Victor, J, Victor, J, Almqvist, K F, Almqvist, K F, Bellemans, J, Bellemans, J, Luyten, F P, & Luyten, F P. 2011. Five-year outcome of characterized chondrocyte implantation versus microfracture for symptomatic cartilage defects of the knee: early treatment matters. *American Journal of Sports Medicine*, **39**(12), 2566–2574.

von Porat, A. 2004. High prevalence of osteoarthritis 14 years after an anterior cruciate ligament tear in male soccer players: a study of radiographic and patient relevant outcomes. *Annals of the rheumatic diseases*, **63**(3), 269–273.

Vunjak-Novakovic, G, Martin, I, Obradovic, B, Treppo, S, Grodzinsky, AJ, Langer, R, & Freed, LE. 1999. Bioreactor cultivation conditions modulate the composition and mechanical properties of tissue-engineered cartilage. *Journal of Orthopaedic Research*, **17**(1), 130–138.

Vunjak-Novakovic, Gordana, Freed, Lisa E, Biron, Robert J, & Langer, Robert. 1996. Effects of mixing on the composition and morphology of tissue-engineered cartilage. *AIChE Journal*, **42**(3), 850–860.

Waldman, SD, Couto, DC, Grynpas, MD, Pilliar, RM, & Kandel, RA. 2006. A single application of cyclic loading can accelerate matrix deposition and enhance the properties of tissue-engineered cartilage. *Osteoarthritis and Cartilage*, **14**(4), 323–330.

Waldman, Stephen D., Spiteri, Caroline G., Grynpas, Marc D., Pilliar, Robert M., & Kandel, Rita A. 2004. Long-term intermittent compressive stimulation improves the composition and mechanical properties of tissue-engineered cartilage. *Tissue Engineering*, **10**(9-10), 1323–1331.

Wang, C. C., Hung, Clark T., & Mow, V C. 2001. An analysis of the effects of depth-dependent aggregate modulus on articular cartilage stress-relaxation behavior in compression. *Journal of Biomechanics*, **34**(1), 75–84.

Wang, Christopher C. B., Deng, Jian-Ming, Ateshian, Gerard A., & Hung, Clark T. 2002a. An Automated Approach for Direct Measurement of Two-Dimensional Strain Distributions Within Articular Cartilage Under Unconfined Compression. *Journal of Biomechanical Engineering-Transactions of the Asme*, **124**(5), 557–567.

Wang, Christopher C. B., Guo, X. Edward, Sun, Dongning, Mow, Van C, Ateshian, Gerard A., & Hung, Clark T. 2002b. The functional environment of chondrocytes within cartilage subjected to compressive loading: a theoretical and experimental approach. *Biorheology*, **39**(1), 11–25.

Wang, Christopher C. B., Chahine, Nadeen O, Hung, Clark T., & Ateshian, Gerard A. 2003. Optical determination of anisotropic material properties of bovine articular cartilage in compression. *Journal of Biomechanics*, **36**(3), 339–353.

Wang, Yongzhong, Kim, Ung-Jin, Blasioli, Dominick J, Kim, Hyeon-Joo, & Kaplan, David L. 2005. In vitro cartilage tissue engineering with 3D porous aqueous-derived silk scaffolds and mesenchymal stem cells. *Biomaterials*, **26**(34), 7082–7094.

Weng, Yulai, Cao, Yilin, Arevalo, Carlos, Vacanti, Martin P, & Vacanti, Charles A. 2001. Tissue-engineered composites of bone and cartilage for mandible condylar reconstruction. *Journal of Oral and Maxillofacial Surgery*, **59**(2), 185–190.

Wernecke, Chloe, Braun, Hillary J, & Dragoo, Jason L. 2015. The Effect of Intra-articular Corticosteroids on Articular Cartilage: A Systematic Review. *Orthopaedic journal of sports medicine*, **3**(5), 2325967115581163.

Whiteside, LA. 1989. Clinical results of Whiteside Ortholoc total knee replacement. *The Orthopedic clinics of North America*, **20**(1), 113–124.

Williams, R J, Peterson, L, & Cole, B. 2007. *Cartilage repair strategies*. Humana Press, Totowa, NJ.

Williamson, Amanda K, Masuda, Koichi, Thonar, Eugene J-MA, & Sah, Robert L. 2003a. Growth of immature articular cartilage in vitro: correlated variation in tensile biomechanical and collagen network properties. *Tissue engineering*, **9**(4), 625–634.

Williamson, Amanda K, Chen, Albert C, Masuda, Koichi, Thonar, Eugene J, & Sah, Robert L. 2003b. Tensile mechanical properties of bovine articular cartilage: variations with growth and relationships to collagen network components. *Journal of Orthopaedic Research*, **21**(5), 872–880.

Wilson, Christopher G, Palmer, Ashley W, Zuo, Fengrong, Eugui, Elsie, Wilson, Stacy, Mackenzie, Rebecca, Sandy, John D, & Levenston, Marc E. 2007. Selective and non-selective metalloproteinase inhibitors reduce IL-1-induced cartilage degradation and loss of mechanical properties. *Matrix biology*, **26**(4), 259–268.

Wilusz, Rebecca E, Weinberg, J Brice, Guilak, Farshid, & McNulty, Amy L. 2008. Inhibition of integrative repair of the meniscus following acute exposure to interleukin-1 in vitro. *Journal of Orthopaedic Research*, **26**(4), 504–512.

Wojdasiewicz, Piotr, Poniatowski, Łukasz A, & Szukiewicz, Dariusz. 2014. The role of inflammatory and anti-inflammatory cytokines in the pathogenesis of osteoarthritis. *Mediators of inflammation*, **2014**(2), 561459–19.

Xu, Tao, Binder, Kyle W, Albanna, Mohammad Z, Dice, Dennis, Zhao, Weixin, Yoo, James J, & Atala, Anthony. 2013. Hybrid printing of mechanically and biologically improved constructs for cartilage tissue engineering applications. *Biofabrication*, **5**(1), 015001.

Yang, K G Auw, Saris, D B F, Verbout, A J, Creemers, L B, & Dhert, Wouter J A. 2006. The Effect of Synovial Fluid from Injured Knee Joints on in Vitro Chondrogenesis. *Tissue Engineering*, **12**(10), 2957–2964.

Yoon, Hee Hun, Yoon, Hee Hun, Bhang, Suk Ho, Bhang, Suk Ho, Shin, Jung-Youn, Shin, Jung-Youn, Shin, Jaehoon, Shin, Jaehoon, Kim, Byung-Soo, & Kim, Byung-Soo. 2012. Enhanced Cartilage Formation via Three-Dimensional Cell Engineering of Human Adipose-Derived Stem Cells. *Tissue Engineering. Part A*, **18**(19-20), 1949–1956.

Zhang, W, Moskowitz, R W, Nuki, G, Abramson, S, Altman, R D, Arden, N, Bierma-Zeinstra, S, Brandt, K D, Croft, P, Doherty, M, Dougados, M, Hochberg, M, Hunter, D J, Kwoh, K, Lohmander, L Stefan, & Tugwell, P. 2008. OARSI recommendations for the management of hip and knee osteoarthritis, Part II: OARSI evidence-based, expert consensus guidelines. *Osteoarthritis and Cartilage*, **16**(2), 137–162.

Zhang, Weijie, Lian, Qin, Li, Dichen, Wang, Kunzheng, Hao, Dingjun, Bian, Weiguo, He, Jiankang, & Jin, Zhongmin. 2014. Cartilage repair and subchondral bone migration using 3D printing osteochondral composites: a one-year-period study in rabbit trochlea. *BioMed research international*, **2014**.

Zolnik, Banu S, & Burgess, Diane J. 2008. Evaluation of in vivo-in vitro release of dexamethasone from PLGA microspheres. *Journal of controlled release : official journal of the Controlled Release Society*, **127**(2), 137–145.

Appendix A Dexamethasone Concentration Determination

A.1 High pressure liquid chromatographic (HPLC) analyses of corticosteroids

The HPLC system is located in Dr. Nuckolls' lab in the Department of Chemistry. Our contact is Dr. Brandon Fowler. Future work with the HPLC will require training on the device, however, there were no costs, aside from raw materials, involved in previous use of the system.

A.1.1 Sample preparation

Several protocols for sample preparation can be found in the literature (Hickey *et al.* , 2002b; Hickey *et al.* , 2002a; Lamiable *et al.* , 1986; Zolnik & Burgess, 2008).

Dexamethasone is insoluble in water in its most common form. Dexamethasone 21-phosphate disodium salt (Sigma D1159) is the compound used in our laboratory for encapsulation in PLGA microspheres. Although poorly water soluble, dexamethasone 21-phosphate disodium salt is soluble in methanol, serving as one part of water in the water-oil-water double emulsion technique used for MS fabrication. Dexamethasone (Sigma D4902) used in our laboratory for standard cell culture is less water soluble than its salt variant. The solubility characteristics of these two compounds should be considered when preparing the sample for analysis.

While HPLC can be used to identify the concentration of multiple compounds within the same sample, to improve the accuracy of results, dexamethasone should be the lone constituent of samples prior to analysis. Identification of either dexamethasone variant from phosphate buffered saline (PBS), chondrogenic medium (CM), or synovial fluid (SF) first requires isolation (extraction) of the compound to remove proteinaceous matter such as collagens and proteoglycans that have been synthesized by the cells and release into the medium. The optimal strategy for isolation of dexamethasone from these fluids has yet to be identified. Collaborating with Dr. Brandon Fowler in Dr. Colin Nuckolls' lab in Columbia University's Department of Chemistry, a current best strategy has been identified. This approach exploits the water solubility of various proteins and molecules within the sample. By diluting the PBS, CM, or SF sample 10-fold in methanol (containing 25 ng equilenin as internal standard), proteins and other water soluble matter will 'crash' out of solution, while less water soluble molecules, such as dexamethasone, will remain preferentially in the

methanol phase. Water and methanol are miscible, meaning that water soluble proteins (collagens and proteoglycans) will come out of solution and form a solid phase. The supernatant, containing dexamethasone (or cortisol), can be removed. This volume can then be evaporated under a stream of nitrogen. The remaining matter can be concentrated in a small volume of methanol (160 µL in this embodiment, but can be changed for injection volume and # of repeats) for HPLC analysis[1].

A.1.2 Standard curve for dexamethasone

The use of HPLC for dexamethasone measurement is predicated on the need to measure the molecule at masses below that which can be determined using a standard spectrophotometer. A protocol for preparation of standard curve is detailed below.

0.0025	g	measured grams of dexamethasone 21-phosphate disodium salt (D1159)		
1.00	mL	1 mL methanol suspension volume		
0.0025	*g/mL*	*concentration dex following suspension in methanol*		
0.0000025	*g/µL*	*concentration of dex in 1 µL of suspended volume*		
20	µL	volume added to 980 µL methanol for 1:50 dilution		
0.00000005	*g/µL*	*concentration of dexamethasone following addition of 20 µL stock to 980 µL methanol*		
50.00	*ng/µL*	*concentration of dexamethasone for addition to standards*		
	100	*ng/µL equilenin in acetonitrile*	**<—- STOCK**	
	100	µL equilenin	<— added to 900 methanol	
in	900	µL methanol	**Total Volume in Standards**	1000
Equilenin Concentration	*10*	*ng/µL*	**HPLC Injection Volume**	50

Figure A.1: Preparation of working solutions of dexamethasone and equilenin for HPLC standards and analysis.

The above table (Figure A.1) should be followed to develop 1x working solutions of both dexamethasone and equilenin. Both 1x working solutions should be used in the standards (prepare duplicates) below (Figure A.2).

[1] Although not explored here, the same extraction protocol may be applied for use with a UV-Vis spectrophotometer.

Vial #	Dex Mass (50 μL injection volume)	1x DEX (μL)	Methanol (μL)	1x Equilenin (μL)	Total Volume (μL)
1	0	0.00	950.00	50.00	1000
2	1	0.40	949.60	50.00	1000
3	10	4.00	946.00	50.00	1000
4	25	10.00	940.00	50.00	1000
5	50	20.00	930.00	50.00	1000
6	75	30.00	920.00	50.00	1000
7	100	40.00	910.00	50.00	1000
8	250	100.00	850.00	50.00	1000
9	500	200.00	750.00	50.00	1000
10	1000	400.00	550.00	50.00	1000

Figure A.2: Preparation of standards for HPLC analysis.

The standards should be prepared in microcentrifuge tubes. For HPLC analysis, 160 µL of the sample should be transferred to glass vials (Sigma 29652-U; package of 100, certified vial kit, 2 mL) with small-volume glass inserts (Sigma 24707; package of 100, insert for 2 mL standard vial, up to 150 µL). Glass vial caps contain a silicone septa (with slit) to allow the machine to enter the vial during injection.

A.1.3 Theory and use of Agilent Infinity LC system

HPLC is a technique to separate, identify, and quantify compounds of interest within a mixture. The sample is injected into a mobile phase, typically comprised of a miscible combination of aqueous and organic solvents, passed through a solid absorbent material (stationary phase) containing a specific particle size, packing structure, and polarity. Understanding the properties of the sample (size, polarity) allows for optimization of the stationary and mobile phase to expedite sample elution from the column. A detector, at the end of the column, will measure absorbance of the sample at a given wavelength (245 nm in this case).

For dexamethasone identification and quantification, we have used a reverse phase set up in which the stationary phase is a C-18 column (non-polar) and the mobile phase (moderately polar) comprises (60:40) 4 mM ammonium acetate buffer:acetonitrile. This arrangement is selected because of the only slightly-polar nature of the dexamethasone (or hydrocortisone) molecule.

Using the above context and below protocol, dexamethasone will elute from the column in ∼5 minutes while the internal standard, equilenin, elutes in ∼12 minutes.

- Samples reconstituted in 160 µL methanol.
- Check miscibility of reagents. (Aqueous solutions versus others.) Replace reagents, if necessary.
- Remove line from previous reagents and clean frit with compressed air. Replace frit on barb and insert to new reagent.
- Select 'BR-DEXAMSETHASONE.mtd' as the method.
  - Select 'Set Up Pump' and indicate which reagent is on what line.
  - Flush the line you just put the frit in to.
    * 100% channel at 5 mL/min with the 'prime valve' open (full counterclockwise turn). Do this for both reagents separately. System can only add channels to 100% and cannot ON OFF pump faster than 5 mL/min because of line pressures.
    * Start the priming by closing out the window and selecting the 'on' box.
    * Monitor line for first air bubbles that come through. Allow five minutes of additional time before switching to the next line.
- During flush, set up 'Sequence Parameters'. (Left click on tray.)
  - Enter the subdirectory 'Brendan'.
  - Select 60 minute wait after loading method.
  - Check the box for post-sequence and 'macro "SHUTDOWN.MAC,go' from the dropdown menu.
  - Select ok to close the window.
  - Delete any values in the 'Fraction Start Location' field. [2]
- Set up 'Sample List' via left click on tray.
  - Create table where vial number reflects position of the vial in the tray.
  - Sample name can be as desired.
  - The method here should be the method chosen above.
  - The # of injections may vary, but in our case is 3.
  - Select okay. Do not run sequence.
- Once lines are flushed, set flow to 0 mL/min. Close the primer knob by rotating all the way to the right.
- Remove and cap any column that is on the instrument. Insert blank (connecting) column and flush the system at 2 mL/min with 100% acetonitrile (~5 mins), then with the prescribed protocol settings (~5 mins). (This is in part because of the use of reverse phase.)

[2] This is because of an error from a previous run. The Fraction Start Location indicates the vial at which the sampler should begin to collect fractions into. We are not purifying sample so we do not need a value here. This is doubly ensuring that the system is not confused.

- Set the flow to 0 mL/min and replace blank column with C-18 column, ensuring that 'flow' is in the correct direction (from the right of the system to the left). In the 'Set up pump' screen, enter protocol settings (solvent ratios, run time, and flow rate), and click 'OK'. [3]
- Place samples in chamber and select 'Start'. Click 'OK' for the 3 windows that pop up.
- Following the end of the runs, cleanse the system with acetonitrile at 100% and 1 mL/min for 10-15 minutes. This will flush the system and leave the column in 100% acetonitrile for storage.
- If possible, remove the column and store (with end caps secure).

A.1.4 Analysis of Agilent Infinity LC System .txt files - .m file

The companion software package for the HPLC system is effective in processing single files, especially when baseline is not on the horizontal. The output plots time on the x-axis and absorbance units (measured at 245 nm) on the y-axis, with the area under the curve of interest being comparable to a curve of a known area. For the purposes of measuring dexamethasone, a standard curve was created for direct comparison of absorbance measurements.

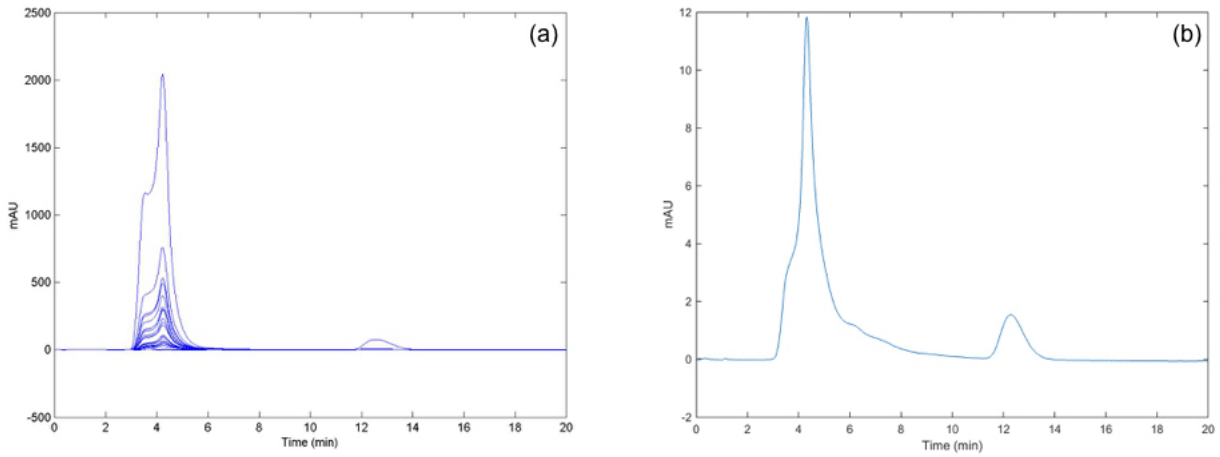

Figure A.3: Chromatographs output from custom .m file. (a) A full set of standards 'running the column' at ∼4 minutes, the length of time required for dex elution. Equilenin, the internal standard, runs the column at ∼12.5 minutes. (b) Depicts a single concentration of dex (500 ng) with equilenin standard (25 ng).

The .m files necessary to process .txt files from the HPLC can be found here. Example output curves, generated by the .m file, are above for the dexamethasone standard curve (Figure A.3a)

[3] While the solvent ratios will be previously entered, run time and flow rate will need to be changed. These values determine the experimental values. For dexamethasone, that means 1 mL/min, 20 min run, and 60/40 C:D (acetate buffer:acetonitrile).

and a sample dexamethasone run, with internal standard equilenin (Figure A.3b). NOTE: This code works only when the baseline is on the horizontal. If there is a shift in the baseline from the beginning of a peak to the end of the peak, the most accurate way to evaluate the area under the curve is via the Agilent Infinity LC system companion software. (With effort, this .m file can be modified to allow for baseline correction. I suggest trying to implement the BEADS package.)

A.2 Spectrophotometric analyses of dexamethasone concentration

Similar to the above protocol for HPLC applications, the protocol below describes preparation of the working solution and standards for spectrophotometric analysis. Standards should be prepared in duplicate, and the buffer should be consistent with the buffer in which the dexamethasone is in.

2.5	mg	measured grams of dexamethasone 21-phosphate disodium salt
1.0	mL	resuspend in 1 mL buffer
0.0025	*g/mL*	*concentration dex following resuspension (stock)*
0.0000	*g/µL*	*concentration of dex in 1 µL of resuspended volume (stock)*
100	µL	volume of stock added to total volume of 15 mL
0.00000001667	*g/µL*	*concentration of dexamethasone following addition of 100 µL stock to 15 mL media*
16.67	*ng/µL*	*concentration of dexamethasone (final) for addition to standards*

	Dilution Label (ng/mL)	Volume Buffer (µL)	Volume 1x Dex (µL)
1	0	1000	0
2	250	985	15
3	500	970	30
4	750	955	45
5	1000	940	60
6	2500	850	150
7	5000	700	300
8	7500	550	450
9	10000	400	600

Figure A.4: Preparation of working reagents (top) and standards (bottom) for absorbance detection of dexamethasone concentration.

Following preparation of the standards (Figure A.4), 100 µL of each standard should be measured at 242 nm in a UV-Vis 96-well plate. Normal assay plates do not allow light in the ultraviolet range

to pass through, necessitating UV-Vis 96-well plates for this assay. Using a UV-Vis capable plate reader, such as the Synergy 2 multi-mode reader, measure the absorbance at 242 nm and plot the absorbance against the concentration. A linear fit should be possible. Most recent efforts fit a line described by (absorbance) = 6 x 10^{-5} x (concentration) + 0.0831, with an R^2= 0.99968.

A.3 Fluorometric analyses of dexamethasone concentration

Similar to the above protocols for HPLC and spectrophotometric applications, the protocol below describes preparation of the working solution and standards for fluorometric analysis. For this assay, dexamethasone fluorescein should be used (Life-Technologies D1383). Note that the working compound is light sensitive.

dex-fluorescein	**D1383**	840.9769	g/mol
0.005	g	mass of powder delivered	
1	mL	resuspension volume for stock	
0.005	*g/mL*	*concentration stock*	
0.000005	*g/µL*	*concentration stock per µL*	
1	µL	volume stock added to buffer	
1999	µL	volume buffer used to dilute stock	
0.0000000025	**g/µL**	**concentration following 2000-fold dilution**	
2.5	**ng/µL**	**concentration of diluted sample**	

	Dilution Label (ng/mL)	Volume Buffer (µL)	Volume 1x Dex (µL)
1	0	1000	0
2	0	1000	0
3	1	999.6	0.4
4	2	999.2	0.8
5	5	998.0	2
6	10	996.0	4
7	25	990.0	10
8	50	980.0	20
9	100	960.0	40
10	200	920.0	80
11	500	800.0	200
12	1000	600.0	400

Figure A.5: Preparation of working reagents (top) and standards (bottom) for fluorescent detection of dexamethasone concentration.

Standards should be prepared in duplicate (Figure A.5), and the buffer should be consistent with the buffer in which the dexamethasone is in. Following preparation of the standards, 100 µL of each standard should be measured in a 96-well plate. If a black plate is available, that is preferable, otherwise, a standard 96-well plate is acceptable. The Synergy 2 multi-mode reader allows for fluorescent analysis of the sample. Excitation wavelength of 493 nm and emission wavelength of 519 nm. Plot the fluorescence against the concentration and a linear fit of the data should be possible. Most recent efforts fit a line described by (absorbance) = 447.19 x (concentration) + 1513, with an R^2= 0.9942.

Appendix B Mechanical Evaluation of Cartilage Integration

B.1 Analysis of push out testing .txt files - .m file

The .m files necessary to process .txt files from the push out testing device can be found here.